

# **Thermal Characterization of Printable Wood Composite and Life Cycle Assessment of a Novel Wood-Based 3D-Printed Exterior Wall**

A Thesis

Presented in Partial Fulfillment of the Requirements for the

Degree of Master of Science

with a

Major in Mechanical Engineering

in the

College of Graduate Studies

University of Idaho

by

Tais I. Mitchell

Approved by:

Major Professor: Damon Woods, Ph.D., PE

Committee Members: Ralph Budwig, Ph.D., PE; Michael Maughan, Ph.D., PE

Department Administrator: Gabriel Potirniche, Ph.D, PE

December 2021

## Abstract

The construction industry is poised for significant transformation with the adoption of additive manufacturing (3D-printing) techniques. The benefits of 3D-printing include reduced cost, labor, and waste, which could result in an overall increase in industry-wide productivity. To maximize sustainability for this emerging technology, a research team at the University of Idaho is developing a method using a recycled wood-based composite as the printing material. The goal of this ongoing project is to take advantage of the benefits of additive manufacturing, while limiting the energy requirements and using renewable materials in the process. This paper details the thermal characterization of the 3D-printed composite and analyzes the total energy impact of this exterior wall assembly.

Initial experimental testing on the wood-based composite was performed using a transient needle probe method. The experiments analyzed a variety of samples with different compositions and wood grain size. The thermal conductivity measurements ranged from 0.08-0.15 W/mK and largely depended on the density of the sample. A correlation between the density and thermal conductivity was found and compared to other wood-based composites currently used in construction.

In addition to the transient needle probe method, an additional steady state method was used to verify results. The scope included designing, fabricating, and verifying a low-cost guarded hot plate apparatus according to ASTM standard C177. Calibration tests found that the apparatus achieved an 8% accuracy when verifying a cast acrylic reference material. The results from the apparatus showed good agreement with the needle probe results that were within 2% difference and validates the usage of the needle probe, which is a faster and less expensive testing method.

A preliminary LCA was performed on a wall section of the 3D-printed wall assembly, as well as for other common residential wall types. The main factor under consideration was the total energy impact. It was found that the proposed 3D-print wall had the best performance in the materials stage and was a close runner up in the building energy usage and end of life stages. Special care should be considered when designing the manufacturing process to ensure low energy usage. The 3D wall design has potential to decrease energy usage in the residential and light commercial building types. If additional incremental improvements are achieved in the envelope performance and manufacturing stages, the 3D-printed wall could become one of the lowest energy consuming wall types available.

## **Acknowledgements**

I would like to thank my major professor Dr. Damon Woods and my committee members Dr. Ralph Budwig and Dr. Mike Maughan. Special thanks to Damon, who has supported me throughout my research over the last year. You have been a great advocate and mentor to me. I also want to thank Ralph for sharing his plentiful knowledge of experimental design and guiding me through the troubleshooting process for the guarded hot plate apparatus. Thank you Dr. Behnaz Rezaie for inspiring me to expand on the environmental analysis in this project and thank you Kenneth Baker for giving me the freedom to include this expanded analysis within my scope of research. I would also like to thank my fellow graduate students in the Integrated Design Lab and in Moscow of whom I had the pleasure working with. Special thanks goes to Berlinda Orji for preparing the wood samples used for thermal testing. Finally, this research would not have been possible without the financial support from the Idaho State Board of Education's Higher Education Research Council.

## **Dedication**

For the memories spent in the mountains and on the water,

To the dedication, support, and love throughout my life.

I would not be the person I am today,

If not for the blessing of my Mom, Dad, and Sister.

## Table of Contents

Abstract.....	II
Acknowledgements.....	III
Dedication.....	IV
List of Figures.....	VII
Chapter 1: Introduction and Background.....	1
1.1 3D-Printing in Construction.....	1
1.2 Thermal Conductivity and Wood Products.....	3
Chapter 2: Thermal Testing of Novel Wood Composite .....	6
2.1 Transient Needle Probe.....	6
2.1.1 Transient Needle Probe Introduction .....	6
2.1.2 Transient Needle Probe Methods.....	9
2.1.3 Transient Needle Probe Results .....	13
2.2 Guarded Hot Plate Apparatus .....	17
2.2.1 Development of a Low Cost Guarded Hot Plate Apparatus .....	17
2.2.2 Guarded Hot Plate Methods.....	31
2.2.3 Guarded Hot Plate Results .....	34
Chapter 3: Life Cycle Assessment of Novel Wood-Based 3D-Printed Exterior Wall Assembly .....	36
3.1 Introduction.....	36
3.2 Methodology.....	37
3.2.1 Materials .....	37
3.2.2 Manufacturing.....	40
3.2.3 Building Energy Usage .....	42
3.2.4 End of Life .....	45
3.3 Overall Comparison and Discussion.....	48
Conclusion .....	53
Future Work.....	54

References.....	55
Appendices .....	60
Appendix A: Transient Needle Probe Method Experimental Results. ....	60
Appendix B: Guarded Hot Plate Details.....	62
Guarded Hot Plate User Manual.....	62
Apparatus Drawings .....	67
Guarded Hot Plate Coding.....	75
Guarded Hot Plate Bill of Materials .....	89
Appendix C: Life Cycle Analysis Details.....	90
Section 1. Pre-Manufacturing Embodied Energy Calculation Tables .....	90
Section 2. Manufacturing Energy Analysis .....	92
Section 3. Added Material Properties Input into EnergyPlus Model.....	93
Section 4. Athena Eco-Indicator Raw Outputs.....	94

## List of Figures

Figure 1. Example of thermal bridging in a wood framed envelope. [15].....	3
Figure 2. Transient needle probe sensor. ....	7
Figure 3. (a) Drilling hole into test sample (left) (b) sample during experimental testing (right). ....	8
Figure 4. Results from needle probe verification experiment.....	8
Figure 5. Needle probe oven drying setup. ....	11
Figure 6. Image of sample during experiment. ....	12
Figure 7. Observation of flaking during the experimental process.....	13
Figure 8. Transient needle probe experimental trials for the 50:50 40-mesh sample. ....	14
Figure 9. Thermal conductivity of 3D-print wood composition vs density.....	15
Figure 10. Comparison of the thermal conductivity – density correlation of the 3D-printed composite (blue), particleboard (grey), fiberboard (orange), and the MacLean model for solid wood (yellow) [20]. .....	15
Figure 11. Rendering of guarded hot plate apparatus. ....	19
Figure 12. Side (left) and bottom (right) side of the hot plate assembly. ....	20
Figure 13. Cold plate assembly.....	20
Figure 14. Temperature sensor location in hot (left) and cold (right) plate assembly. ....	21
Figure 15. Calibration curve for a temperature sensor. ....	22
Figure 16. Results from temperature stability test at steady state.....	23
Figure 17. Circuit diagram for the center plate (left) and guard plate (right). ....	25
Figure 18. Voltage across central heating pad. Vertical division: 100 mV. Horizontal division: 1 ms. 25	
Figure 19. Guarded hot plate calibration testing results with cast acrylic samples. ....	26
Figure 20. 95% confidence interval from calibration experiments.....	28
Figure 21. Thermal conductivity measurement of OSB sample.....	29
Figure 22. Guarded hot plate oven drying setup.....	31
Figure 23. Insulation surrounding the sample to limit heat loss. ....	33
Figure 24. Comparison of guarded hot plate results to transient needle probe results .....	34
Figure 25. Composition of a wood framed wall. ....	37
Figure 26. Composition of a SIPs Wall .....	37
Figure 27. Composition of a CMU Wall. ....	38
Figure 28. Structural matrix of proposed 3D-printed wall .....	39
Figure 29. Composition of proposed 3D-print wall.....	39
Figure 30. Material embodied energy comparison. ....	40

Figure 31. Preliminary 3D-print wall manufacturing process. ....	41
Figure 32. Rendering of PNNL single family residential model. ....	43
Figure 33. Embodied energy of the end-of-life stage. ....	46
Figure 34. Total energy impact comparison. ....	48
Figure 35. Sensitivity analysis comparing the relative effects of insulation and infiltration. ....	49
Figure 36. 3D-printed envelope energy saving compared with baseline envelope for different climate zones. ....	50
Figure 37. Transient needle probe experimental trials for the 70:30 40-mesh sample. ....	60
Figure 38. Transient needle probe experimental trials for the 60:40 40-mesh sample. ....	60
Figure 39. Transient needle probe experimental trials for the 60:40 whole wood sample. ....	61
Figure 40. Transient needle probe experimental trials for the 50:50 whole wood sample. ....	61
Figure 41. Image of hot plate temperature within Arduino code. ....	62
Figure 42. Constant temperature water bath controls. ....	62
Figure 43. Image showing thickness measurement. ....	63
Figure 44. Process to install insulation onto the sides (top left and right), front (bottom right) and back (bottom right), of the apparatus. ....	64
Figure 45. Inputs into the Python code. ....	65
Figure 46. Image of start button. ....	65



# Chapter 1: Introduction and Background

## 1.1 3D-Printing in Construction

Additive manufacturing, better known as 3D-printing, is a manufacturing technique that builds a given part from a feedstock material assembled in a layer-by-layer process. The ability to produce complex products with an all-in-one machine has sparked multiple industrial sectors to develop hardware and software that can print parts using novel materials. One of these industries is the construction sector. Several startup companies are developing printing methods to create small to medium residential and light commercial projects.

3D-printing in construction had an estimated market size of \$7 million in 2020 and is projected to reach \$1.2 billion by 2028 globally [1], which demonstrates the high demand for this construction method. There are several market factors that are driving construction towards 3D-printing. The first market pain is a shortage of affordable housing within the US. This is a key challenge faced by many growing cities [2]. The second issue facing construction is a long-term shortage of skilled construction workers. In 2018, a survey of over 2,500 construction firms conducted by the Associated General Contractors of America found that 80% of firms had a difficult time filling open positions [3]. This issue is compounded by the construction sector having lower productivity gains in the last several years compared to other sectors of the economy [4]. Lastly, the construction sector needs to improve energy efficiency in the built environment to slow the effects of climate change.

3D-printing has several benefits that can address these issues. The key benefit to the technology is reducing the cost and labor. The cost to build a 3D-printed structure is around 50-75% less compared to traditional construction methods on a cost per square foot basis [5]. The time during construction is also reduced, ranging from a couple of days to a couple of weeks depending on the project size. Other notable benefits of 3D-printed construction include reducing waste during construction, limiting human error on the construction site, and enabling complex building forms to be built without financial penalty. The major barriers towards widespread market adoption include rewriting building codes and standards with guidance for 3D-printing, scaling the printer design to construct larger buildings, and creating demand within the general public. There has been a lot of progress to meet these challenges with the use of concrete as the primary feedstock material.

One of the first attempts to use 3D-printing for full scale construction was contour crafting and primarily utilized concrete. The process used a gantry style printer design that could build the walls layer by layer while incorporating an additional crane to place supports for windows and doors [6].

Concrete has since become a popular feedstock material to use in 3D-printed construction. Some of the benefits with concrete include being easily extruded during the printing process and having a high mechanical strength when fully cured. As a result, there are several startup companies that are currently using concrete and have successfully completed demonstration projects.

While concrete is a popular material for 3D-printing, it has some drawbacks when it comes to energy intensity. Concrete has a high volumetric embodied energy value compared to other common building materials because of the 2,700°F temperature required during the manufacturing process, making it very difficult to produce without the use of fossil fuels [7]. Another issue with concrete is that it is not as insulative as other common construction materials. In 2018, one of the first demonstration projects attempted in the US to create affordable housing was not able to meet the local energy codes [8]. However, the company was able to get an exemption in order to obtain an occupancy permit for the project. This is concerning because if regulators allow energy codes to be ignored in order to promote this new construction method, 3D-printed houses could become more energy intensive to run than the current building stock. A numerical study evaluating the energy performance of 3D printed concrete walls found that most configurations analyzed do not meet standard regulations, with the average insulation rating of  $RSI-1.38 \text{ m}^2 \cdot \text{K}/\text{W}$  ( $R-9.09 \text{ Hr} \cdot \text{ft}^2 \cdot \text{F}/\text{Btu}$ ) [9]. Commercial and residential buildings currently consume around 40% of the total energy produced in the United States [10]. There is a growing demand for buildings to become more energy efficient in order to slow down the rate of carbon dioxide being released into the atmosphere. To meet these needs, concrete printed structures require additional envelope design considerations including added insulation, and computational analysis to ensure the envelopes meet energy codes [11].

With these limitations of concrete, other feedstock materials for printing buildings are being explored. One novel material is a recycled wood-based composite. This could retain the benefits of utilizing 3D-printed construction discussed above and could reduce the energy required compared to concrete.

This study characterizes the thermal properties of this wood-based 3D-printable feedstock material. This work includes the development of a low cost guarded hot plate apparatus that measures thermal conductivity, and compares the results using a transient probe experimental approach. These results are then used to predict the resultant life cycle energy performance for a full exterior wall envelope using this novel material compared to other common building envelopes available on the market.

## 1.2 Thermal Conductivity and Wood Products

The thermal envelope plays a large role in determining the energy usage within buildings. Highly efficient building envelopes were found to save above 30% of the total building energy usage compared to a minimum code compliant envelope [12]. The International Energy Conservation Code sets a minimum insulation resistance of RSI-3.52 (R-20) for a single family residence in climate zone 5B [13]. As a result, improving envelope design and effectiveness is one major tool that can be used to meet the goal of decarbonization within the built environment.

Discontinuities can occur in a building envelope because of structural needs. This can lead to thermal bridging that transfers heat more easily through a given part of the envelope. The overall effects of thermal bridging have been found to increase the heat loss by 9% [14]. This can be visualized in the wood framed wall shown in Figure 1. The image shows that the heat flux is higher through the wood studs than the insulation with the outside temperature set at  $-18^{\circ}\text{C}$  and the interior temperature set at  $21^{\circ}\text{C}$ .

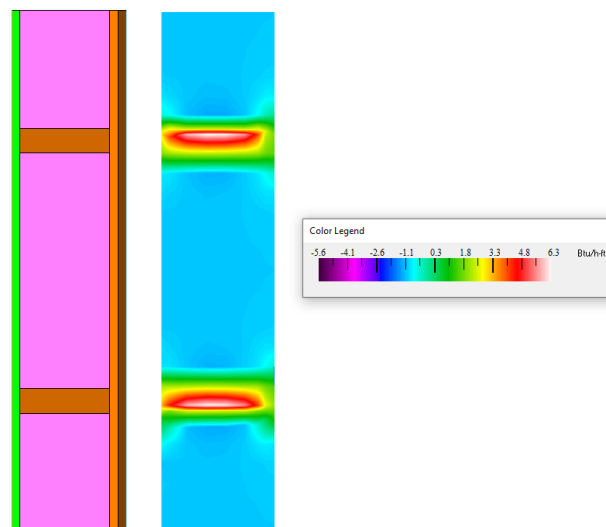


Figure 1. Example of thermal bridging in a wood framed envelope. [15]

A promising opportunity with 3D-printing assemblies is the ability to create custom geometric envelope systems that can limit thermal bridging. This has the potential for optimization of the structural matrix, which could further reduce energy consumption.

To begin this work, the thermal properties of the materials used in the envelope system need to be understood. This can be determined by utilizing the thermal conductivity of each material in the assembly. Thermal conductivity is a material property that relates the rate of heat transfer through a given material at a set temperature differential. This indicates how effective the material is at

transferring heat. The goal of insulation is to isolate heat loss or heat gain in a building; therefore, a lower thermal conductivity value indicates better performing materials.

Thermal conductivity measurements are normally given for homogenous and isotropic materials, where heat flows evenly throughout a material. Solid wood is an anisotropic material because of the grain structure from the fibers in the wood. This results in heat transferring around 1.8 times more easily along the grain direction as oppose to across the grain [16]. However, grain direction is not a major consideration when characterizing wood products. The primary reason is the wood grain structure is broken down into small particles and combined together with an adhesive, resulting in an isotropic material. The thermal conductivity of woods normally falls in the range of 0.08-0.18 W/mK [16]. This largely depends on the variety of wood tested, density, and moisture content.

In a typical residential or light commercial building, it is common to use wood panels as part of the envelope system. Engineered wood-based composites combine wood materials and additives resulting in improved structural strength, and better moisture and fire-resistant properties. Wood composites are usually made with wood fibers of varying sizes and binding resin. Typical wood composites in construction include medium density fiberboard, plywood, and oriented strand board [16]. The adhesives typically used in these panels are formaldehyde-based resins including phenol-formaldehyde, urea formaldehyde, and melamine formaldehyde. The different combinations of particle size, additives, and manufacturing process can affect the overall thermal properties of the end product [17]. The formaldehyde-based resins can also cause negative health effects in humans by off-gassing into the indoor environment once installed. As a result, these resins are highly regulated [18].

There are other characteristics that affect the thermal conductivity specifically within wood panels. The first property is the density of the panels [16]. Lower density wood panels have more air voids within the material, which causes higher thermal resistance compared to the solid wood [19]. Another common factor that affects wood is the moisture content. The thermal conductivity of wood products increases and becomes less insulative as the moisture content increases. Other studies have determined correlations based on the specific wood product and each of these parameters [16], [20]. As a result, sample conditioning of the wood needs to be taken into consideration before the thermal experiment begins in order to achieve repeatable results.

The specific thermal conductivity for each type of wood panel product can be seen in Table 1 below:

Table 1. Thermal conductivity of common wood products.

Material	Thermal Conductivity (W/m*K)
Plywood [21]	0.11-0.15
OSB [22]	0.13
Medium density fiberboard [20]	0.09-0.14

## Chapter 2: Thermal Testing of Novel Wood Composite

### 2.1 Transient Needle Probe

#### 2.1.1 Transient Needle Probe Introduction

The transient needle probe is one of several experimental methods that can measure thermal conductivity. This method utilizes the derivation of the heat equation based on the transient line source method with a continuous line heat source boundary condition [23]. This testing method works by inserting a needle with an embedded heating element and a temperature sensor into the sample material. The probe measures the change in temperature with a known power input applied to the heating element. Transient methods of testing thermal conductivity can capture the effects of high moisture content within a specimen and generally require less material and less time compared to steady state methods. The theory behind the method is discussed within the operational manual and associated literature [24], [25]. The end-use governing equation used to determine the thermal conductivity is shown in equation 1.

$$K = \frac{Q}{4\pi} * \frac{\ln(t) - \gamma - 1}{\Delta T} \quad (1)$$

Where K is the thermal conductivity (W/mK), Q is the heat applied to the line source (W), t is the time (s),  $\Delta T$  is the change in temperature ( $^{\circ}\text{C}$ ), and  $\gamma$  is Euler's constant. For large values of time, the relationship between the natural logarithm of time and the change in temperature can be found through a linear regression of recorded data. The three main assumptions for this method are as follows: the needle is sufficiently long enough to be treated as an infinitely long heating source, the sample is both homogenous and isotropic, and the sample and the probe have the same starting temperature at the beginning of the experiment.

The thermal probe, shown in Figure 2, is primarily used by geologists to measure thermal conductivity in soil and soft rocks. This method has been standardized within ASTM standard D5334 [23]. Additional applications of this testing method include measuring insulation, food products, nuclear rods, and other materials with a high moisture content. The sensor used during the course of this research has a thermal conductivity range between 0.02-2 W/mK and has a rated accuracy of 5% when paired with a Campbell Scientific Datalogger. The sample should surround the thermal probe with at least 1.5 cm of material to ensure there are no edge effects on the heat flow through the material. In addition, thermal grease is recommended when working with hard, grainy material. While this method is not traditionally used to measure building materials, the relatively small sample size and the

purchase price for the equipment made it appealing for obtaining preliminary results for the 3D-printed material.

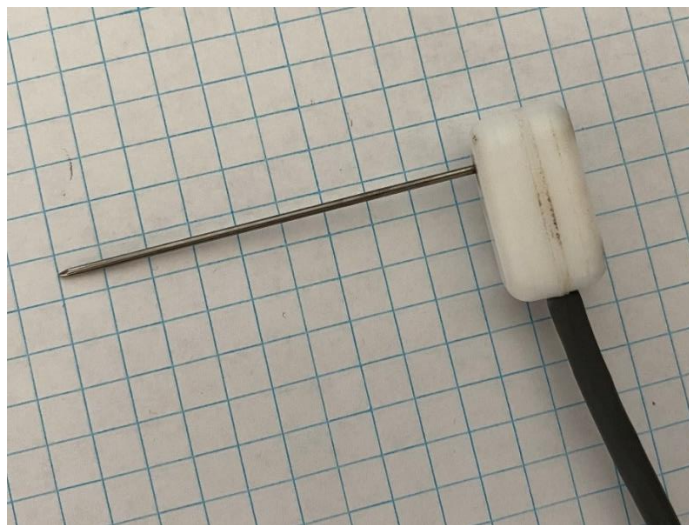


Figure 2. Transient needle probe sensor.

Before testing began on the 3D-printed wood composite, an initial calibration experiment utilizing cast acrylic was performed to verify the accuracy of the sensor. Cast acrylic was chosen as a primary reference material because of the close thermal conductivity value in relation to wood. The National Physical Laboratory proposed cast acrylic as a possible standard reference material [26]. In one study, researchers were able to characterize cast acrylic using a transient hot wire method in conjunction with a finite-element model that resulted in a standard deviation of 0.09% [27]. Other references are in close agreement with this research, although larger uncertainties were found between testing laboratories, resulting in a uncertainty range from 4% to 13% with contact resistance being the most likely cause for this uncertainty [28], [29]. Nonetheless, the close range and consistent measurements makes cast acrylic an ideal candidate to verify the experimental testing within this research.

The experimental procedure using the cast acrylic samples consisted of the following steps. A 30 mm diameter cast acrylic rod was purchased from McMaster-Carr. The rod was cut into two 75 mm long rods. Once cut, the samples were placed into a milling machine and a #55 drill was used to pre-drill a hole in the center of the rods, shown in Figure 3a.

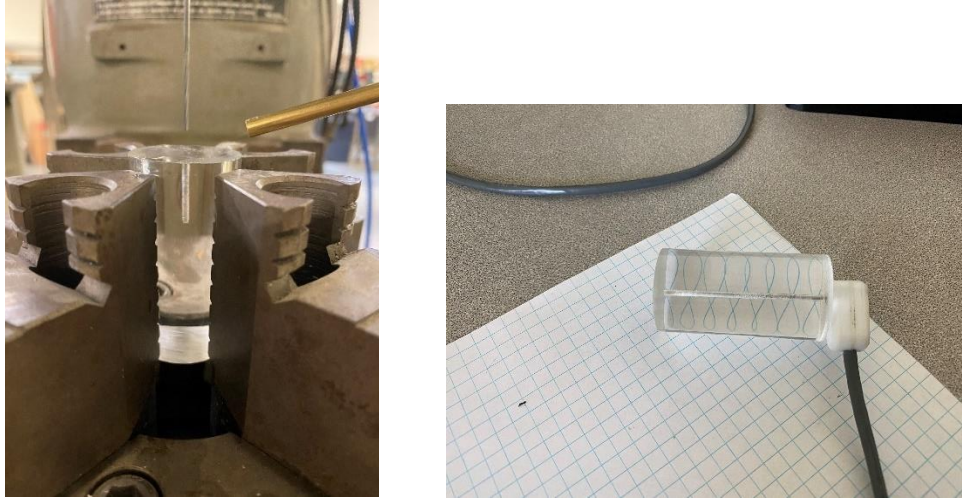


Figure 3. (a) Drilling hole into test sample (left) (b) sample during experimental testing (right).

Once the hole was drilled, it was filled with thermal grease as directed in the manual. Afterwards, the needle probe was inserted into the hole and a waiting period of 15 minutes was observed to let the temperature equalize between the needle and the sample, shown in Figure 3b. The preprogrammed experiment was run two times. The results from the calibration testing can be seen in Figure 4. The results demonstrated that the transient method worked well in estimating the thermal conductivity within this sample and can produce satisfactory results for the 3D-printed composite material.

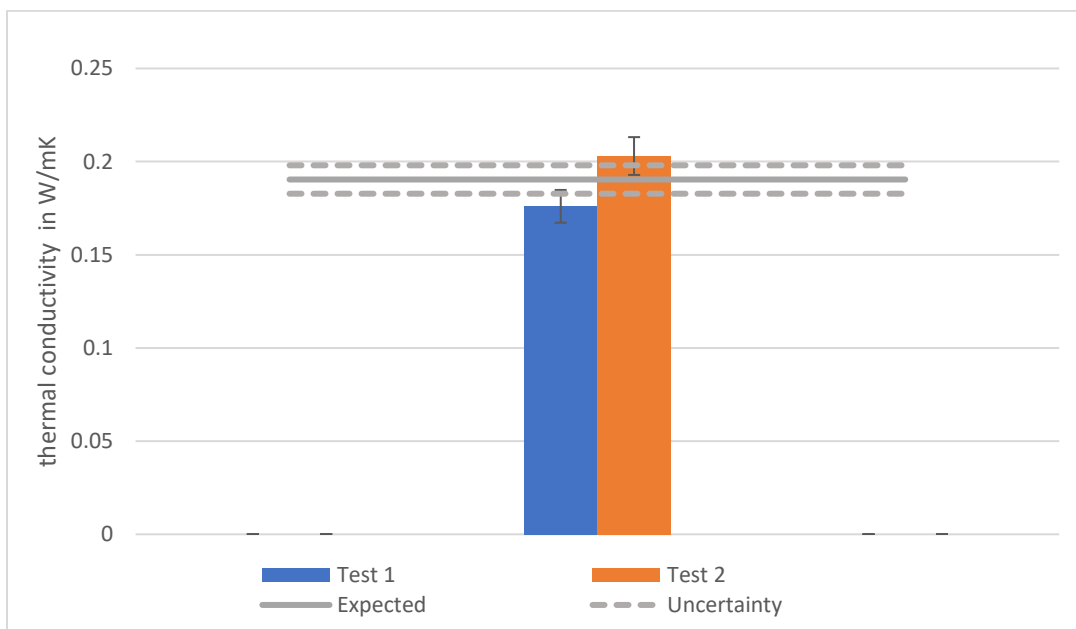


Figure 4. Results from needle probe verification experiment.



### 2.1.2 Transient Needle Probe Methods

With the transient needle probe apparatus working properly, the thermal testing with the 3D-printed wood composite began. Since the manufacturing process can affect thermal conductivity in wood products, a detailed description of the sample preparation is provided in the paragraphs below.

The 3D-printed wood material is primarily composed of waste wood chips and sodium silicate. The wood chips were sourced from Plummer Forest Products, Post Falls, ID, and the samples were prepared in Moscow, ID. Two wood particle sizes were prepared. The first particle size was less than 0.425 mm and was obtained by using a mill and a 40-mesh sieve, which is ten times larger than those used in medium density fiberboard [30], [31]. The other particle size was unchanged from the provided wood chips. The binding material used for the 3D-printed process is sodium silicate ( $\text{Na}_2\text{O}_3\text{Si}$ ) sourced from Thermo Fisher Scientific, Carlsbad, CA. The binder is in solution with water with a weight ratio of 37% sodium silicate and 63% water.

The 40-mesh wood particle size and the sodium silicate were mixed together using a food processor in weight ratios of 50:50, 60:40 and 70:30 respectively. The whole wood particles were also combined with sodium silicate to produce samples with 50:50 and 60:40 compositions. Once the samples were mixed together, they were placed into a circular press. The samples were then cured in a 100 °C drying oven until the water in the sodium silicate solution evaporated. Once this process was complete, the samples were placed into airtight bags and shipped to Boise for the thermal testing. The mass and density properties for each sample can be seen in Table 2.

Table 2. Density properties of samples on arrival.

Composition (Wood wt% : Binder wt%) and Number		Mass (g)	Thickness (in)	Density (g/cm <sup>3</sup> )
< 40 mesh Wood / SS				
50:50	1	39.8	0.583	0.589
	2	33.7	0.466	0.624
	3	45.0	0.604	0.643
60:40	1	36.3	0.776	0.404
	2	34.6	0.621	0.481
	3	25.9	0.398	0.562
70:30	1	13.7	0.257	0.460
	2	37.8	0.792	0.412
	3	40.5	0.757	0.462
Whole wood / SS				
50:50	1	49.5	0.716	0.589
	2	73.0	0.993	0.635
60:40	1	35.9	0.531	0.584
	2	44.0	0.740	0.513

One of the limitations with the transient probe apparatus is the required sample size. The apparatus requires 15 mm of material around the probe in order to avoid errors with the experiment [24]. To address this issue, additional preparation was performed. The samples for each composition were combined into one continuous puck. Sodium silicate was used to bond each composition type together and was generously spread between the surfaces. Once the adhesive was applied, the samples were again placed into a 100°C drying oven to cure with an applied pressure from a 5-pound metal plate. This process is shown in Figure 5.



Figure 5. Needle probe oven drying setup.

To check if the drying process is complete, the weight of each sample was measured at 12-hour intervals until the weight stayed consistent. Each of the samples took 24 hours to cure. The density of the sample was determined after the drying oven process was complete. Next, a pilot hole was drilled into the sample using a #55 drill bit and a mill. Afterwards, the samples were stored in an airtight bag until thermal testing began.

The steps for the thermal testing are as follows: thermal grease was inserted into the pilot hole to ensure good thermal contact between the probe and the sample, as recommended by East 30 Sensors [24]. A waiting period of 15 minutes was observed afterwards to ensure that the temperature between the probe and the sample could equalize. Finally, the preprogramed experiment ran for one minute. These steps were repeated five separate times with at least one hour between heating cycles. Between the second and fourth experiment, the thermal probe was removed from the sample and reinserted with additional thermal grease. After each experiment, the moisture content of the sample was measured with a MT270 digital moisture meter manufactured by Tavoil. These readings showed that the moisture content was less than 1%. This ensured that the thermal conductivity corresponded with a dry measurement as intended for this experiment. An image of the experiment setup is shown in Figure 6.



Figure 6. Image of sample during experiment.

### 2.1.3 Transient Needle Probe Results

During the testing process, The 70:30 composition samples shed wood particles around the circular edge of the material. This occurred during normal handling and can be seen in Figure 7.

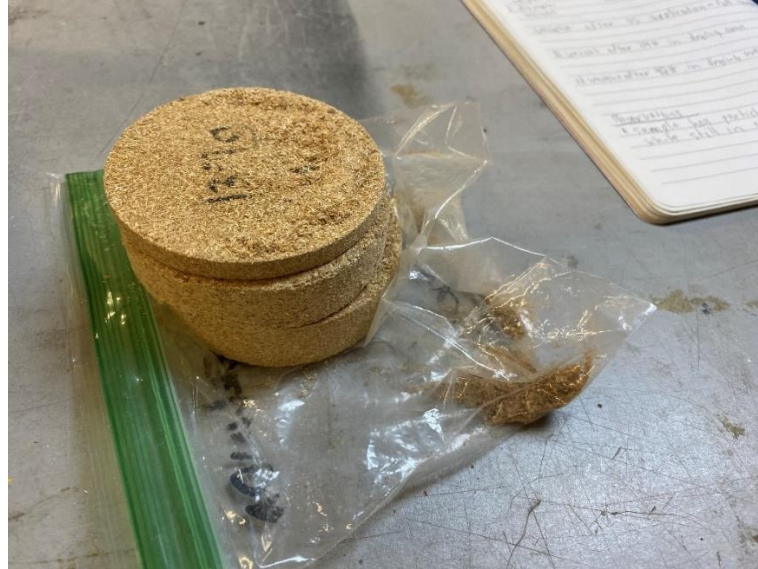


Figure 7. Observation of flaking during the experimental process.

The shedding is likely caused by not using enough binding material within the composition. As a result, this composition will likely not have the required mechanical strength for the wall assembly. The summary table for all of the experimental data is shown in Table 3 and a sample of the full experimental results from the 50:50 wood mesh composition is shown in Figure 8. The rest of the experimental results can be found in Appendix A.

Table 3: Summary of transient needle probe experiments by composition.

Sample Composition	Binder Weight Percentage	Density (kg/m <sup>3</sup> )	Average Thermal Conductivity (W/m*K)	Uncertainty Range (W/m*K)
70:30 40-Wood Mesh	30%	456	0.081	± 0.004
60:40 40-Wood Mesh	40%	537	0.104	± 0.005
50:50 40-Wood Mesh	50%	655	0.146	± 0.007
60:40 full-Wood Mesh	40%	553	0.118	± 0.006
50:50 full-Wood Mesh	50%	651	0.141	± 0.007

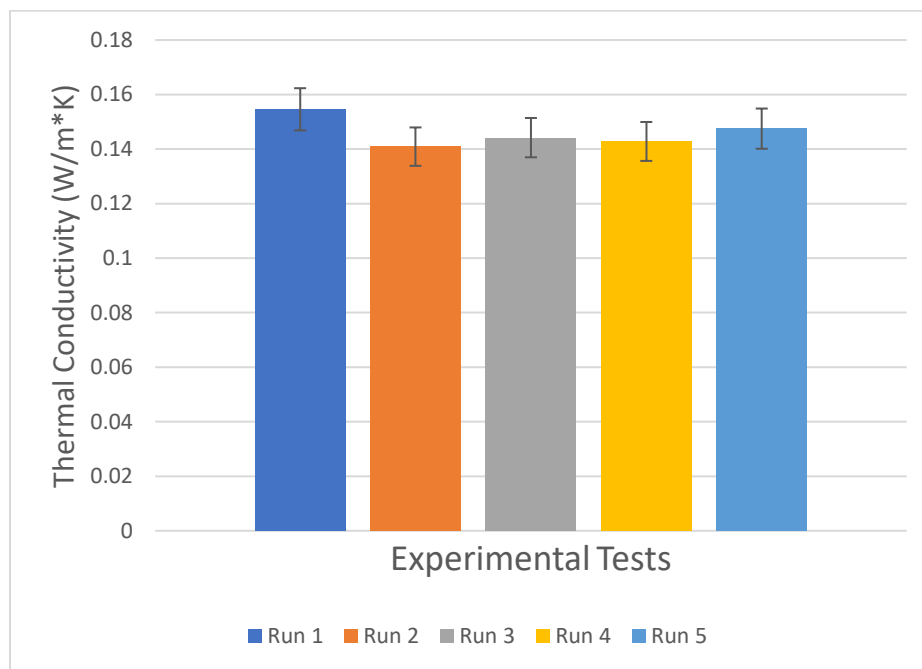


Figure 8. Transient needle probe experimental trials for the 50:50 40-mesh sample.

The results from the experiments are very consistent between each of the trial runs and fall within the stated uncertainty of 5%. The thermal conductivity is shown to vary between 0.081 and 0.141 W/mK across the compositions. This is caused by the change in the density. This is a well-documented correlation within the literature for other engineered wood products [16], [20], [32]. The following graphs show the strength of the correlation between the density and the thermal conductivity within the

samples tested (Figure 9) and compares this relationship to other common wood products used in the construction industry (Figure 10).

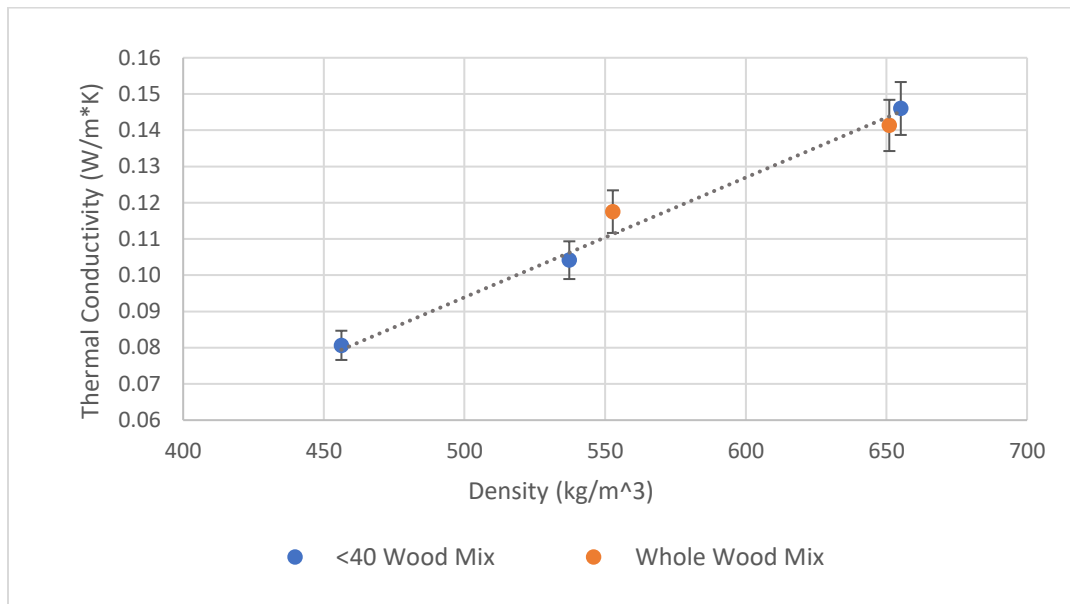


Figure 9. Thermal conductivity of 3D-print wood composition vs density.

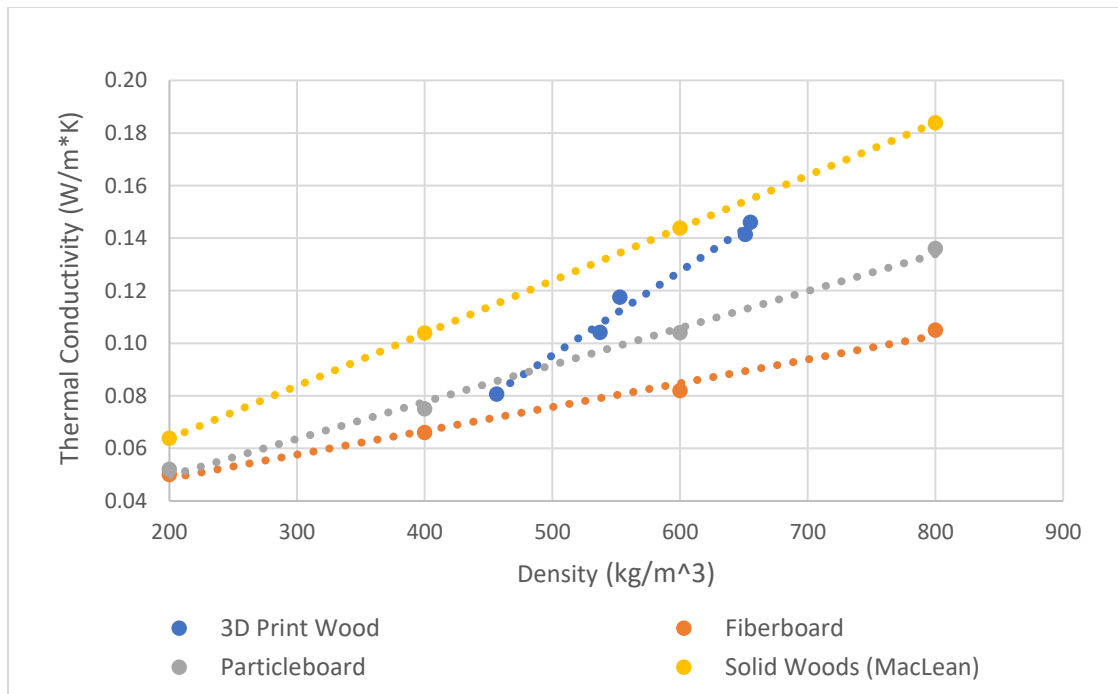


Figure 10. Comparison of the thermal conductivity – density correlation of the 3D-printed composite (blue), particleboard (grey), fiberboard (orange), and the MacLean model for solid wood (yellow) [20].

As Figure 9 shows, the difference in particle size between the whole wood and the 40 mesh samples doesn't have a significant effect on the density vs conductivity correlation. This is most likely due to only utilizing one binding resin. The composition weight percentages could also be a factor. The mixtures used for testing varied from 30-50% by weight compared to the 6% typically found with formaldehyde-based resin composites. This extra binding material could fill in the small air pockets and effectively reduce the particle size effect on thermal conductivity.

Figure 10 shows the correlation has a similar trend compared to other wood products. The slope of this line is greater than the slopes found in other wood-based composites. This can be attributed to the different binding material used within the process. The traditional phenol formaldehyde resin has a lower thermal conductivity value (0.2 W/mK [33]) compared to the sodium silicate resin used in the 3D-printed composite (1.1 W/mK [34]).

Further discussion of these results and a comparison to another testing method can be found in section 2.2.3.



## 2.2 Guarded Hot Plate Apparatus

### 2.2.1 Development of a Low Cost Guarded Hot Plate Apparatus

While the results from the transient needle probe method appear to be conclusive, the thermal testing procedure is not widely recognized within building codes and standards. A more conventional testing setup based on the ASTM C177 guarded hot plate apparatus is therefore needed to verify previous testing results and better position the material for energy code adoption. While a normal guarded hot plate apparatus is one of the most accurate methods to measure thermal conductivity, the commercial price for these starts in the range of \$22,000-32,000 and was beyond the current project's budget. With the advancement of consumer electronics offering highly accurate sensors at an affordable price point, the team decided to design and build a low cost guarded hot plate using consumer grade electronics. The presented work details the design requirements, development, and overall performance for this apparatus.

The ASTM C177 standard is a direct measurement method to quantify the thermal conductivity for homogenous materials. This is the preferred method because it can achieve highly accurate results and doesn't rely on external calibration to a reference material. This standard covers a wide array of apparatus designs, testing and operating conditions, but is generally used to measure relatively insulative materials under 16 W/mK.

The testing method for a single specimen sample consists of creating a hot and cold isothermal surface on each side of the material, which induces a heat flux through the sample. The thermal conductivity can then be calculated using Fourier's one-dimensional conduction heat transfer equation:

$$K = \frac{QL}{A\Delta T} \quad (2)$$

Where Q is the heat flux (W), L is the sample's thickness (m), A is the cross-sectional area of the sample (m<sup>2</sup>), and ΔT is the temperature difference between the isothermal layers (C).

While the theory is relatively straightforward, the implementation of this apparatus can be difficult to achieve [35]. One of the major sources of error is edge heat loss. This effect can be mitigated by implementing auxiliary heating plates, known as heat guards, and adding insulation on the sides of the material. This helps direct the heat flow through the material instead of around it. The next issue with the guarded hot plate is the length of time needed to achieve a steady state temperature. A long

exposure time to a high temperature could change the material or chemical properties of a sample. Moisture content can also affect the thermal properties of wood-based composites, and has been well documented within literature [16], [17], [19], [20]. The last potential source of error is contact resistance between the isothermal plates and the sample. If not addressed, this could result in an under-estimation of the thermal conductivity. Table 4 summarizes the design requirements for a guarded hot plate given by ASTM C177.

Table 4. Design requirements from ASTM C177 [35].

Section Number	Design Requirement Description
6.3.1.1	Surface plainness departure from the plane should be 0.025% of the linear dimensions
6.3.1.2	The difference in temperature between the guarded plate and the metered plate should be less than 0.2 K
6.3.1.3	The surface of the plate should be a high emittance surface
6.4	The metered section and the primary guard should be separated by a gap and the area of the gap should be less than 5% of the area of the metered section
6.6	Testing temperature should be close to room temperature to limit edge heat losses
6.7	A clamping force should be used to ensure good contact between the sample and hot and cold plates
6.8.1	A temperature imbalance detector should be used to ensure temperature difference between guard and metered section are within requirement 6.3.1.2
6.8.2.3	Thermocouples should be mounted into grooves in the surface plate
6.8.2.5	The number of temperature sensors in the metered section should be greater than 2
6.9	Thickness measurement should be within 0.5%
6.11(a)	Accuracy of the temperature measurement should be within 0.1 K.
6.11(b)	Accuracy of the metered power should be within 0.2%

## Design of Apparatus

The apparatus was designed to test an 200 mm square sample with varying thicknesses between 6.5 to 50 mm, as seen in Figure 11. The apparatus is designed for easy fabrication and assembly by using aluminum stock and commonly found machine fasteners. The apparatus is composed of three main assemblies: the hot plate assembly, the cold plate assembly, and the electronic controls and sensors. The full plans for the apparatus including machining diagrams, software program, and bill of materials can be found in Appendix B.

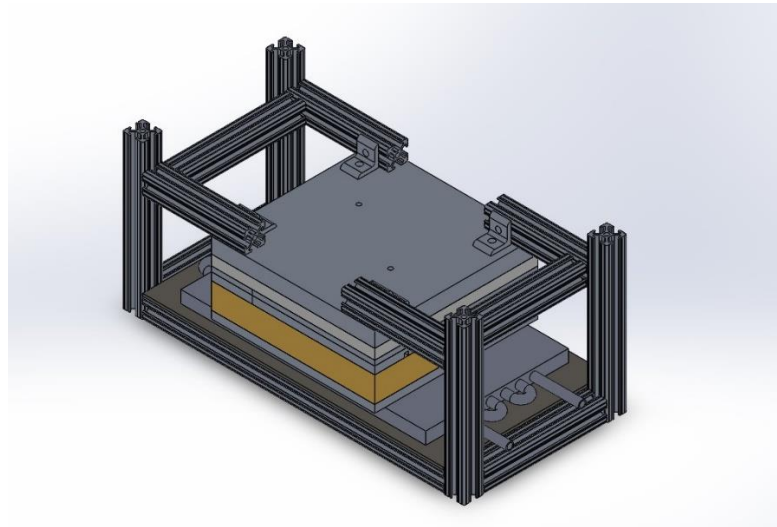


Figure 11. Rendering of guarded hot plate apparatus.

The hot plate shown in Figure 12 consists of five separate resistive heating pads that are sandwiched in between two 6061 aluminum plates (1). Aluminum was chosen because of the ability to evenly distribute the heat from the heating pads onto the top surface of the sample material. The aluminum plates are configured into one central heating plate (2) and four exterior guard plates (3). There is an intentional gap between the central plate and the guard plate (4) to isolate the lateral heat transfer across the surface and direct the heat flow to move one directionally through the sample material. The heating plates are connected via screws to a top connection plate (5) and are separated by a layer of insulation (6). The specific dimensions of the center and guard plates were designed to meet requirement 6.4. The weight of the top assembly produces around 0.95 kPa of pressure on the sample material, satisfying requirement 6.7.

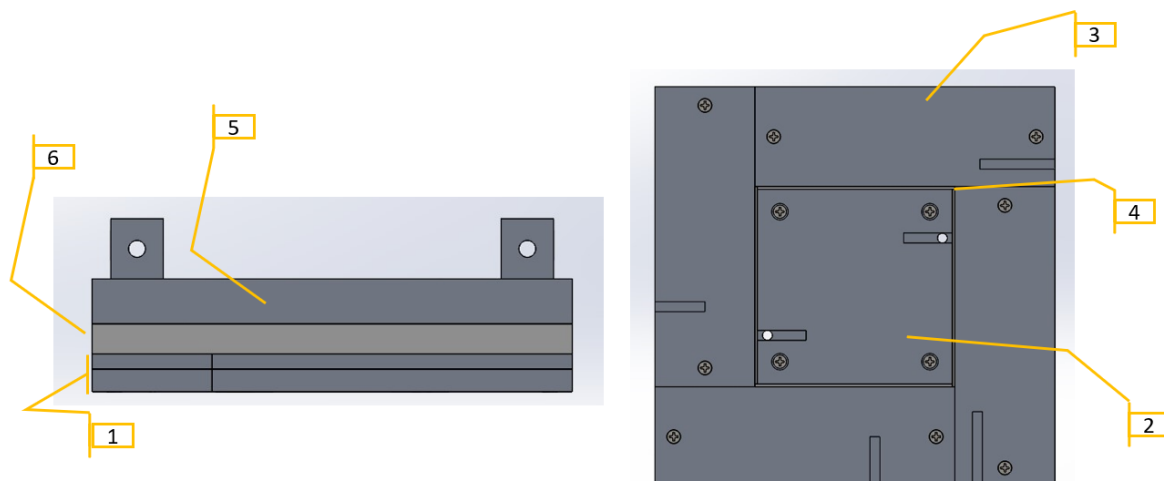


Figure 12. Side (left) and bottom (right) side of the hot plate assembly.

The cold plate assembly consists of a 200 mm square aluminum plate (6061), a 6-pass water cooled heat sink, and a constant temperature water bath made by Cole-Parmer. The water bath can maintain a constant temperature within 0.1°C. The aluminum cold plate is in direct contact with the heat sink to maintain a constant cold temperature at the bottom of the sample. The assembly is shown in Figure 13

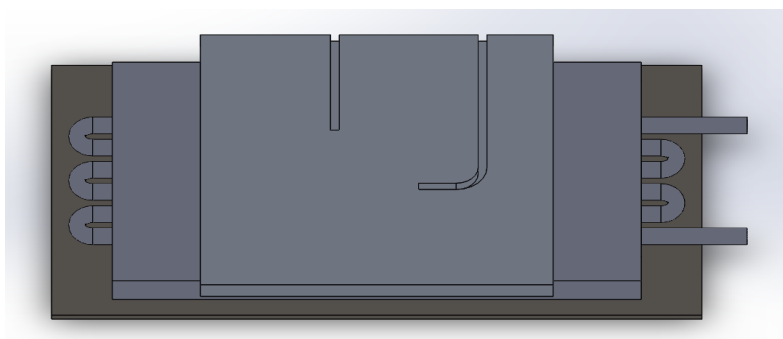


Figure 13. Cold plate assembly.

The electronics utilize a variety of different sensors and breakout boards. There are seven different temperature sensors on the apparatus with two sensors being on both the center hot plate and cold plate, and one sensor on each of the guard plates, meeting requirement 6.8.2.5. The locations of the sensor are denoted by the green dots shown in Figure 14.

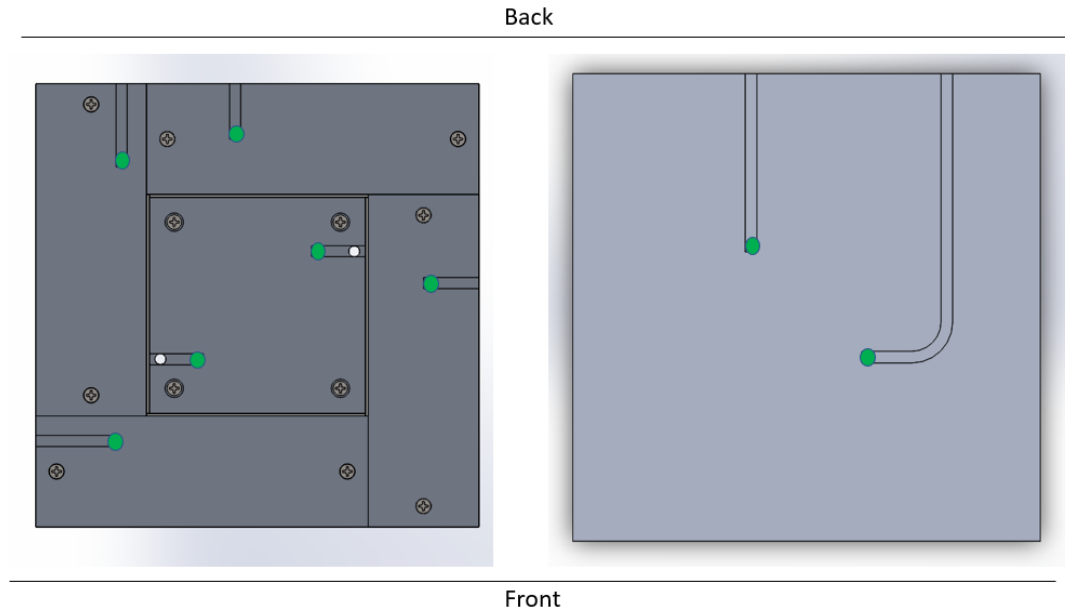


Figure 14. Temperature sensor location in hot (left) and cold (right) plate assembly.

Normally, thermocouples are used to measure temperature on the samples surface. However, this design uses Dallas DS18B20 digital temperature sensors, which offers a resolution of  $0.0625^{\circ}\text{C}$ . The temperature sensors in the center plate and the cold plate were calibrated to a NIST-certified RTD temperature sensor accurate to  $0.01^{\circ}\text{C}$ . The temperature sensors were placed directly onto the water-cooled heat sink and were surrounded by extruded polystyrene insulation. Once the heat sink reached the desired temperature, the calibration period began. Each calibration period lasted around 15 minutes with a 30-second sampling rate from both sensors. This was repeated for temperatures ranging from  $15\text{-}35^{\circ}\text{C}$  with a  $3^{\circ}\text{C}$  increment. After the calibration tests were completed, an evenly distributed 7-point calibration curve was utilized to calibrate the sensors as seen below in Figure 15. An analysis of the standard error from the calibration curve found that the requirement 6.11(a) was satisfied, having a standard error less than  $0.1^{\circ}\text{C}$  for each sensor.

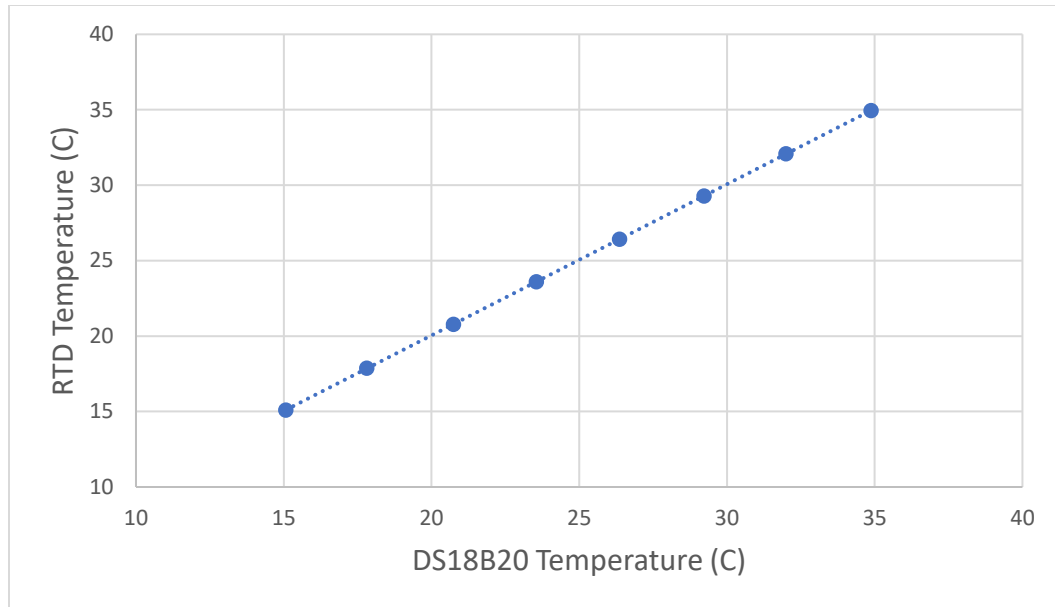


Figure 15. Calibration curve for a temperature sensor.

Once the temperature sensors were calibrated, they were connected to the machined grooves on the hot and cold plate. The hot plate assembly was then assembled, and the control sequence began development. Five low side N-channel MOSFET transistors were used in conjunction with a PI control sequence to reach and maintain a desired temperature in the guard and center plates

At this point in the development process, a reference material was used to help verify the apparatus' performance. Cast acrylic was chosen as the reference material because it had a similar thermal conductivity range as wood products [27], [28], [29]. The thickness of the cast acrylic sample was measured with calipers accurate to within 0.01 mm at each of the four corners of the sample, satisfying requirement 6.9. The ambient temperature was measured in the room and the hot and cold plate temperatures were set with the mean temperature equaling the ambient temperature, in accordance with requirement 6.6. The final step in the setup was to surround the apparatus in EPS insulation to limit the heat loss through the sides and top of the apparatus.

Once the experimental setup was complete, a sample trial run was performed to verify temperature stability of the hot plate. The results showed the temperature of each plate stayed within the 0.2°C requirements of 6.3.1.2. as shown in Figure 16. A detection algorithm was also programmed to alert the operator if a temperature imbalance within the hot and cold plate occurred during the steady-state duration of the test. The detection algorithm satisfies requirement 6.3.1.2.

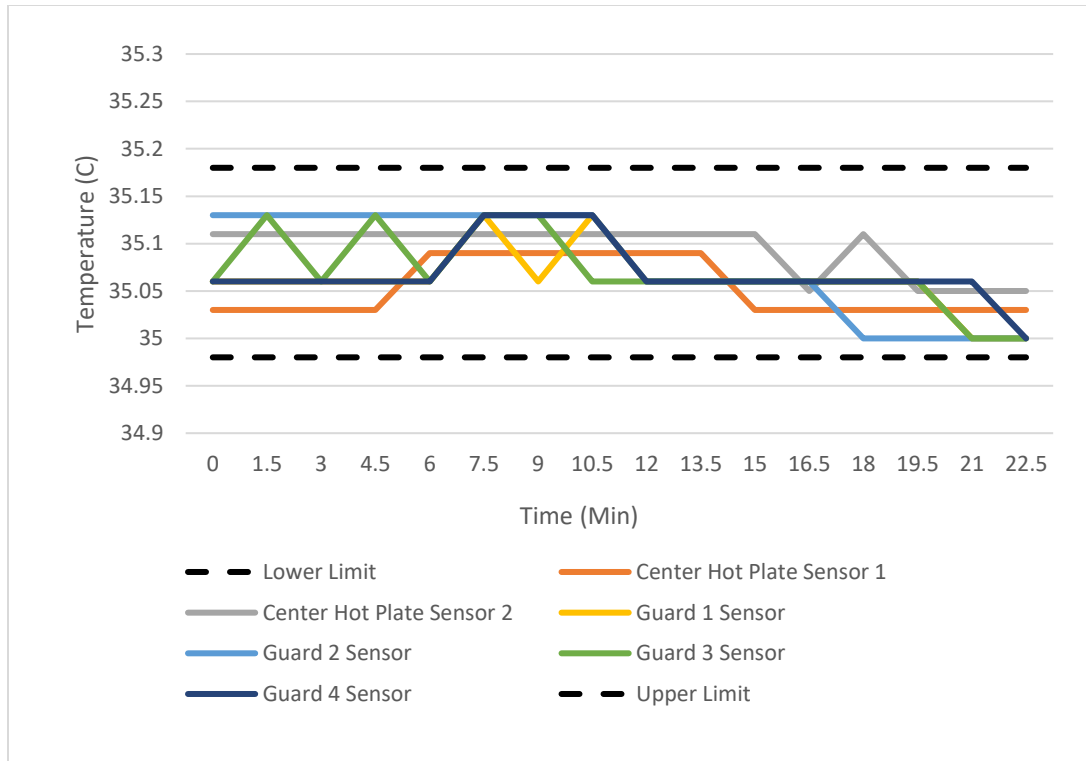


Figure 16. Results from temperature stability test at steady state.

While the temperature stability met the consistency requirement, the applied power to the center and guard heaters oscillated throughout the experiment to maintain the temperatures of the hot plates. To achieve a steadier heating setting during the steady state stage, while still limiting the warmup time, a two-stage PI control sequence was programmed into the microcontroller. The first stage is designed to quickly get the temperature of the hot plate to the desired temperature for the experiment. Once the temperature gets close, the second stage in the PI sequence is activated, which slows down the responsiveness of the system to provide a steadier power supply to the heaters. With additional experiments, the oscillating power output was reduced and remained fairly constant. Despite the steady controls implemented, the calculation of thermal conductivity was producing a significantly low value for the thermal conductivity and was around 90% lower than the expected value.

A parametric analysis was used to find the source of this error and applied to each parameter in equation 2. The analysis initially showed that the thickness of the sample, area of the center plate and the temperature readings were very unlikely sources of error. This left two possible sources of error: the thermal contact resistance and the power supplied to the central plate.

The first parameter troubleshot was thermal contact resistance. If there is not good contact between the hot and cold plates and the sample, excess contact resistance can occur. This can result in

a lower thermal conductivity reading and create a measurement bias in the apparatus. By comparing the calculated thermal contact resistance from the experiment to known values, thermal contact alone was unlikely to have produced the full error, requiring the thermal resistance to be two orders of magnitude higher than typically found. However, the resistance could have been caused by an air gap between the sample and the hot/cold plate. To eliminate the airgap between two materials, it is common to apply thermal grease. A follow-up experiment was performed with the addition of thermal grease between the aluminum plates and the cast acrylic. This experiment found that there was a marginal improvement of a couple percentage points and was not the main source of error. However, this did inspire a solution to deal with the upcoming roughness of the wood samples.

While adding a layer of thermal grease didn't solve the original problem, it addresses the issue of excess contact resistance that can come from measuring solid materials. However, a concern that arose for the wood samples is that the thermal grease could imbed itself within the pores of the wood because of the applied pressure, changing the thermal properties of the wood. A novel solution is to have a layer of thermal grease on the hot and cold plate with an additional layer of aluminum foil. This method merges both benefits of filling in the air gap without changing the properties of the wood samples. The effect of adding the thermal aluminum foil was studied with the cast acrylic sample. The measurement before and after the application indicated a negligible change in the measured thermal conductivity, as expected. With this unique solution in place, the purpose of requirement 6.3.1.1 to ensure good contact between the isothermal plates and the sample material was accomplished. The aluminum foil goes against requirement 6.3.1.3 and has a low emittance surface. However, the effect of a low emittance surface is small when working with plate temperatures that are close to room temperatures. For radiation heat transfer to be a primary mode of heat transfer, it requires a high temperature difference between the body and the surrounding.

Since the thermal contact wasn't found to be the source of error, attention shifted to the power parameter. Initially, the power was calculated by using the input voltage supplied to the apparatus, the resistance of the heating pad, and the duty cycle of the PWM signal. To verify that this method was accurate, two Fluke 117 multimeters were used to measure the voltage and current in the resistive heating pad to compare to the software measurements. Because the power supplied to the resistors was using PWM electrical signals, the true RMS setting was used to accurately measure power to the resistors. A difference between the two readings was found. By using the multimeters, the thermal conductivity values were providing more reasonable results that fell within 15-30% uncertainty. With this finding, additional electronic components were needed to obtain a more accurate power measurement.



The next iteration of the electronic components included the addition of two breakout boards and an RC filter. The first breakout board was a DC driver board acting as a high side switch for the circuit. The RC filter was needed to smooth out the PWM signal generated by the DC driver board. The last breakout board was an Adafruit INA260 current and voltage sensor board. This board can measure DC current and voltage to within 0.15% and 0.1% respectively, meeting requirement 6.11(b). Figure 17 shows the completed circuit diagram for the center plate. The original circuit was kept for the 4 guard plates because power measurements on the guard plates are not needed.

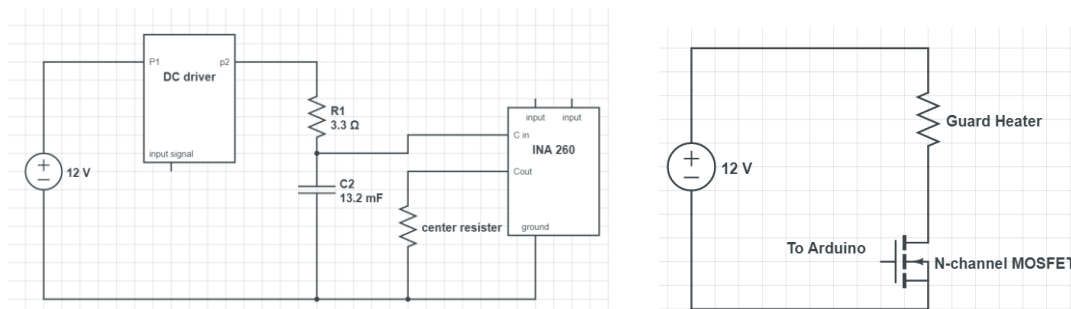


Figure 17. Circuit diagram for the center plate (left) and guard plate (right).

A couple of follow-up measurements were used to ensure accurate power readings. The first measurement used an oscilloscope to see the resultant voltage signal entering the center heating pad. The PWM signal was set to a 50% duty cycle for the test. An image of the waveform can be seen in Figure 18.

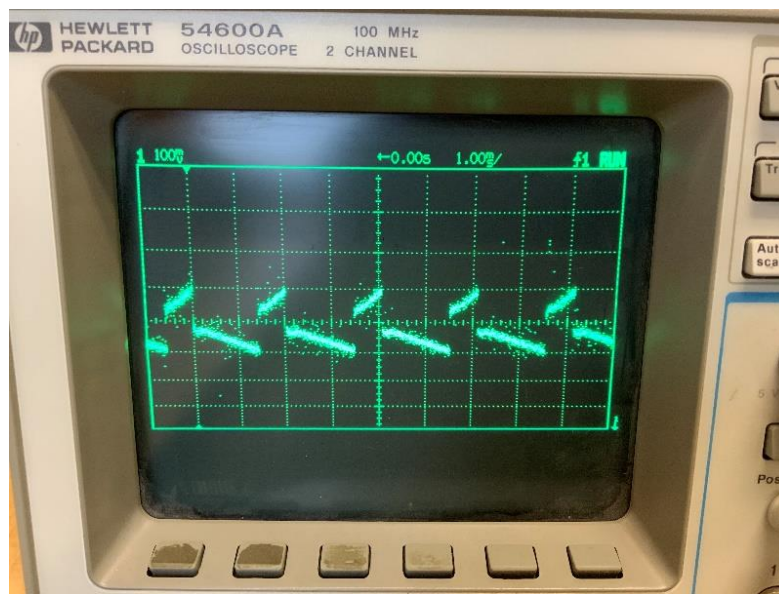


Figure 18. Voltage across central heating pad. Vertical division: 100 mV. Horizontal division: 1 ms.

The oscilloscope found a 20 mV variation peak to valley within the voltage supplied to the resistor. To account for the excess noise, a digital averaging filter built within the INA260 program library was also incorporated to further smooth out the wave. The second verification measurement used a calibrated Fluke 117 True RMS multimeter to verify both the current and voltage reading. The readings between the multimeter and the breakout board were within 0.005 V and 0.002 A respectively.

Once the revised power measurement system passed the verification process, cast acrylic samples were again used to further refine minor issues with the apparatus. At the end of the refinement period, the full verification trials for the apparatus began.

### Full Testing Verification

The full verification trial consisted of performing four independent experiments on three 200 mm square cast acrylic sheets with thicknesses of 6 mm, 12 mm, and 25 mm. The testing procedure remained the same as before. The thickness of the sample was measured with calipers at each of the four corners of the sample and averaged. The mean temperature in the room was measured before the experiment to set the temperature of the hot and cold plates. Finally, the cast acrylic samples were pre-conditioned to the testing chamber 12 hours before the experiment began. The summary of the results of the experiments can be seen in Figure 19.

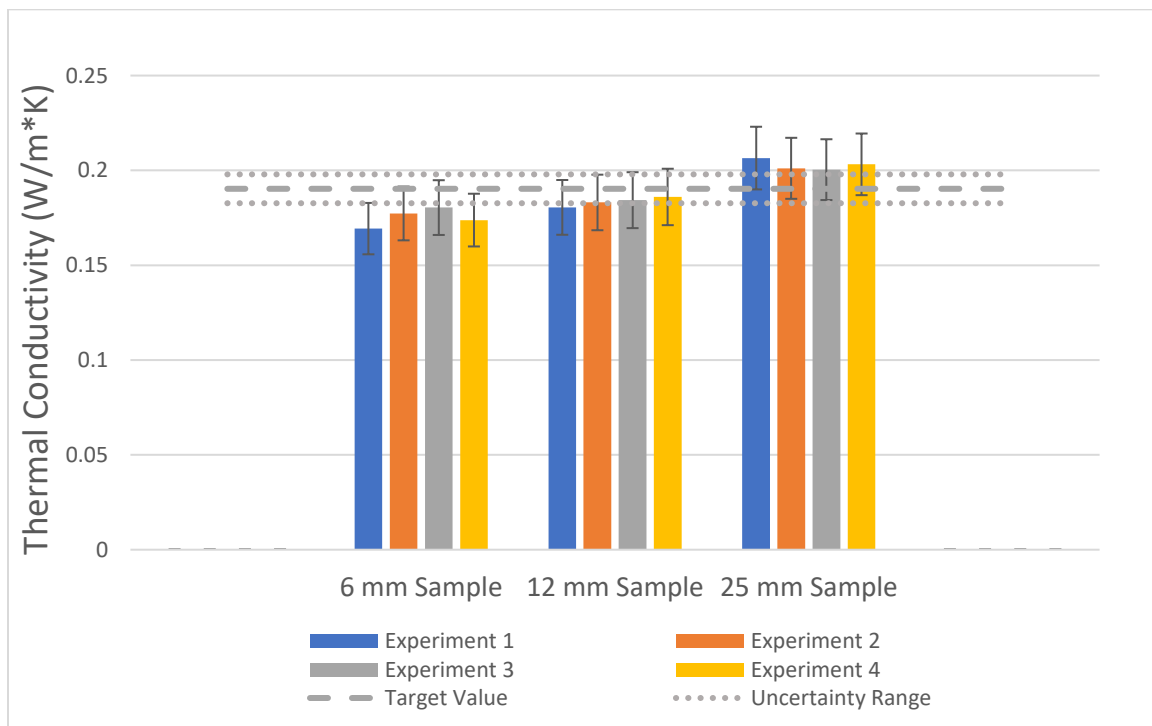


Figure 19. Guarded hot plate calibration testing results with cast acrylic samples.

The results found that the apparatus was successful in measuring the thermal conductivity when considering the combined uncertainty within the apparatus (shown as error bars) and the uncertainty in the calibration material (shown in the dotted grey line) [27], [28]. The 6 mm and the 12 mm sample appear to have very consistent results between each other, consistently measuring around 0.01 W/mK lower than the recognized value. This result in isolation would appear to have a systematic negative bias. However, the 25 mm sample does not seem to follow this trend. This difference could be attributed to a combination of several different factors.

The first factor could be a lower heat flux in the 25 mm sample. With a smaller heat flux, a higher percentage of heat produced by the heating pad could escape through the fitted insulation around the apparatus and subsequently cause a higher power reading. Another factor could be contact resistance between the plates and the 6 mm and 12 mm samples. The last factor is the variation in the thermal conductivity of the reference material. The results shown above is most likely a combination of each of these factors.

Initially, the 25 mm sample was tested under the same testing conditions as the 6 mm and 12 mm samples. It was found that during these tests, the measurement of thermal conductivity was about 12% higher than the expected value (not shown in Figure 19). During these tests, the power required to maintain the hot plate temperature was lower compared to the other tests, as expected. This lower power requirement could have made the power supplied to the hot plate more sensitive to edge heat losses in the sample. A follow-up test was performed on the 25 mm sample with a higher temperature difference between the hot and cold plates to attempt to reduce this sensitivity. The results of the modified experiment, showed in Figure 19, found an improvement over the previous experiments and demonstrated a need to have a minimum heat flux through the sample material to limit the excess heat loss to the surrounding environment.

Several different methods were used to analyze the sources of error. First, a 95% confidence interval was calculated using the 12 experiments. The interval appears to align well with the uncertainty range of the cast acrylic but is slightly lower. This result supports that the source of the error is within contact resistance; however, it is difficult to judge based on the limited data set used to generate the interval.



Figure 20. 95% confidence interval from calibration experiments.

To understand the uncertainty within each sample, a parametric uncertainty analysis was calculated. The uncertainty values used in the analysis are shown in Table 5.

Table 5. Uncertainty values for guarded hot plate apparatus

Parameter	Uncertainty value	Source
Area	$2.9 (10^{-3}) \text{ m}^2$	Measured uncertainty from calipers
Thickness	0.25 mm	Uncertainty of using calipers to measure thickness and sample thickness variation
Hot plate temperature	0.1 °C	Calibration uncertainty results
Cold plate temperature	0.1 °C	Calibration uncertainty results
Current	0.15% of reading	INA 260 spec sheet
Voltage	0.1% of reading	INA 260 spec sheet

One notable source of error involved the thickness measurement. For a given sample, the measured thickness could vary up to 0.25 mm between the four corners of the sample. This is larger than the precision of the calipers used to measure the thickness at around 0.01 mm. This larger variation was updated in the parametric analysis and increased the overall uncertainty in the thermal conductivity measurement. Table 6 shows the results of the parametric uncertainty analysis.

Table 6. Uncertainty across varying calibration materials.

Sample Thickness	Absolute Uncertainty (W/m*K)	Relative Uncertainty
6 mm acrylic	0.0076	4.07%
12 mm acrylic	0.0041	2.29%
25 mm acrylic	0.0027	1.35%

The other explanation for this discrepancy in results could be a natural variation within the cast acrylic material. The cast acrylic has an uncertainty rating of 4% [28], and different testing labs have found variations up to 13% [27]. When taking this into consideration with the apparatus parametric uncertainty, these values fall within the stated error range of the material.

Given the analysis of the apparatus performance, it was able to achieve an accuracy of around 8%. This number is based on the maximum discrepancy found during the testing and verification process detailed above. This number could improve with additional modifications to the apparatus.

In addition to the cast acrylic calibration, a OSB sample was also used to run a secondary verification experiment. The sample was preconditioned in the testing room and the same testing procedure as before was followed. The density of the OSB sample was calculated using dimensions measured with calipers and a mass scale. The results of this secondary verification can be found in Figure 21. The OSB sample was not chosen as a primary calibration material because of the wide variation in the thermal conductivity values, depending on the manufacturing method, density of the material and the specific additives used. The thermal conductivity measurement for OSB can range from 0.109-0.17 W/mK within literature, although a standard rating is assumed to be around 0.13 W/mK by industry [17], [22].

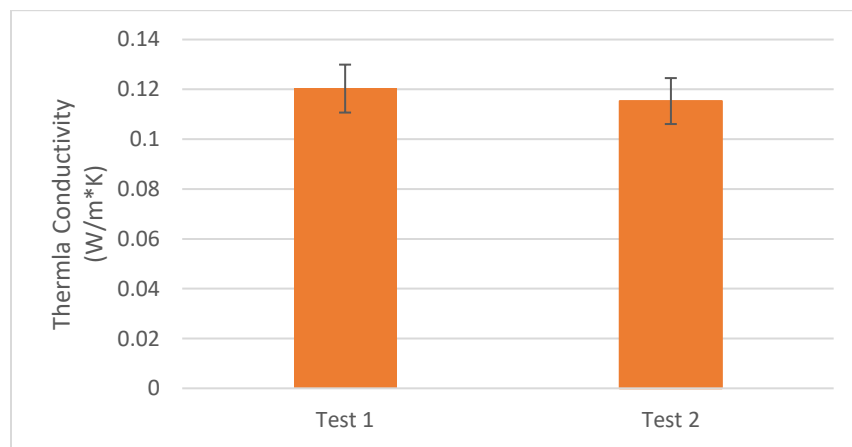


Figure 21. Thermal conductivity measurement of OSB sample

## Cost of Assembly

Below is the cost of all the material used to build the apparatus summarized into the major components. The most expensive piece of equipment required is the constant temperature water bath, accounting for about 80% of the total material cost. The fabrication of the different components for the apparatus took around 4 weeks to complete with the help of a university machine shop supervisor. A fully detailed bill of materials is available in Appendix B.

Table 7. Summary of material costs.

Hot plate assembly	\$93.80
Cold plate assembly	\$3,100.48
Framing	\$239.20
Electronics	\$220.62
Other material	\$59.66
Total costs	\$3,713.76

## Discussion of Calibration Results

Overall, 8% accuracy is a positive outcome for this project considering the consumer grade electronics used in the apparatus. This accuracy could improve with additional calibration testing and other minor improvements. Additional steps that could improve the apparatus include designing a permanent insulated enclosure that limits heat loss in the apparatus, running a fly cut pass using a mill on the top assembly for a flatter surface, and using a NIST certified reference material with a more precise uncertainty for further verification.

Other low-cost apparatuses were able to achieve a higher level of accuracy but required additional analysis and correction to achieve this. One inherent flaw within the apparatus is parasitic heat loss through the top and side of the apparatus. To limit the intrinsic error, one study utilized a finite element analysis to quantify the parasitic heat loss at varying thicknesses. The result was a calibration curve that adjusted the effective area based on this analysis [36]. While this method resulted in an uncertainty around 1.5%, this method goes against the guidelines of the ASTM standards used to design the current apparatus. While this correction may increase accuracy, this analysis was beyond the scope of this project.

### 2.2.2 Guarded Hot Plate Methods

With the guarded hot plate fabricated and verified, the next step is to test the 3D-printed samples. During the timeframe of the guarded hot plate development process, the research team narrowed down the composition to the 50:50 mix based on mechanical and printing properties. As a result, the following testing procedure will focus on this composition. Similar to the needle probe method's section, a detailed description of the manufacturing process is given in the following paragraphs.

The 3D-printed wood material is primarily composed of waste wood chips and sodium silicate. The wood chips were sourced from Plummer Forest Products, Post Falls, ID, and the samples were prepared in Moscow, ID. The wood particle size was less than 0.425 mm and was obtained by using a 40-mesh sieve. The binding material used for the 3D-printed process is sodium silicate ( $\text{Na}_2\text{O}_3\text{Si}$ ) sourced from Thermo Fisher Scientific, Carlsbad, CA. The binder is in solution with water with a weight ratio of 37% sodium silicate and 63% water.

The 40-mesh wood particle size and the sodium silicate were mixed together using a food processor with a weight ratio of 50:50. Once mixed, the samples were placed into a 125 mm square press with a pressure of 18.6 psi, then cured in a drying oven at 60°C for a 72-hour period. Once this was complete, the samples were then shipped to Boise for thermal testing.

Upon arrival, the density, weight, and moisture content of the samples were measured. The moisture content of the sample was measured with a MT270 digital moisture meter manufactured by Tavool. The moisture content of the sample ranged from 5% to 8%. To match the testing conditions of the transient needle probe method, the samples were placed into a drying oven set at 100°C for a 20-hour period, as seen in Figure 22. The weight of each sample was checked at the 16-hour and 20-hour mark to ensure the samples were dry. Afterwards, the samples were placed into an airtight bag until thermal testing.



Figure 22. Guarded hot plate oven drying setup.

Table 8. Weight and density properties of guarded hot plate samples.

Sample Number	Weight on Arrival (g)	Weight after Drying (g)	Sample Volume (m <sup>3</sup> )	Density of Dried Sample (kg/m <sup>3</sup> )
Pressed Sample 1	98.06	92	0.000134	685
Pressed Sample 2	113.91	108	0.000149	723
Pressed Sample 3	133.13	126	0.000167	750

The thermal testing sequence is similar to the calibration process discussed earlier in the chapter. The density of the sample was measured by using calipers and a mass scale. The thickness was measured at each of the four corners of the sample and averaged together. The temperature of the room was measured, and the hot and cold plates were set to a 20°C difference with a mean temperature equaling the ambient temperature. Finally, the sample was placed in the apparatus and surrounded with insulation

One issue with the experiment is the size of the sample. The apparatus was designed to measure 200 mm square samples, which is the minimum sample size given by the ASTM standard. The prepared samples were 125 mm squares and were limited in size because of the available square press. The size of samples falls outside the range of the ASTM standard; therefore, the thermal experiments does not fully comply with ASTM standard C177. However, the apparatus should still be able to measure the thermal conductivity of these samples. The central metered plate in the apparatus is a 100 mm square and the sample was a 125 mm square with thicknesses of around 9 mm; therefore, it is possible to still get a reasonable measurement. When measuring smaller samples is that as long as the thickness is smaller than the length from the edge of the center plate to the edge of the sample, a reasonable measurement should be achievable [37]. However, there could be additional side heat losses that could add uncertainty to the measurement. To reduce the lateral and edge heat loss, additional EPS insulation strips were placed between the outer edges of the hot and cold plate shown in Figure 23. These strips were made slightly thinner than the samples used for testing to avoid a bad connection between the plates and the sample.





Figure 23. Insulation surrounding the sample to limit heat loss.

Once the sample was installed, the rest of the insulation was placed around the device and the programmed experiment ran for around five hours. The experiment was repeated three separate times per sample on consecutive days.

### 2.2.3 Guarded Hot Plate Results

Table 9. Summary of guarded hot plate experiments by sample.

Sample Number	Density of Dried Sample (kg/m <sup>3</sup> )	Averaged Measured Thermal Conductivity (W/m <sup>2</sup> *K)	Measurement Uncertainty (W/m <sup>2</sup> *K)
Pressed Sample 1	685.3	0.1581	±0.013
Pressed Sample 2	724.0	0.1693	±0.014
Pressed Sample 3	750.3	0.1734	±0.014

The results from the guarded hot plate experiment are summarized in Table 9. The measured thermal conductivity ranges from 0.15-0.17 W/mk. This result is slightly higher than the previous testing method; however, the densities of the samples are also higher. If the correlation from the needle probe method is extrapolated to the higher density values, an estimation of the thermal conductivity can be compared between the testing methods. The variation between these values was found to be within a 2% difference. As a result, the correlation found in the needle probe testing agrees with the guarded hot plate experiment. The correlation can be seen in Figure 24.

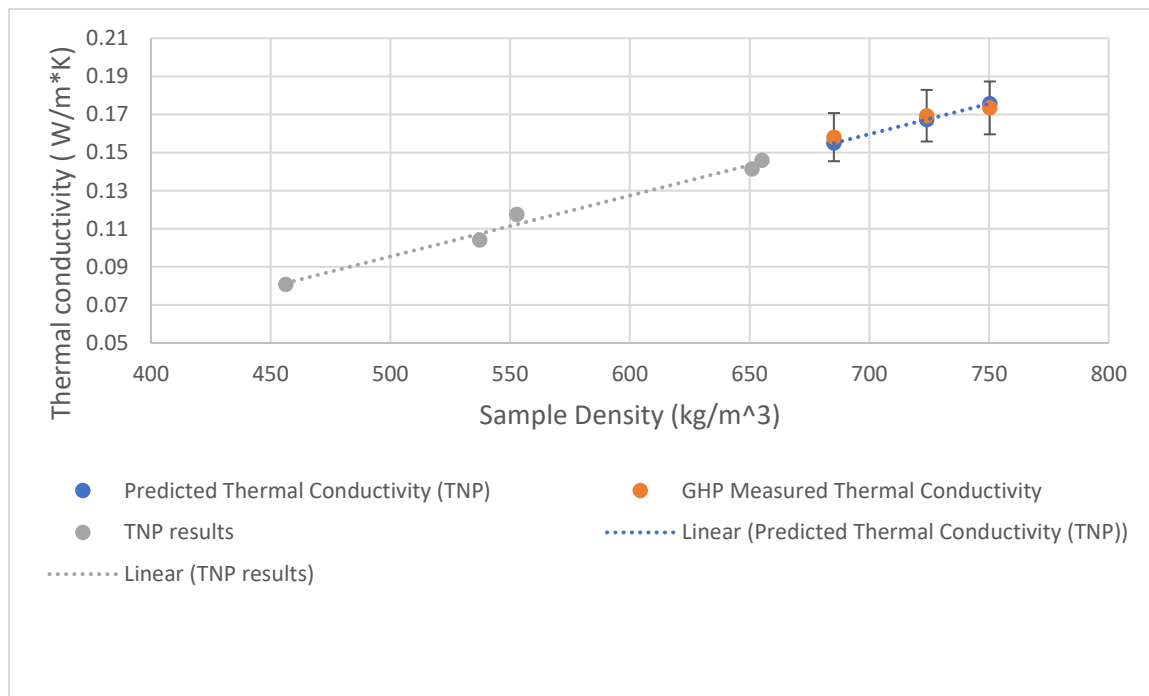


Figure 24. Comparison of guarded hot plate results to transient needle probe results

The measurements from the guarded hot plate apparatus confirm the earlier testing results. There is a very good agreement between the predicted thermal conductivity from the transient needle probe method and the measurements from the guarded hot plate. This is encouraging because it shows that the transient needle probe method can reliably estimate the thermal conductivity in the wood samples. This is a benefit for the overall project because the thermal experiments can be done relatively quickly and can be performed on larger and more complex shapes fabricated using the 3D-printing process. With this strong correlation between density and thermal conductivity, a determination of direct causality is still yet to be determined. There is some evidence from the guarded hot plate measurements that supports the direct causality, however more experimental data is needed to make a definitive claim.

One discrepancy between the testing methods was the use of thermal grease on the samples. Both methods used thermal grease, however there was an aluminum foil shield used for the hot plate apparatus that wasn't used on the needle probe. The rationale is as follows: The transient probe method used thermal grease for a relatively short period under little pressure pushing the material into the sample. In comparison, the guarded hot plate apparatus had factors that could make this problematic. The first reason is a longer exposure time and the second is an applied pressure on the samples. These two factors could make it more likely for the grease to diffuse into the samples open pores. This could cause thermal measurements to be higher than normal.

Another discussion point to note is the drying process. The scope of this research focused on characterizing the thermal properties of dried samples. The initial curing time and temperature ranged from 60°C for around a 72-hour period. To be consistent between the needle probe and the guarded hot plate sample preparations, the guarded hot plate samples were also placed in a 100 °C drying oven to dry out the samples. It is possible that during the second drying process at the higher temperatures, the binding material in the sample could have been further cured, resulting in different material properties.

## **Chapter 3: Life Cycle Assessment of Novel Wood-Based 3D-Printed Exterior Wall Assembly**

### **3.1 Introduction**

With the results of the thermal testing completed, the thermal conductivity can be used to estimate the overall envelope performance for a 3D-printed exterior wall. 3D-printing can create complex forms to improve the envelope performance. Highly efficient building envelopes were found to save 30% of the total building energy usage compared to a minimum code compliant envelope [12]. In addition, a main goal of the project is to produce a wall assembly that can reduce material and energy consumption by utilizing recycled wood waste. To better understand the holistic environmental effects of the 3D-printed wall assembly, a life cycle assessment of the building envelope is needed.

A life cycle assessment (LCA) can quantify the environmental effects through eco-indicators in each stage of a product's life cycle including the premanufacturing of the raw materials, product manufacturing, transportation, product usage, and end-of-life disposal / recycling. Numerous LCA studies on building materials have compared different envelope systems using a variety of methods and simulation software [38]. Despite the early phase of the project, a LCA of the proposed wall assembly is a valuable metric that can be used to better inform future design decisions in terms of reducing the most significant environmental impacts of the assembly.

The following LCA is focused on a typical 2.4 m square (8x8 ft) exterior wall section by quantifying the embodied energy and other eco-indicators. Embodied energy is a quantification of all the required energy to produce a given product or service. The four life stages that will be analyzed are raw materials, manufacturing, building energy usage, and the end-of-life [39]. The analysis compares the 3D-print wall assembly, a conventional wood frame wall, a concrete masonry unit (CMU) wall, and a high performing structural insulated panel (SIP) wall. Finally, the total energy impact for each wall type will be compared along with other eco-indicators using the Athena Building Impact Estimator.

## 3.2 Methodology

### 3.2.1 Materials

To quantify the embodied energy for each wall assembly throughout the product life cycle, the first step is to determine the composition for each wall assembly. The typical wood-framed wall consists of the following material listed from outside to inside:


<ol style="list-style-type: none"> <li>1. 6.35 mm (1/2-in) Wood Siding</li> <li>2. Vapor Barrier</li> <li>3. 6.35 mm (1/2-in) OSB Sheathing</li> <li>4. 60 x 180 cm (2x6-ft) Wood Studs, 40 cm (16-in) on centers, Filled with Fiberglass Insulation in the Cavity</li> <li>5. 6.35 mm (1/2-in) Gypsum Board</li> </ol>	
---	---

Figure 25. Composition of a wood framed wall.

The next wall assembly of interest is SIPs wall, which is produced by sandwiching an insulated foam core between two sheathing layers. This wall assembly takes advantage of off-site manufacturing methods and can be easily assembled on site. The typical wall composition given by the the Engineering Wood Association is detailed as follows [40]:

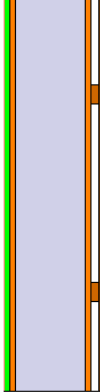
<ol style="list-style-type: none"> <li>1. 6.35 mm (1/2-in) Wood Siding</li> <li>2. Furring Strip</li> <li>3. Vapor Barrier</li> <li>4. 11.1 mm (7/16-in) OSB Sheathing</li> <li>5. 14.8 cm (5-5/8-in) EPS Insulation</li> <li>6. 11.1 mm (7/16-in) OSB Sheathing</li> <li>7. 6.35 mm (1/2-in) Gypsum Board</li> </ol>	
---	---

Figure 26. Composition of a SIPs Wall

Concrete masonry units are also a common wall assembly for residential housing, especially in the southern United States. These envelopes have a special classification within the International Energy Conservation Code (IECC) because the extra mass of the building material acts like a thermal

damper and can smooth out the daily heating and cooling needs of a building. In a Pacific Northwest National Lab report that studied residential mass framed walls, the researchers detailed the typical construction of a CMU wall and modeled the energy usage in several different climate locations [41]. To make this wall code compliant with the most recent energy code, an additional layer of continuous insulation was added, resulting in a RSI-56 (R-10) insulation rating. This modified baseline wall has the composition listed below.

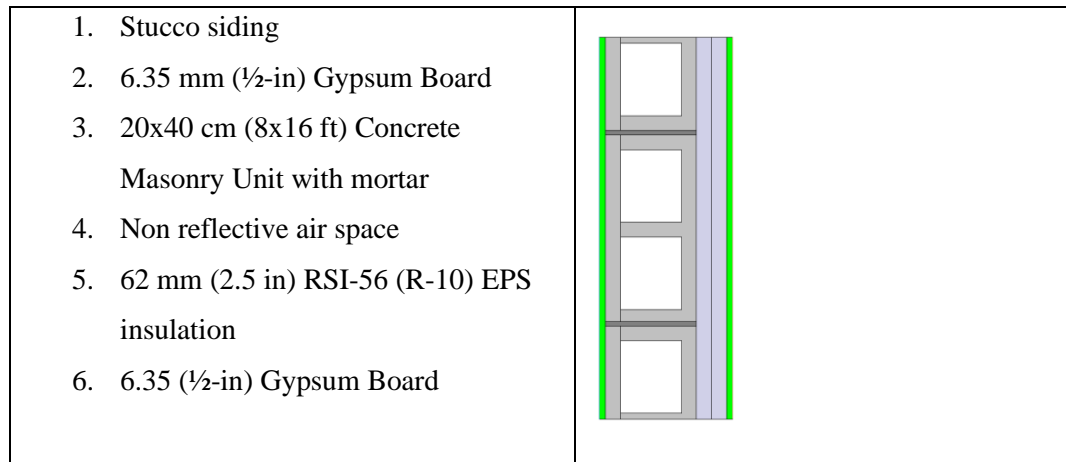


Figure 27. Composition of a CMU Wall.

The last wall composition that will be considered is a preliminary version of the 3D-printed wall assembly. The specific product details is still undergoing continual development. In an interview with Kenneth Baker, the project's principal investigator, he discussed some assumptions for the overall composition of the wall [42]. The wall is initially conceived to act like a combination between a conventional wood frame wall and a SIP wall. The overall design would have a core structural matrix made up of a wood-based composite with cellulose insulation filling in the open voids in the matrix. Figure 28 shows an initial conception of this proposed structure matrix using a honeycomb design. The matrix will be enclosed within 3D-printed panels. Dr. Baker estimates that there will be a 30% reduction in the structural wood volume compared to a wood frame wall. The exterior and interior finish could then be installed on site as specified by a prospective home buyer. These elements are assumed to be wood siding, gypsum board, and a vapor barrier. The final estimated composition and geometrical shape of the structural matrix is given as follows:

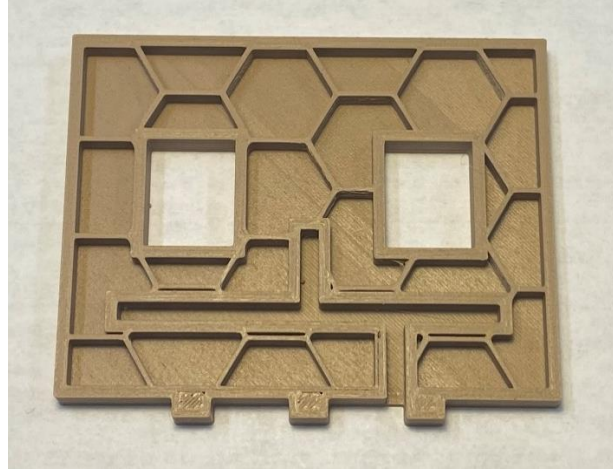


Figure 28. Structural matrix of proposed 3D-printed wall

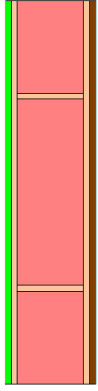
<ol style="list-style-type: none"> <li>1. 6.35 mm (1/2-in) wood siding</li> <li>2. Vapor Barrier</li> <li>3. 6.35 mm (1/2-in) 3D wood Panel end</li> <li>4. 3D wood matrix, with infill Cellulose insulation</li> <li>5. 6.35 mm (1/2-in) 3D wood Panel end</li> <li>6. 6.35 mm (1/2-in) Gypsum board</li> </ol>	
--	--

Figure 29. Composition of proposed 3D-print wall

Exterior wall compositions for residential applications depend on the climate zone, structural loads and other design decisions by architects and contractors. The wall compositions used in this LCA is based on the IECC 2018 standards for climate zone 5B [13].

The raw material for each assembly is included in the material analysis using a cradle-to-gate approach. Embodied energy is difficult to accurately quantify and can have variations between different geographic location, specific processes, and individual practices of a facility [43]. The Inventory of Carbon and Energy Database was chosen to quantify the embodied energy for this life stage [44] and contains estimated embodied energy and material densities for each of the components listed in the above wall assemblies.

Using the volumetric dimensions, the material density, and embodied energy density, the embodied energy for an 2.4 m square wall section can be calculated. Figure 30 shows the results of this analysis. Tables of the embodied energy calculations for each wall assembly can be found in Appendix C.

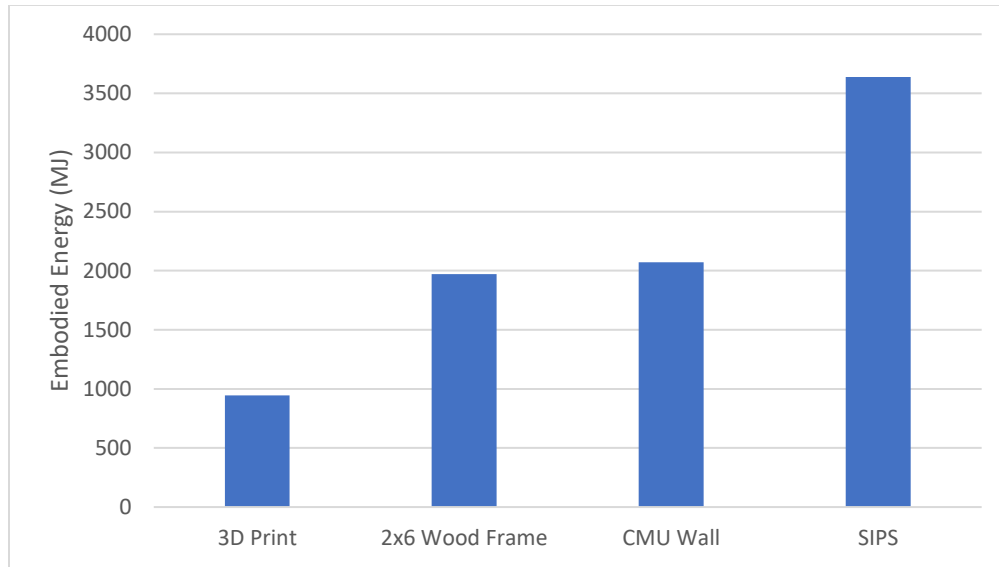


Figure 30. Material embodied energy comparison.

The proposed 3D-printed wall is estimated to have the lowest embodied energy in terms of material usage. This can be attributed to the utilization of cellulose insulation over traditional fiberglass insulation used in the wood framed wall, and the lower embodied energy of the recycled wood material compared to dimensional lumber. The SIPs wall has substantially more embodied energy due to the heavy use of an EPS insulation core, which contributes a little less than half of the total embodied energy for the assembly. The CMU wall has a similar overall embodied energy value compared to the wood-framed wall, but requires a high amount of added interior insulation to meet current energy codes. The OSB sheathing is also a major contributor to the embodied energy in the wood framed and the SIPs wall assembly.

### 3.2.2 Manufacturing

Traditional residential construction techniques largely rely on manual labor and small power equipment. This results in a vast majority of residential life cycle assessments neglecting the manufacturing stage [39]. Those who did include this stage have concluded that the total life cycle impact is less than 8% [45]. However, most of these studies focused on the wood and steel framed building envelopes for commercial construction projects. While this assumption in these studies might hold true for traditional construction techniques, this assumption might not be valid for offsite manufacturing techniques used for the SIPs and the proposed 3D-printed panel, especially with automation trends increasing within the construction sector. The following section will review the manufacturing processes for the SIPs wall and the 3D-printed wall. It is assumed that the CMU wall



and the wood framed wall assembly largely follow the general consensus for the literature for this stage in life.

Both the SIPs and 3D-printed wall utilize off-site manufacturing in their construction. To better understand the energy needs in this stage, A literature search has been conducted to understand the energy used during the manufacturing phase for a SIPs wall. However, there were no available studies that fully detailed the energy usage in a SIPs manufacturing facility. This part of the report will therefore walk through the steps for each process and estimate the energy needed to produce a 3D-printed wall.

The construction of a SIPs wall begins with the raw material entering into the factory. Adhesive material is applied on each side of the EPS insulation and OSB sheathing. The next step in the process is to press the material together with a large hot press. It normally takes 5 minutes for the sandwiched pieces to cure in the press. The last step in the process involves cutting walls and doors into the wall frame as specified by the individual design of the building [46]. Once this step is completed, the wall assembly can be shipped out to the site to be assembled. Given the limited number of steps and analyzing to compared to traditional construction techniques, it was determined that the manufacturing process of the SIPs wall assembly would be marginally higher than the other construction techniques.

The process to manufacture the 3D-print wall assembly is currently under development. The research team is still determining the optimal composition of the structural wood composite for the 3D-printing process and the resultant mechanical and thermal properties. With this in mind, the conceptual manufacturing process will be discussed as a high level overview. The preliminary production process can be seen in the process-flow diagram in Figure 31.

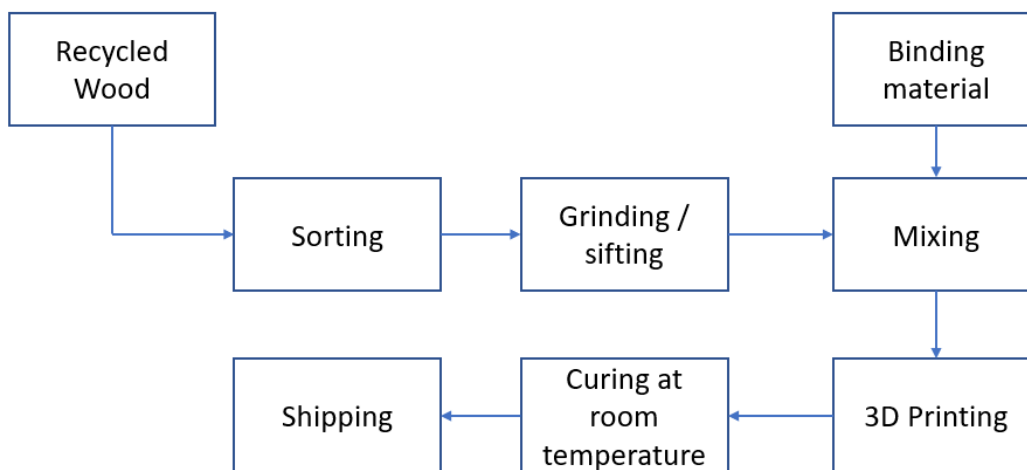


Figure 31. Preliminary 3D-print wall manufacturing process.

The manufacturing process starts by having recycled wood enter the facility. The wood would go through a sorting process to remove undesirable debris. The next step consists of chipping, milling, and sifting to get the desired 40 wood mesh flour [30]. The estimation for the energy used during this process is based on available industrial equipment and typical processing times [47], [48]. Once this process is completed, the wood flour can be stored on site until a wall assembly is ready to print. The wood flour and the binding material would be mixed together within a large mixing chamber and then be immediately printed into the desired wall form using a large-scale 3D-printer. Once the wall section is finished printing, the assembly should be able to cure at room temperature. This assumption is based on early testing of the printed material and the curing process. The curing time for the wall could range from a couple of days to a couple weeks and depends on how larger samples are able to cure. Once the panel has been fully cured, it will be ready for shipping.

There are a few assumptions that have to be considered to estimate the eventual power usage to produce a wall section. The first assumption is that the motors used on the current prototype 3D-printer would scale linearly with the size of the printer. The prototype printer is designed to print a 60 cm square section; therefore, the size of the motors is estimated to be around 4 times more powerful. The mixing stage power requirement is also scaled linearly based on volume output. The last estimation is that the curing process can be done at room temperature and the required energy usage is negligible compared to the other manufacturing steps.

Given all these estimations, the added embodied energy from the manufacturing stage for the 3D-print wall is roughly estimated to be around 62 MJ to process the recycled wood into the wood flour and 2,500 MJ to print the wall section. Further details of this estimation can be seen in Appendix C.

### 3.2.3 Building Energy Usage

The next life cycle stage is associated with the energy usage during the building's operational lifetime. According to the Energy Information Administration, around 30% of residential energy usage is used for climate control [10]. The building's envelope plays a large role in determining the energy consumption needs. There are six parameters of the envelope that affect the energy usage of buildings: solar gains, sun protection, thermal insulation, thermal storage, air tightness, and air infiltration [49]. The thermal insulation is a driving parameter in quasi steady state energy modeling software, but it is limited in scope and does not consider the dynamic effects of building energy usage. Changes in the building envelope can affect the heating and cooling loads, fan usage and internal heat gains. Each of these factors has interdependent ripple effects with one another and changes to the building envelope can have a complex effect on the overall energy needs of a building.

EnergyPlus is a building energy simulation engine that utilizes each of these parameters to estimate the change in a building's overall energy usage. In addition, the Pacific Northwest National Lab has created open-source prototype models of single family residences with varying heating and cooling systems and foundation types. These models were developed to compare the average energy savings between different energy standards in a variety of climates zones located throughout the United States. The prototype residence is a 2 story, 2,400 square feet, 3-bedroom, 2-bath house with a 15% window to wall ratio. The models used in this analysis are designed to meet IECC 2018 standards [13]. A picture of the prototype model can be seen in Figure 32. The prototype model for climate Zone 5B with a gas furnace and a crawlspace was selected because of the commonality of those specifications in the pacific northwest.



Figure 32. Rendering of PNNL single family residential model.

The model's exterior walls will be modified to compare the energy usage across the envelopes. The two main parameters that will change is the wall composition and the air infiltration rate. Most of the component material properties are included in the original PNNL model, with two exceptions. The 3D-printed panel and the structural matrix were added to the model based on the experimental testing and are detailed in Appendix C.

The independent variables in the building model include the envelope's insulation and the effective air infiltration rate in the living space. The SIP's air infiltration rate will be reduced by 80% compared to a wood framed wall and is based on findings from an Oak Ridge National Laboratory study [50]. Dr. Baker estimates that a 70% reduction in air filtration rate is achievable with the 3D-printing technique and the quality control improvement using off-site manufacturing [42]. The air infiltration reduction is incorporated into both models as a reduction in effective air leakage area. The overall exterior wall U-factor and infiltration area is summarized in Table 10.

The main output of interest from the simulations will be the overall energy usage of the house. This method aligns with similar studies looking at life cycle assessments for differing building envelopes [39], [51]. A relative comparison between each wall type is used to account for all the interdependencies of changing the building envelope. The wall assembly with the lowest overall energy usage sets a benchmark for a high-efficient home. The other envelopes show the additional energy requirements compared to the benchmark. The additional energy requirements are scaled down by the total exterior wall area to match the wall section analyzed earlier, shown in equation 3. A lifetime of 50 years will be assumed to calculate the additional lifetime energy consumption, shown in equation 4 [52]. The results can be found in Table 10.

$$\text{Column 4} = (\text{Building energy usage} - \text{Benchmark energy usage}) * \frac{64 \text{ ft}^2}{\text{Gross Wall Area (ft}^2\text{)}} \quad (3)$$

$$\text{Column 5} = (\text{Annual additional energy requirements}) * 50 \text{ Years} * 1.055 \text{ (kBtu to MJ conversion)} \quad (4)$$

Table 10. EnergyPlus simulation summary.

Assembly	U-factor (BTU/(hr *ft <sup>2</sup> *F))	Effective Air Leakage Area (cm <sup>2</sup> )	Total Building Source Energy Use (kBtu)	Annual Additional Energy Requirements (kBtu)	Additional Lifetime Energy Consumption (MJ)
3D-Print	0.044	107.20	173,690.90	6.84	361.02
2x6 Wood Frame	0.058	357.40	191,903.38	459.92	24,260.53
SIPS	0.035	71.48	173,415.79	Benchmark	Benchmark
CMU	0.069	357.40	193,625.29	502.75	26,520.13

The results from the simulations demonstrate the importance of the building envelope with regard to the energy usage during the lifespan of the building. As expected, the SIPs wall had the lowest energy consumption, saving around 9.6% compared to a wood framed wall. The theoretical 3D-print wall assembly is estimated to save around 9.5%. Upon further inspection of the simulations, most of the energy savings is associated with reduced heating loads during the wintertime. The 3D-printed wall was found to have the lowest cooling load requirements, as well as the lowest fan energy usage. The

CMU wall was found to have the greatest energy usage out of the selected walls for climate zone 5b. CMU walls are typically found in warmer climate zones that can take better advantage of the thermal mass properties of the wall to reduce the daily heating and cooling needs of the building. It is also worth noting that the additional energy usage could be greater if the building lifetime was extended beyond 50 years.

### 3.2.4 End of Life

The end-of-life disposal of buildings doesn't receive much attention in building life cycle assessments. While most studies focus on the energy and emissions for material and building energy usage, they leave out the end-of-life disposal in their life cycle analysis and early design stage framework [39]. However, end of life disposal should not be entirely ignored since over 60% of all non-industrial waste is created from the construction and demolition of buildings [53]. Beyond the energy requirements, there are a number of parameters based on specific air pollutants, ground water pollution and overall ecotoxicology that contribute to the full negative environmental impacts.

To analyze the energy consumption in this life stage, the energy requirements for typical waste disposal will be estimated using the EPA Waste Reduction Model (WARM). This is a software designed for municipal waste management to help quantify the greenhouse gas emissions and energy consumption measures before and after implementing different waste management policies [54]. While the ideal method of the end-of-life stage is to reuse and recycle materials into new buildings, the current practice in the United States is to send most waste to a landfill [55]. The geometric dimension and associated weight for the wall section uses the same method as the materials phase.

Some material substitutions were required to use the WARM model for each wall assembly. OSB board was modeled as medium density fiberboard because they are both wood products produced using similar binding materials. The other substitution is cellulose insulation. Since cellulose is primarily created using recycled paper, general mixed paper was chosen to be the best material substitute. The last substitution made was for the 3D wood printing material. Since the specific composition is still under development, it was assumed that the best material selection to use in its place was dimensional lumber. The resulting energy consumption for each wall assembly can be seen in Figure 33.

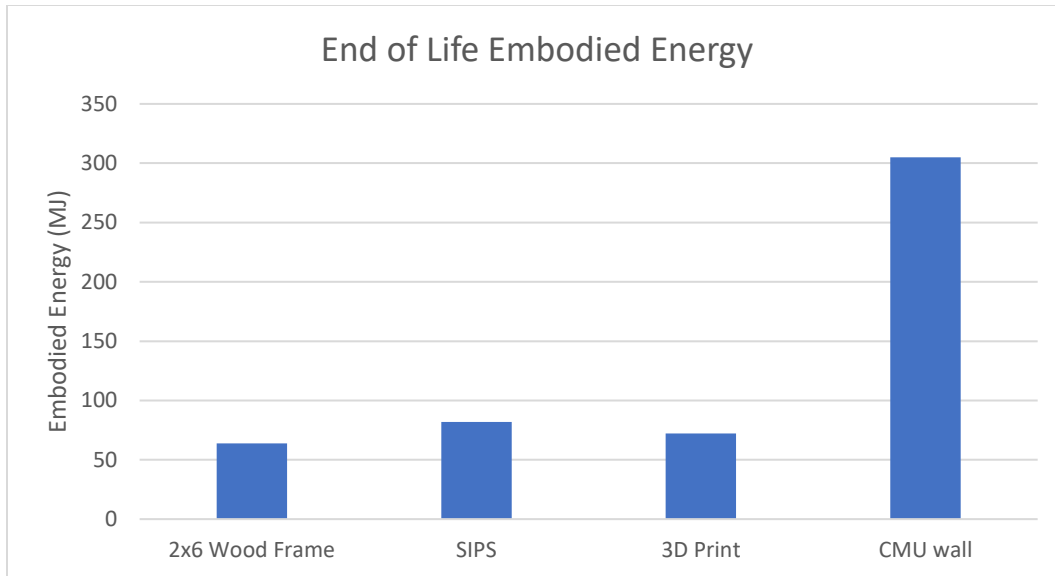


Figure 33. Embodied energy of the end-of-life stage.

The result of the life stage shows that the wood framed wall has the lowest estimated effect with energy needs for disposal, followed closely by the 3D-print wall. The primary cause is that the 3D-print wall has an extra sheathing layer to contain the loose fill insulation during manufacturing. Further analysis of the WARM model shows that the general mixed paper used to simulate the cellulose insulation in the 3D-printed wall has a negative energy value when placed in a landfill. If this material was omitted from the overall composition, the 3D-printed wall would have a marginally higher embodied energy. The CMU wall is the big outlier of the group, with a high energy requirement to landfill concrete. Overall, these results are very small compared to the other life stages in terms of embodied energy, accounting for around 2% of the total energy impact. While the embodied energy analysis for the end-of-life stage is inconclusive between the wall types, energy usage is a limited indicator to the overall environmental impact.

In addition to quantifying the embodied energy, other eco-indicators were analyzed over the entire life cycle. The analysis used Athena's Impact Estimator for Buildings, which is a software designed to perform life cycle assessments for buildings. Each envelope type was inputted into the software program similar to the materials section. The eco-indicators chosen to compare the assemblies were global warming potential, acidification, airborne particulates, ozone depletion, and smog potential. The 3D-printed envelope was estimated by using a wood framed wall, with cellulose insulation and plywood sheathing. Table 11 shows the results from the program based on a 1 to 5 rating scale with 1 being the least harmful and 5 being the most harmful in each category. The total score is

the sum of each individual category and was weighted equally amongst the indicators. The raw outputs from the software analysis can be seen in Appendix C.

Table 11. Normalized Athena eco-indicator results.

	Global Warming Potential	Acidification	Airborne Particles	Ozone Depletion	Smog Potential	Total Score
3D-Print	1.0	1.0	1.3	1.0	1.1	<b>5.5</b>
CMU	5.0	5.0	5.0	5.0	5.0	<b>25.0</b>
SIPs	1.8	2.0	1.0	1.0	1.9	<b>7.7</b>
Wood Frame	1.1	1.1	1.0	1.1	1.0	<b>5.3</b>

The results from this analysis show that the CMU walls have the poorest rating in each category by a healthy margin. The SIPs wall type closely resembles the wood frame and 3D-print wall but has a higher environmental cost in global warming potential, acidification, and smog. This is most likely caused by the production of the EPS insulation core. As modeled, the 3D-print wall is close to the top in terms of environmental impact, but the method to quantify the environmental effects within the printed material is flawed. The 3D-print composite has a sodium silicate binding resin, which is a less harmful material compared to formaldehyde-based resins. When the sodium silicate cures within air, it reacts into silicon dioxide and is a commonly found material in the natural environment. The research team should look into recycling capabilities with the printed wood composite.

### 3.3 Overall Comparison and Discussion

In a typical LCA, it is standard to incorporate a weighting factor associated with the severity of the effects in one life stage. In this analysis, there is a common unit measured between each life stage and can simply be summed together. Since the building energy usage stage incorporated a relative energy comparison, there is no additional energy associated with the SIPs wall frame. The overall comparison can be seen in Figure 34.

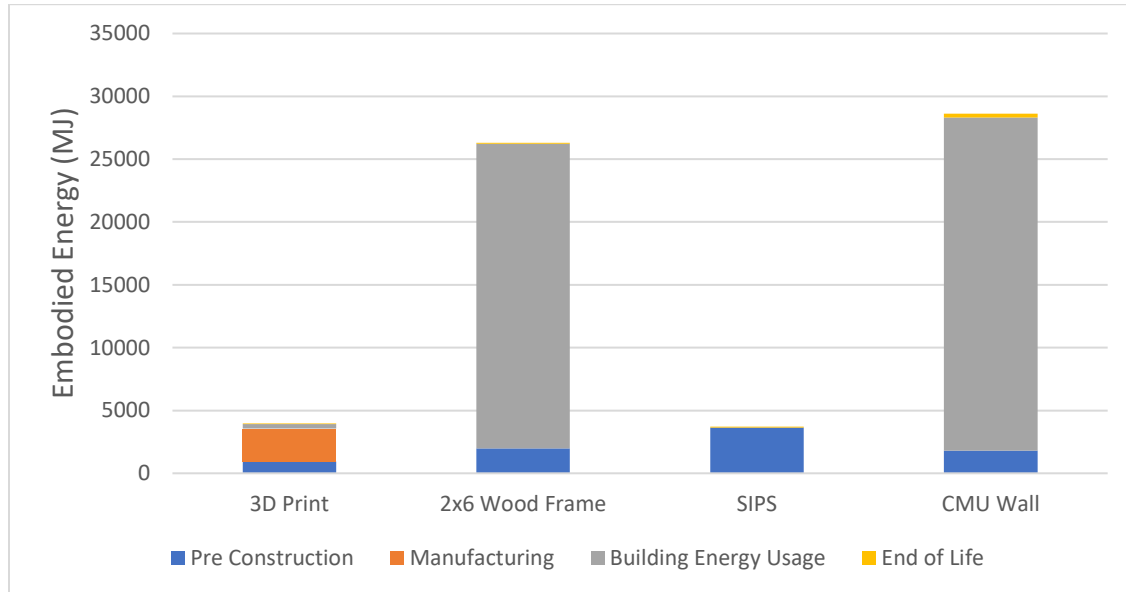


Figure 34. Total energy impact comparison.

The first thing to note is that the end-of-life energy consumption was found to contribute less than 2% in all envelopes. As mention before, embodied energy is not an effective metric to convey the environmental costs when it comes to end-of-life disposal of items in a landfill. Other environmental indicators such as global warming potential and acidification are a better measurement for the overall environmental impact.

In terms of the total energy impact score, the SIPs wall assembly has the lowest embodied energy, followed closely by the 3D-printed wall. The building energy usage stage is the largest contributor to the overall embodied energy. The raw material stage played a very light role with the 3D-print wall having the lowest material energy score. The SIPs wall was still able to edge out the 3D-print wall having the lowest material energy score. The SIPs wall was still able to edge out the 3D-print wall with a slightly better envelope performance. Lastly, the estimated manufacturing stage for the 3D-print wall assembly was larger than expected and should be considered by the research team as the project progresses.



A further understanding of the correlation between the building energy usage and infiltration / insulation was explored because of the preliminary nature of the 3D-printed wall assembly. A sensitivity analysis was performed to compare the energy usage for the full building with an incremental performance change of 10 and 20%. The analysis was done by changing the thermal conductivity of the 3D-printed matrix and the effective air leakage area. The results of the sensitivity analysis can be seen in Figure 35.

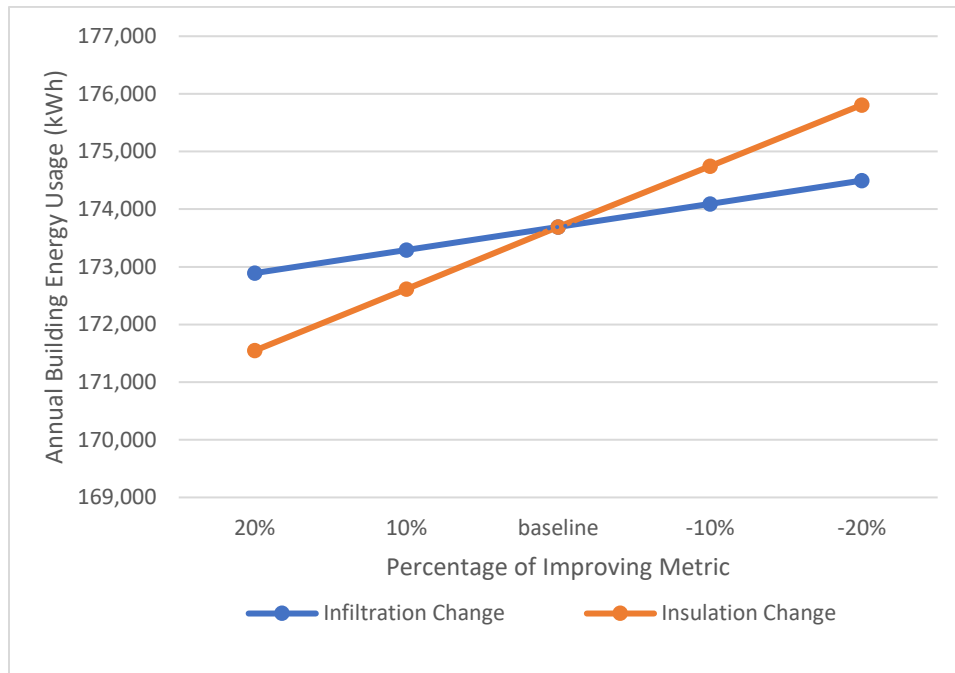


Figure 35. Sensitivity analysis comparing the relative effects of insulation and infiltration.

The result of the sensitivity analysis shows a linear correlation between infiltration / insulation and annual building energy usage when simulated independently. Insulation is about 2.4 times more effective at changing the energy usage than improving infiltration with the same incremental improvement. Both parameters should continue to be monitored throughout the 3D-printed wall development process. Thermal performance of the 3D-printed matrix should be further explored by comparing different printing geometries. With further improvement in design, the 3D-printed wall could become the lowest energy consuming wall type for each stage in the life cycle.

A parallel analysis was conducted to judge the independent effect from the infiltration and insulation. The individual savings from infiltration and insulation were compared to a typical wood framed wall baseline. By separating these changes in the energy plus simulations, the overall effects could be evaluated. Table 12 shows the individual contributions of the savings from each parameter.

Table 12. Sensitivity analysis of insulation savings vs infiltration savings

Simulation Run	Site Energy Usage (kBtu)	Energy Savings in (kBtu)	Energy Usage Percent Improvement
Wood-Framed Wall Baseline	105,037	N/a	N/a
Infiltration Only	95,433	9,603	9%
Insulation Only	98,285	6,752	7%
Combined Savings	89,003	16,033	16%

The overall effects of the infiltration and the insulation gains over the baseline case are about equal. This is due in part that there was a larger incremental gain in the infiltration (70% improvement) compared to the improvement due to insulation (27% improvement). This shows that both infiltration and insulation performance are vital improvements for the 3D-print envelope's performance.

Building energy usage is highly dependent on the surrounding climate, which can vary widely within the United States. The IECC has separate requirements for residential and commercial buildings based on regional climate. Additional simulations of the PNNL residential prototype were ran to understand how the 3D-print envelope would perform in other climates in terms of energy savings over a wood-frame envelope. Figure 36 shows the total energy savings over multiple climate zones.

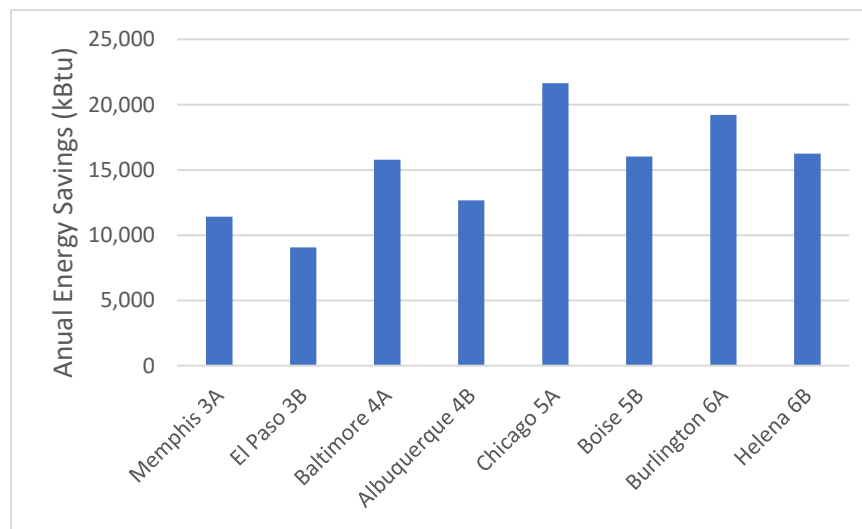


Figure 36. 3D-printed envelope energy saving compared with baseline envelope for different climate zones.

There is greater potential for energy savings in colder climates. The total source energy savings ranges from 10% to 17%. The overall improvement shows that there is a good potential for this wall envelope to reduce energy usage in a variety of climates across the United States.

The final analysis performed on the 3D-printed envelope is a preliminary market analysis to estimate the aggregate impact this technology could have if it becomes widely available. The Department of Energy's Scout tool was used to evaluate the technical potential energy and cost savings. The input parameters include the envelope performance, an assumed cost of \$7.00 per square foot, and a market entry year of 2024. These estimations are based on the overall team's research within the project. The analysis found that there could be a net savings of 446 Tbtu and an energy cost savings of \$6.4 billion by 2040. The key takeaway is a better understanding of how effective high-efficient building envelopes can be at reducing energy usage in the built environment if they became cost competitive with baseline envelopes.

The associated energy usage with the building life stage is not an absolute metric and was determined to be a comparison between each of the exterior wall types. There are many factors that go into determining the overall energy usage of a building, including internal loads, building envelope, size of the heating and cooling equipment, ventilation design, and building occupant behavior. Each of these parameters has a codependence on one another. For example, if there is more insulation installed on a building, there will be an increase in the cooling load because less heat can escape during the cooling season. This was observed in the SIPs wall type model. The energy savings were primarily associated with a reduction in heating requirements. These interdependencies show the importance of a holistic building design. An early building stage energy model can help inform architects and engineers of different site-specific strategies to reduce the overall energy usage of a building.

The specific source of energy used in a building can also have a sizable impact on the surrounding environment and depends on regional energy production. The energy source for the materials life cycle stage was included in the embodied energy density values provided by the Inventory of Carbon and Energy database; however, the electricity consumption was based off British electricity mixes. For the building energy usage stage, EnergyPlus has incorporated general site to source energy conversion factors based on the United States overall electricity production. For the end-of-life stage, the WARM software includes energy usage associated with transportation and landfilling energy requirements based off the United States national average.

The final point of discussion that the LCA does not consider is the possible reduction in construction waste in between each of the life stages. As mentioned before, off-site manufacturing

benefits by being able to optimize the raw material inputs. 3D-printing walls also has the potential to further reduce, if not eliminate, wasted materials. However, quantifying this effect was beyond the original scope of work.

## Conclusion

Considering the rapid development in 3D-printing technologies, the construction industry is poised to increase productivity and lower the cost of housing by using additive manufacturing methods. The benefits of 3D-printing in construction include reduced cost, labor, and waste, leading to an overall increase in productivity. One innovative process utilizing a recycled wood-based composite feedstock material is under development. The goal of the project is to take advantage of the benefits of additive manufacturing, while limiting the energy and raw materials while in the process. This paper details the thermal and environmental analysis of this novel envelope.

First, experimental testing of the wood composite was performed using a transient needle probe method. The experiments tested a variety of samples with different composition and wood grain size and found that the thermal conductivity ranged from 0.08-0.15 W/mK. A correlation between the density of these samples and their corresponding thermal conductivity was found and compared to other known wood-based composites.

In addition to the transient needle probe method, an additional steady state method was used. The scope of work included designing, fabricating, and verifying a low cost guarded hot plate apparatus designed to ASTM standard C177. Calibration tests found that the apparatus was able to achieve an 8% accuracy using a cast acrylic reference material. The results from the apparatus showed good agreement with the needle probe results that were within 2% difference and validates the usage of the needle probe, which is a faster and less expensive testing method.

A preliminary LCA was performed on a wall section of the 3D-printed wall assembly, as well as for other common residential wall types. The main factor under consideration was the total energy impact. It was found that the proposed 3D-print wall had the best performance in the materials stage and was a close runner up in the building energy usage and end of life stages. Special care should be considered when designing the manufacturing process to ensure low energy usage. The 3D wall design has potential to decrease energy usage in the residential and light commercial building types. If additional incremental improvements are achieved in the envelope performance and manufacturing stages, the 3D-printed wall could become one of the lowest energy consuming wall types available.

## Future Work

The transient needle probe should continue to be used when testing variations with the binding resin, particle size, binder content, and additional additives for the wood composite. The benefits with the needle probe is a reduction in time while maintaining reliable measurements. The probe can also be used for thermal testing of the wood material during manufacturing, leading to improved thermal management designs for the extruder. Lastly, the transient needle probe should be used to verify thermal properties on larger and more complex 3D-printed shapes.

Once the capability of creating larger wood composite samples is achieved, followup testing with the guarded hot plate apparatus should commence. Several samples with the same composition should be made with thicknesses larger than 12 mm. The increased thickness is needed to mitigate the effects of sample warpage.

There are a couple of improvements that could be made on the guarded hot plate apparatus to increase accuracy. One improvement is designing a permanent insulated enclosure to limit heat loss. Another improvement is replacing the aluminum foil on the hot and cold plate with a shrink wrap material to further limit air pockets between the plates and the sample. The last improvement is using a NIST certified reference material with a more precise thermal uncertainty to better verify the accuracy of the apparatus.

Finally, the life cycle assessment should be continually updated as development continues with the 3D-printing process. Another area of research is to look into reusing the 3D printed composite to form a closed loop material flow cycle. Current research with room temperature curing and the infusion of CO<sub>2</sub> into the wood composite should be further explored and thermally characterized. Once the prototype 3D-printer is complete and has successfully printed an object, thermal optimization of the 3D-printed wall envelope should begin.

## References

- [1] Grand View Research, "3D Printing Construction Market Size Report," Grand View Research, San Francisco, 2021.
- [2] E. Christoffer, "July / August: The Housing Shortage," July 2021. [Online]. Available: <https://www.nar.realtor/realtor-magazine/july/august-2021-the-housing-shortage>.
- [3] Association General Contractors of America, "Workforce Development Plan 2.0," Association General Contractors of America, 2018.
- [4] J. M. Stupak, "Productivity Growth Across the Economy," Congressional Research Services, Washington DC, 2018.
- [5] F. Saleen, "World's Largest 3D Printed Building in Dubai," Engineering.com, 29 January 2020. [Online]. Available: <https://www.engineering.com/story/worlds-largest-3d-printed-building-in-dubai>. [Accessed July 2021].
- [6] M. R. Khorramshahi and A. Mokhtari, "Automatic Construction by Contour Crafting Technology," *Emerging Science Journal*, pp. 28-33, 2017.
- [7] Portland Cement Association, "How Cement is Made," 2019. [Online]. Available: <https://www.cement.org/cement-concrete/how-cement-is-made>.
- [8] A. Verzoni, "Printing Buildings," *National Fire Protection Association*, 2020.
- [9] T. Suntharalingam, I. Upasiri and P. Gatheeshgar, "Energy Performance of 3D-Printed Concrete Walls: A Numerical Study," *Buildings*, vol. 11, no. 10, pp. 432-454, 2021.
- [10] EIA, "Annual Energy Outlook 2020," Energi Information Administration, Washington DC, 2020.
- [11] P. A. K. Sanguinetti and e.t., "Evaluating the Potential of High Performance Concrete 3D-Printing for Zero Energy Homes," in *16th IBPSA Internal Conference and Exhibition*, Rome, It, 2019.
- [12] S. B. Sadineni, S. Madala and R. Boehm, "Passive Building Energy Savings: A Review of Building Envelope Components," *Renewable and Sustainable Energy Reviews*, pp. 3617-3631, 2011.

- [13] International Codes Council, International Energy Conservation Code, Country Club Hills, IL: International Codes Council, 2018.
- [14] P. Bianchi, G. Baldinelli and E.T., "Infrared Thermography Assessment of thermal Bridges in Building Envelope: Experimental Validation in a Test Room Setup," *Sustainability*, pp. 7107-7120, 2014.
- [15] Lorraine Berkeley National Laboratory, *Therm*, Berkeley: Lawrence Berkeley National Laboratory, 2021.
- [16] R. J. Ross, "Wood Handbook: Wood as an Engineering Material," USDA Forest Service: Forest Products Laboratory, Washington DC, 2010.
- [17] F. Yapici and G. Gunduzm, "The effect of some Production Factors on Thermal Conductivity of Oriented Strand Board," *Technology*, pp. 65-70, 2010.
- [18] The Engineered Wood Association, "Formaldehyde and Engineered Wood Products," APA, Tacoma, WA, 2018.
- [19] d. S. Bertilini and C. E. Moralis, "Acoustic Absorption and Thermal Insulation of Wood Panels: Influence of Porosity," *Bioresources*, pp. 3746-3757, 2019.
- [20] A. TenWolde, D. McNatt and L. Krain, "Thermal Properties of Wood And Wood Panel Products for Use in Buildings," Forest Service: Forest Products Lab, Madison, WI, 1988.
- [21] MatWeb, "Plywood," 2021. [Online]. [Accessed 15 September 2021].
- [22] Swiss Kronor, "OSB boards: Technical Data," [Online]. [Accessed 2021].
- [23] ASTM International, "Standard Test Method for Determination of Thermal Conductivity of Soil and Soft Rock by Thermal Needle Probe Procedure," ASTM International, West Conshohocken, PA, 2021.
- [24] East 30 sensors, *Thermal Conductivity*, Pullman, WA: East 30 sensors, 2020.
- [25] H. He and M. Dyck, "Development and application of the Heat Pulse Method for Soil Physical Measurements," *Review of Geophysics*, vol. 56, no. Print, pp. 567-720, 2018.



- [26] R. Tye and D. Salmon, "Thermal Conductivity of Reference Materials: Pyrex 7740," National Physics Laboratory, Teddington, England, 2003.
- [27] m. Assael, S. Botsios and K. Gialou, "Thermal Conductivity of Polymethyl Methacrylate (PMMA) and Morosilicate Crown Glass BK7," *International Journal of Thermophysics*, vol. 26, no. 5, pp. 1595-1605, 2005.
- [28] Thermtest, "Reference Materials - Measurement of thermal Conductivity," 26 October 2020. [Online]. [Accessed 25 February 2021].
- [29] S. Rudtsch and U. Hammerschmidt, "Intercomparison of measurements of the thermophysical properties of polymethyl methacrylate," *International Journal of Thermophysics*, vol. 25, no. 5, pp. 1475-1482, 2004.
- [30] C. m. Clemons, "Wood Flour," in *Functional Filler for Plastics*, Newark, NJ, Wiley-VCH, 2010, pp. 269-290.
- [31] T. Ding, "A comparative study of morphological characteristics of medium-density fiberboard dust by sieve and image analyses," *Journal of Wood Sciences*, vol. 66, no. 1, pp. 1-9, 2020.
- [32] W. Sonderegger and P. Niemz, "Thermal Conductivity and Water Vapour Transmission Properties of Wood Based Materials," *European Journal of Wood and Wood Products*, pp. 313-321, 2009.
- [33] S. Claucherty and H. Sakaue, "Phenol-formaldehyde resin for optical-chemical temperature sensing," *Sensors*, vol. 18, no. 6, p. 1756, 2018.
- [34] M. Kleiner and S. Kuhn, "Thermal conductivity measurements of thin silicon dioxide films in integrated circuits," *IEEE Transactions on electron devices*, vol. 43, no. 9, pp. 1602-1609, 1996.
- [35] ASTM International, *Standard Test Method for Steady-State Heat Flux Measurements and Thermal Transmission Properties by Means of the Guarded-Hot-Plate Apparatus*, West Conshohocken, Pa: ASTM International, 2019.
- [36] S. Dubois and L. Frédéric, "Design, construction and validation of a guarded hot plate apparatus for thermal conductivity measurement of high thickness crop-based specimens," *Materials and Structures*, vol. 48.1, no. Print, pp. 407-421, 2015.

- [37] D. Hume, Interviewee, *Thermal Conductivity Meeting*. [Interview]. 2021.
- [38] Rios, Grau and Chong, "Reducing Exterior Wall Framing Systems: a Cradle-to Cradle Comparative Life Cycle Assessment," *Waste Management*, pp. 120-135, 2019.
- [39] Kahhat and Crittenden, "Environmental Impacts Over the Life Cycle of a Residential Building Using Different Exterior Wall Systems," *Journal of Infrastructure Systems*, pp. 211-221, 2009.
- [40] APA, "Standard for Performance-Rated Structural Insulated Panels In Wall Applications," The Engineered Wood Association, Tacoma, WA, 2018.
- [41] Hart and M. Taylor, "Residential Wall Type Energy Impact Analysis," Florida Masonry Apprentices & Educational Forum, Orlando, 2014.
- [42] K. Baker, Interviewee, *3D Printed Envelope Assumption*. [Interview]. November 2020.
- [43] M. Dixit and J. Fernandez-Solis, "Identification of Parameters for Embodied Energy Measurements: A Literature Review," *Energy and Buildings*, pp. 1238-1247, 2010.
- [44] G. Hammond and G. Jones, *Inventory of Carbon & Energy: ICE Vol. 5, Bath* : Department of Mechanical Engineering, university of Bath, 2008.
- [45] D. Kellenburger and H. Althaus, "Relevance of Simplification in LCA of Building Components," *Building and Environment*, pp. 818-825., 2009.
- [46] C. Guthrie and J. McIntosh, "What are 'Structural Insulated Panels' and are they the sustainable Solution to Standard light framing Load Bearing Wall Construction," in *International Conference on Sustainability Engineering and Science*, Auckland, NZ, 2007.
- [47] Munson, "Attrition Mills," Munson, 2021. [Online]. Available: <https://www.munsonmachinery.com/Attrition-Mills/>. [Accessed September 2021].
- [48] Vecoplan, *Horizontal Drum Chippers*, Archdale NC: Vecoplan, 2010.
- [49] A. M. Papadopoulos, "Forty Years of Regulation on the Thermal Performance of the Building Envelope in Europe: Achievements, Perspectives and Challenges," *Energy and Buildings*, pp. 942-952, 2016.

- [50] C. Jeff, "High Performance Homes That Use 50% Less Energy Than the DOE Building America Benchmark Building.," Oak Ridge National Lab, Oak Ridge, TN, 2011.
- [51] A. Aksamija and T. Peters, "Heat Transfer in Facade Systems and Energy Use: Comparative Study of Different Exterior Wall Types," *Journal of Architectural Engineering*, 2017.
- [52] C. B. Aktas and M. M. Bilec, "Impact of Lifetime on US Residential Building LCA Results," *The International Journal of Life Cycle Assessments*, pp. 337-349, 2012.
- [53] S. S. Shrestha and K. Biswas, "A Protocol for Lifetime Energy and Environmental Impact Assessment of Building Insulation Material," *Environmental Impact Assessment Review*, pp. 25-31, 2014.
- [54] Environmental Protection Agency, "Waste reduction Model," 2019. [Online]. [Accessed November 2020].
- [55] V. Diyamandoglu and L. M. Fortuna, "Deconstruction of Wood Framed Houses: Material Recovery and Environmental Impact," *Resources Conservation and Recycling*, pp. 21-30, 2015.
- [56] Department of Energy: Office of Energy Efficiency and Renewable energy, "Prototype Building Models," 2021. [Online]. [Accessed November 2020].
- [57] H. He and R. H. E. Dyck, "Development and Application of the Heat Pulse Method for soil Physical Measurements.," *Review of Geophysics*, pp. 567-620, 2018.
- [58] P. Kotoulek, "Basic Thermal Properties and Geometrical Characteristics of wood and oriented Strand Board Used in Low Energy Buildings," *Journal of Processing and Energy in Agriculture*, pp. 73-75, 2018.

## Appendices

### Appendix A: Transient Needle Probe Method Experimental Results.

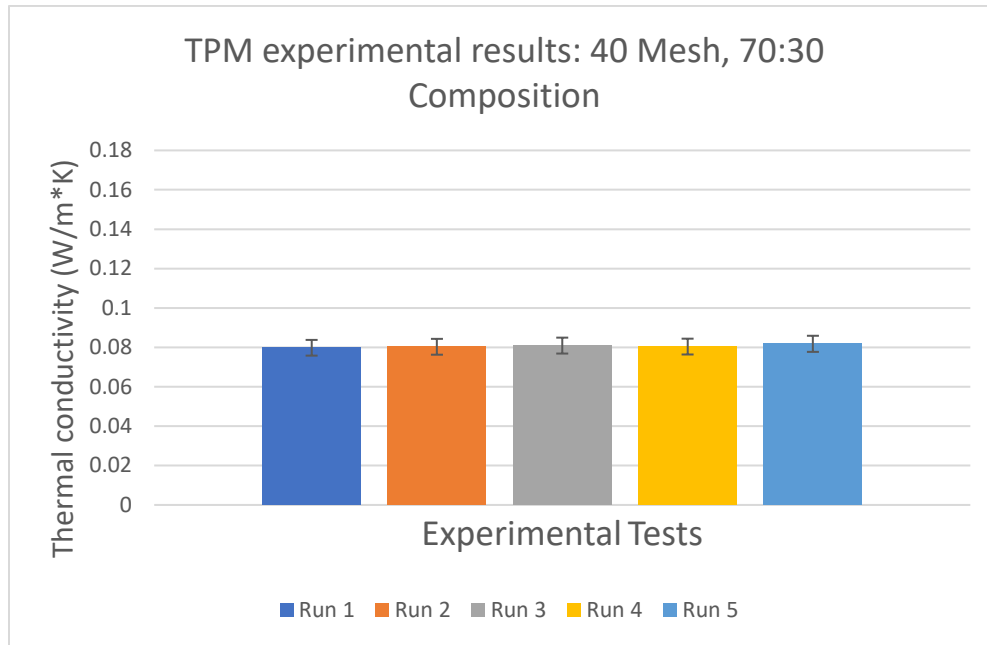


Figure 37. Transient needle probe experimental trials for the 70:30 40-mesh sample.

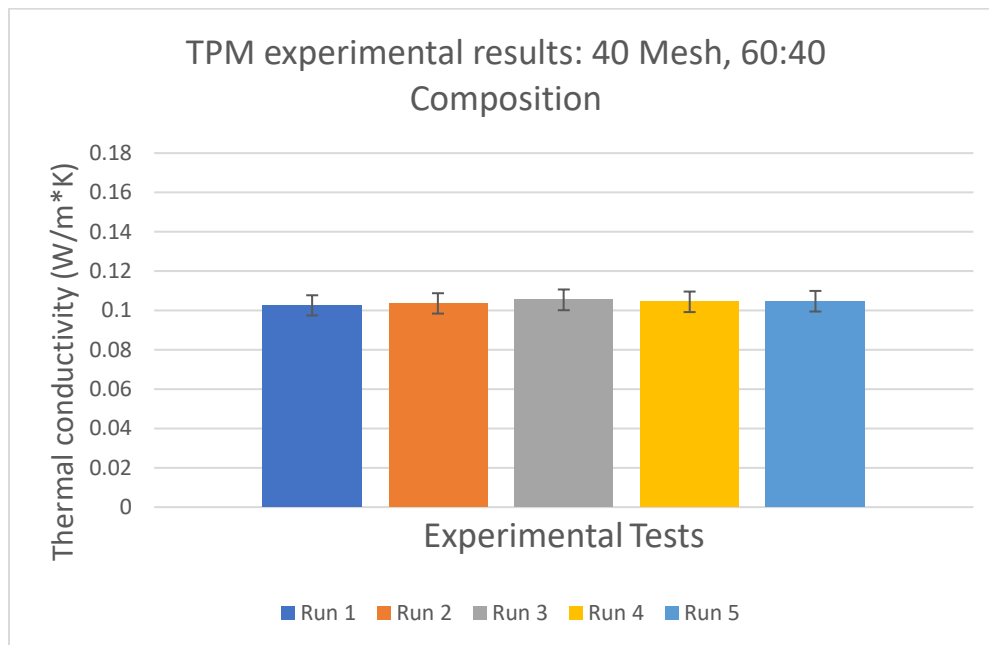


Figure 38. Transient needle probe experimental trials for the 60:40 40-mesh sample.

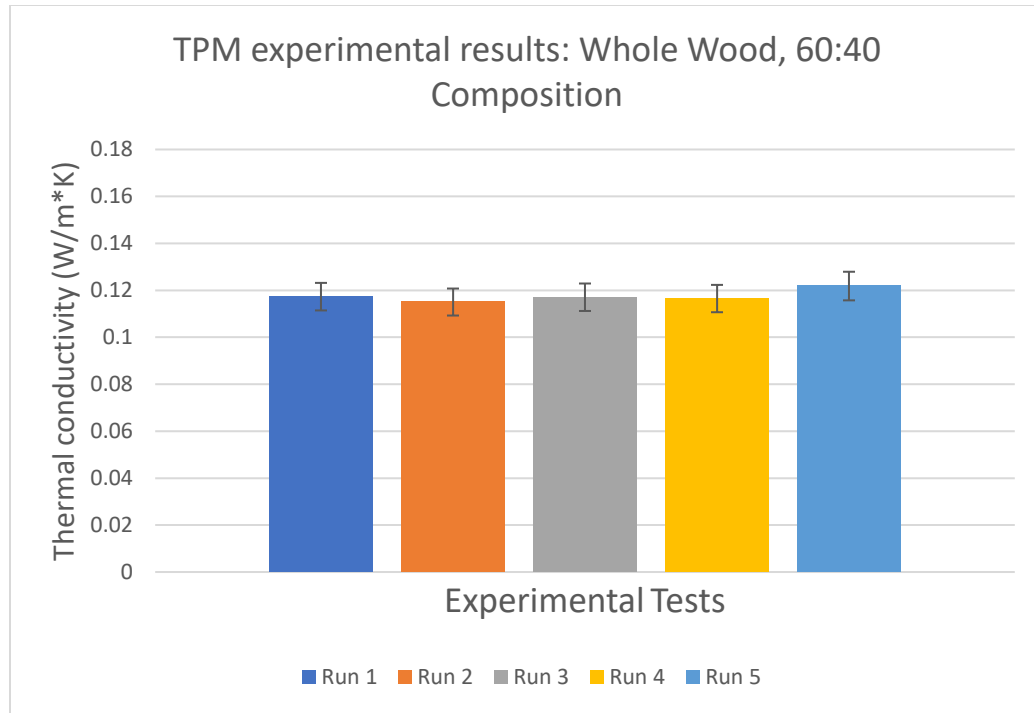


Figure 39. Transient needle probe experimental trials for the 60:40 whole wood sample.

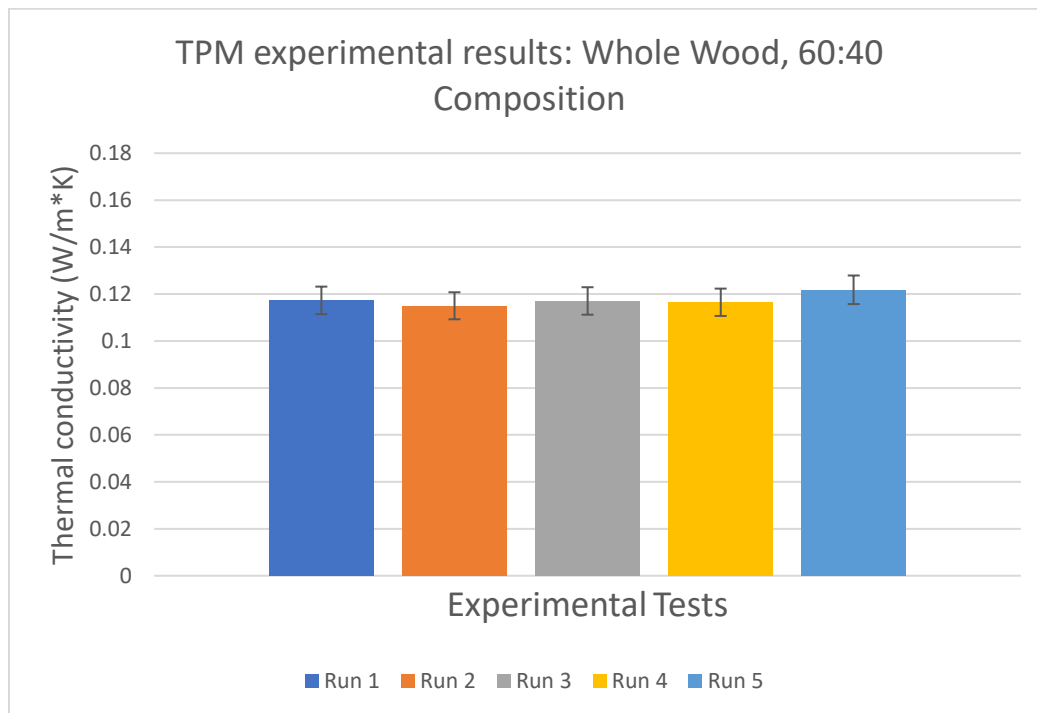


Figure 40. Transient needle probe experimental trials for the 50:50 whole wood sample.

## Appendix B: Guarded Hot Plate Details

### Guarded Hot Plate User Manual

This apparatus is designed to measure the thermal conductivity of 8x8 in samples ranging from ¼-in to 2.5-in., according to ASTM standard C177. Through thermal testing, It has an uncertainty range of 8%.

#### Steps

1. Measure the room temperature. This can be done by plugging in the Arduino USB cord and seeing the temperature readout on the LCD display.
2. If the mean temperature is off by a 1-2 degrees from the last experiment, the temperatures need to be adjusted, see below.
3. Checking / Changing the Hot plate temperature.
  - a. Open the Arduino program,
  - b. load the script INO\_SS script
  - c. change the temperature to 5° above the mean temperature
  - d. Upload the updated script to the Arduino.
4. Changing the cold plate temperature
  - a. Take the mean temperature and subtract 5°C from it to get the cold plate temperature
  - b. Adjust the chiller to corresponding Low temperature setting, I suggest lowering the temperature by 0.5°C from the desired cold plate temperature to adjust for the temperature difference between the fluid and surface of the cold plate
5. Measure and record the four corners of the sample material with a pair of calipers.

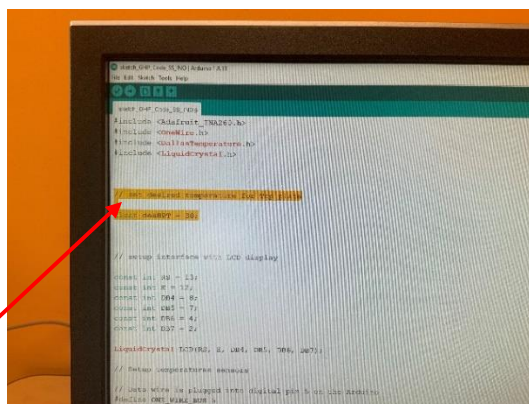


Figure 41. Image of hot plate temperature within Arduino code



Figure 42. Constant temperature water bath controls



Figure 43. Image showing thickness measurement.

- a. Note: the accuracy of the thermal conductivity measurement depends of the accuracy of the thickness measurements. The sample may require a fly pass with a mill depending on the flatness of the material.
6. Put the sample into the apparatus and lower the top plate onto the sample
  7. Place insulation around the device. I recommend putting the insulation on the sides in first and placing wedges to ensure a tight fit, then put in the front and back insulation



Figure 44. Process to install insulation onto the sides (top left and right), front (bottom right) and back (bottom right), of the apparatus.

8. Turn on the 12 V power supply, the fan should be spinning
9. On the computer, open Anaconda, then Spyder,
10. Change the filename
11. Update the thickness measurements highlighted in the figure below



```

1 #-*- coding: utf-8 -*-
2 """
3 Created on Wed Jan 27 12:47:58 2021
4
5 @author: tmitchell
6 """
7
8 # arduino example get data and store in vstiable
9
10
11
12 # import packages for code
13
14
15
16 import numpy as np;
17 import pandas as pd;
18 import datetime;
19 import serial;
20
21
22
23 # update these items for each test
24
25 filename = "Hemp_risi_exp1.xlsx"
26
27 thickness = 40.7 # in mm
28
29
30
31
32 #filename2 = "warmup_risi_exp1.xlsx"
33
34
35
36
37 # Connect to arduino
38
39 try:
40     arduino = serial.Serial('COM4', timeout=None, baudrate=9600)
41     print('connected')

```

Figure 45. Inputs into the Python code

12. Push run on the Python code, it should confirm that it successfully connected to the Arduino in the readout
13. Push the button on the breadboard to confirm to run the experiment seen in the picture below, the display on the Python code should slow down on the readout

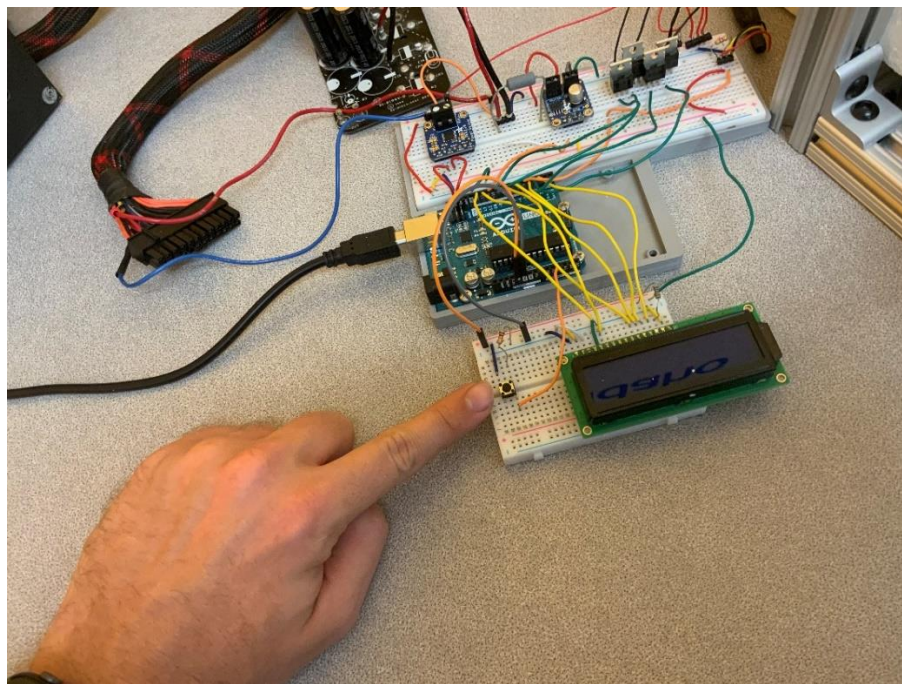
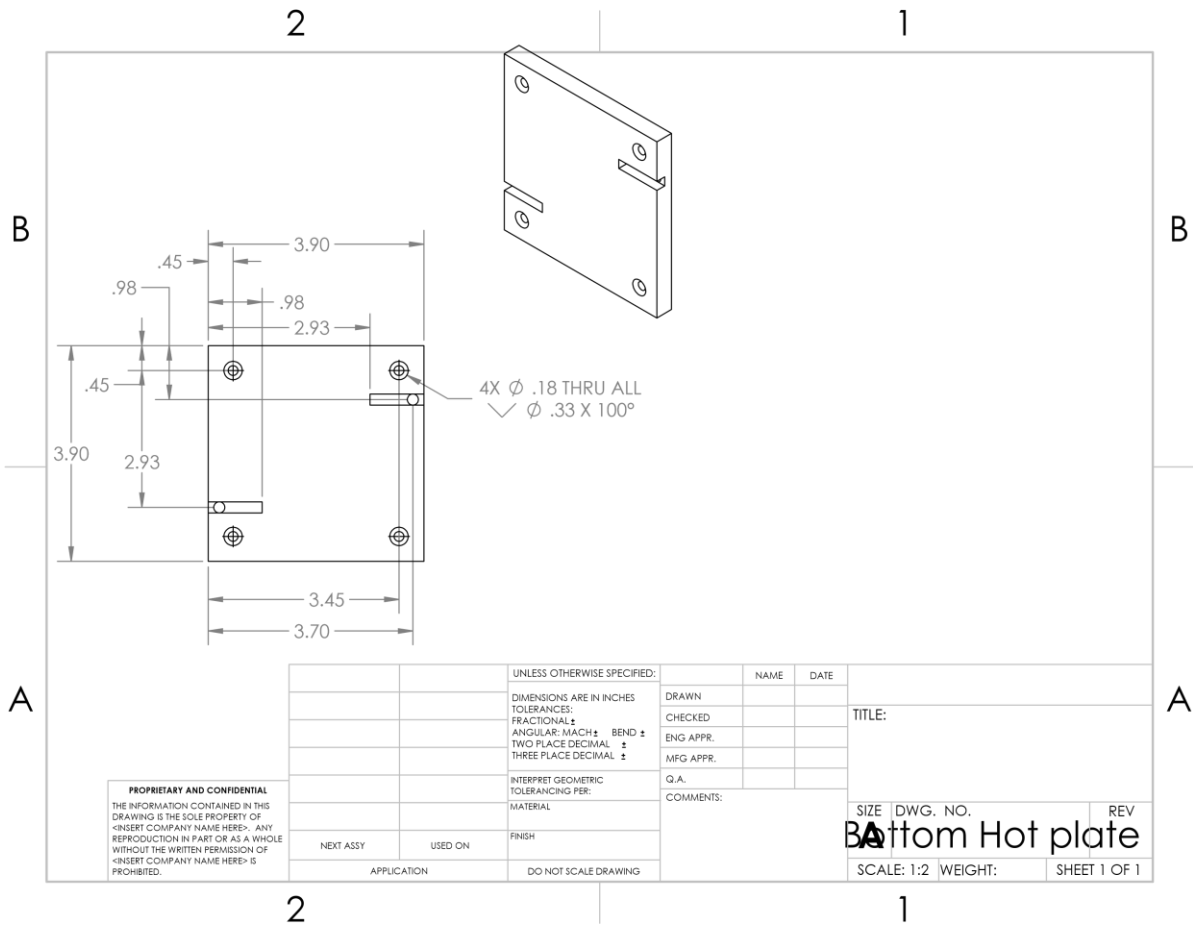


Figure 46. Image of start button.

14. Wait around 3-5 Hours for the experiment to run. It is ideal to start this process in the morning.
15. Once the experiment is over, Turn off the chiller and the 12 V power supply, then unplug the Arduino USB from the computer. The results are stored in a separate excel file within the Python script folder – transfer to an appropriate location on the Server to keep the folder cleanish
16. If for any reason that an experiment needs to be stopped, you can either push the button to save the experiment, then unplug the USB cable to the computer. Afterwards, turn off the power supply and the chiller.
17. DONE!!

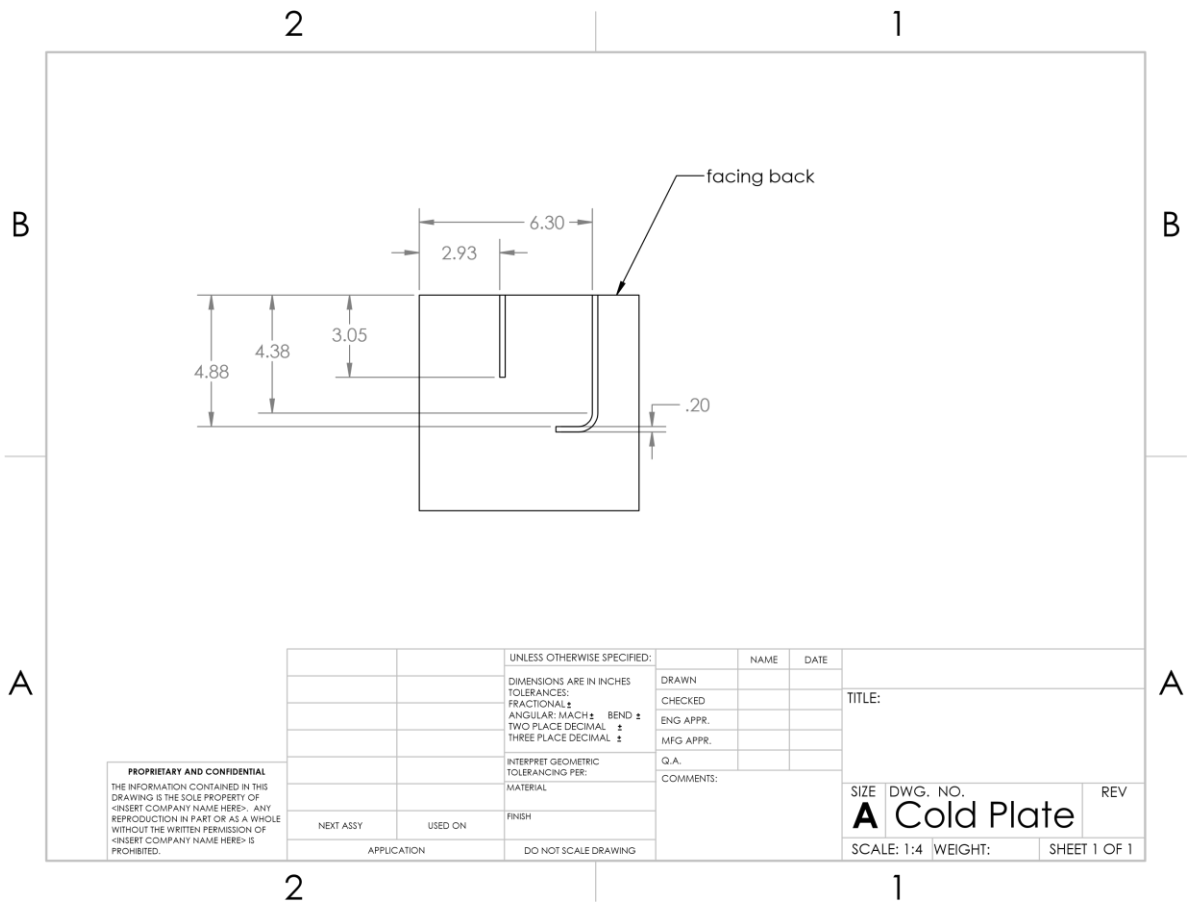
# Apparatus Drawings



**PROPRIETARY AND CONFIDENTIAL**  
 THE INFORMATION CONTAINED IN THIS DRAWING IS THE SOLE PROPERTY OF <INSERT COMPANY NAME HERE>. ANY REPRODUCTION IN PART OR AS A WHOLE WITHOUT THE WRITTEN PERMISSION OF <INSERT COMPANY NAME HERE> IS PROHIBITED.

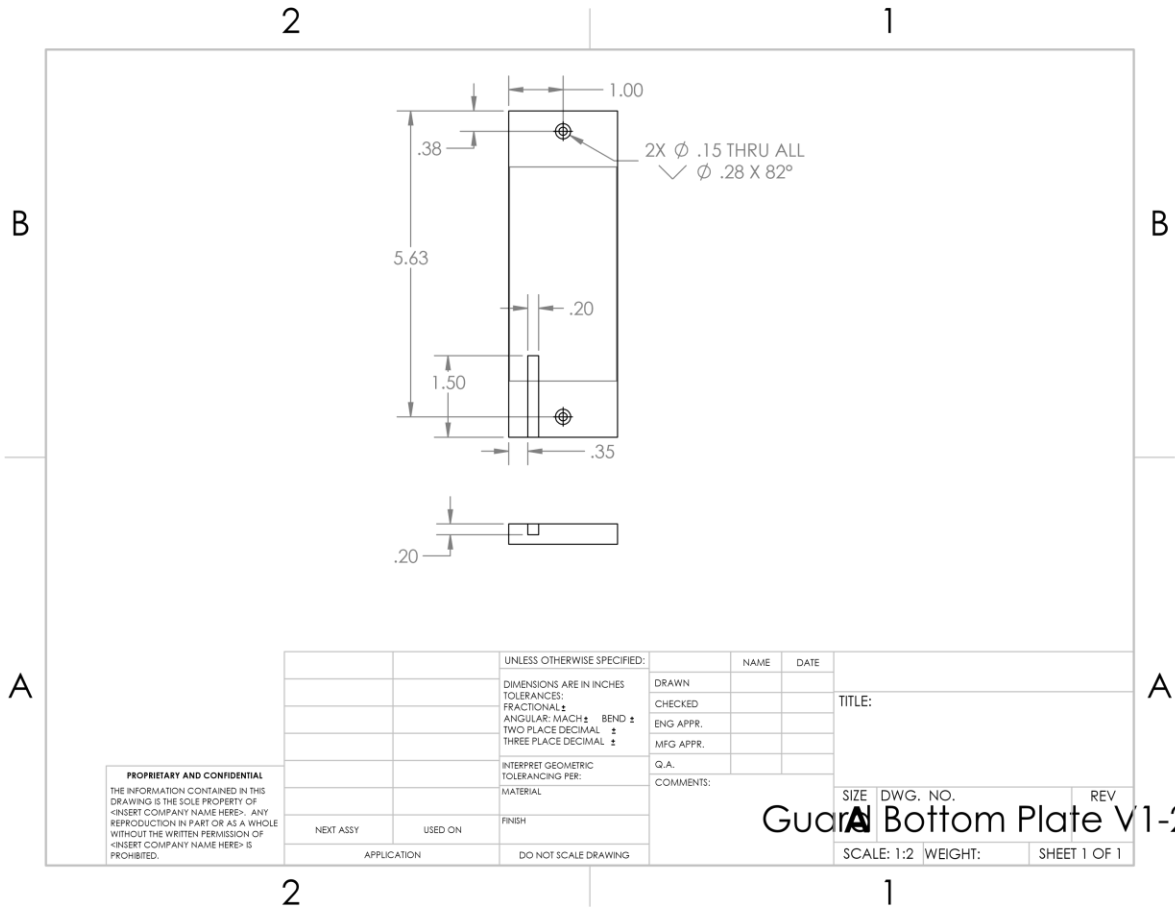
		UNLESS OTHERWISE SPECIFIED:		NAME	DATE
		DIMENSIONS ARE IN INCHES	DRAWN		
		TOLERANCES:	CHECKED		
		FRACTIONAL ±	ENG APPR.		
		ANGULAR: MACH ± BEND ±	MFG APPR.		
		TWO PLACE DECIMAL ±	Q.A.		
		THREE PLACE DECIMAL ±	COMMENTS:		
		INTERPRET GEOMETRIC TOLERANCING PER:			
		MATERIAL			
		FINISH			
NEXT ASSY	USED ON				
APPLICATION	DO NOT SCALE DRAWING				

TITLE:		
SIZE	DWG. NO.	REV
<b>Bottom Hot plate</b>		
SCALE: 1:2	WEIGHT:	SHEET 1 OF 1



**PROPRIETARY AND CONFIDENTIAL**  
 THE INFORMATION CONTAINED IN THIS DRAWING IS THE SOLE PROPERTY OF [INSERT COMPANY NAME HERE]. ANY REPRODUCTION IN PART OR AS A WHOLE WITHOUT THE WRITTEN PERMISSION OF [INSERT COMPANY NAME HERE] IS PROHIBITED.

		UNLESS OTHERWISE SPECIFIED:		NAME	DATE	
		DIMENSIONS ARE IN INCHES		DRAWN		
		TOLERANCES:		CHECKED		TITLE:
		FRACTIONAL: ±		ENG APPR.		
		ANGULAR: MACH ± BEND ±		MFG APPR.		
		TWO PLACE DECIMAL ±		Q.A.		
		THREE PLACE DECIMAL ±		COMMENTS:		
		INTERPRET GEOMETRIC TOLERANCING PER:				SIZE DWG. NO. REV
		MATERIAL				<b>A Cold Plate</b>
NEXT ASSY	USED ON	FINISH				
	APPLICATION	DO NOT SCALE DRAWING				SCALE: 1:4 WEIGHT: SHEET 1 OF 1

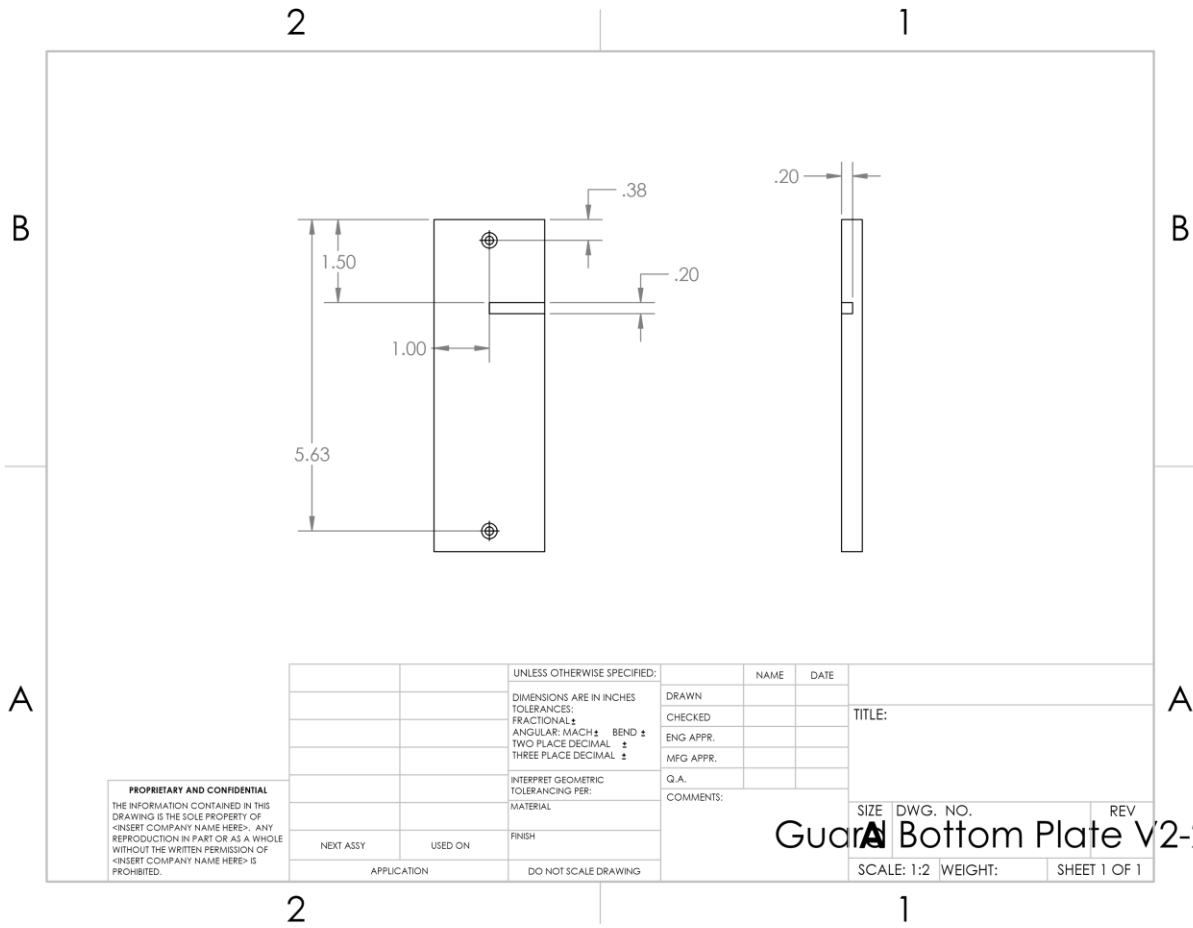


**PROPRIETARY AND CONFIDENTIAL**  
 THE INFORMATION CONTAINED IN THIS DRAWING IS THE SOLE PROPERTY OF <INSERT COMPANY NAME HERE>. ANY REPRODUCTION IN PART OR AS A WHOLE WITHOUT THE WRITTEN PERMISSION OF <INSERT COMPANY NAME HERE> IS PROHIBITED.

		UNLESS OTHERWISE SPECIFIED:	NAME	DATE
		DIMENSIONS ARE IN INCHES	DRAWN	
		TOLERANCES:	CHECKED	
		FRACTIONAL ±	ENG APPR.	
		ANGULAR: MACH ± BEND ±	MFG APPR.	
		TWO PLACE DECIMAL ±	Q.A.	
		THREE PLACE DECIMAL ±	COMMENTS:	
		INTERPRET GEOMETRIC TOLERANCING PER:		
		MATERIAL:		
NEXT ASSY	USED ON	FINISH		
APPLICATION		DO NOT SCALE DRAWING		

SIZE	DWG. NO.	REV
SCALE: 1:2	WEIGHT:	SHEET 1 OF 1

**Guard Bottom Plate V1-2**

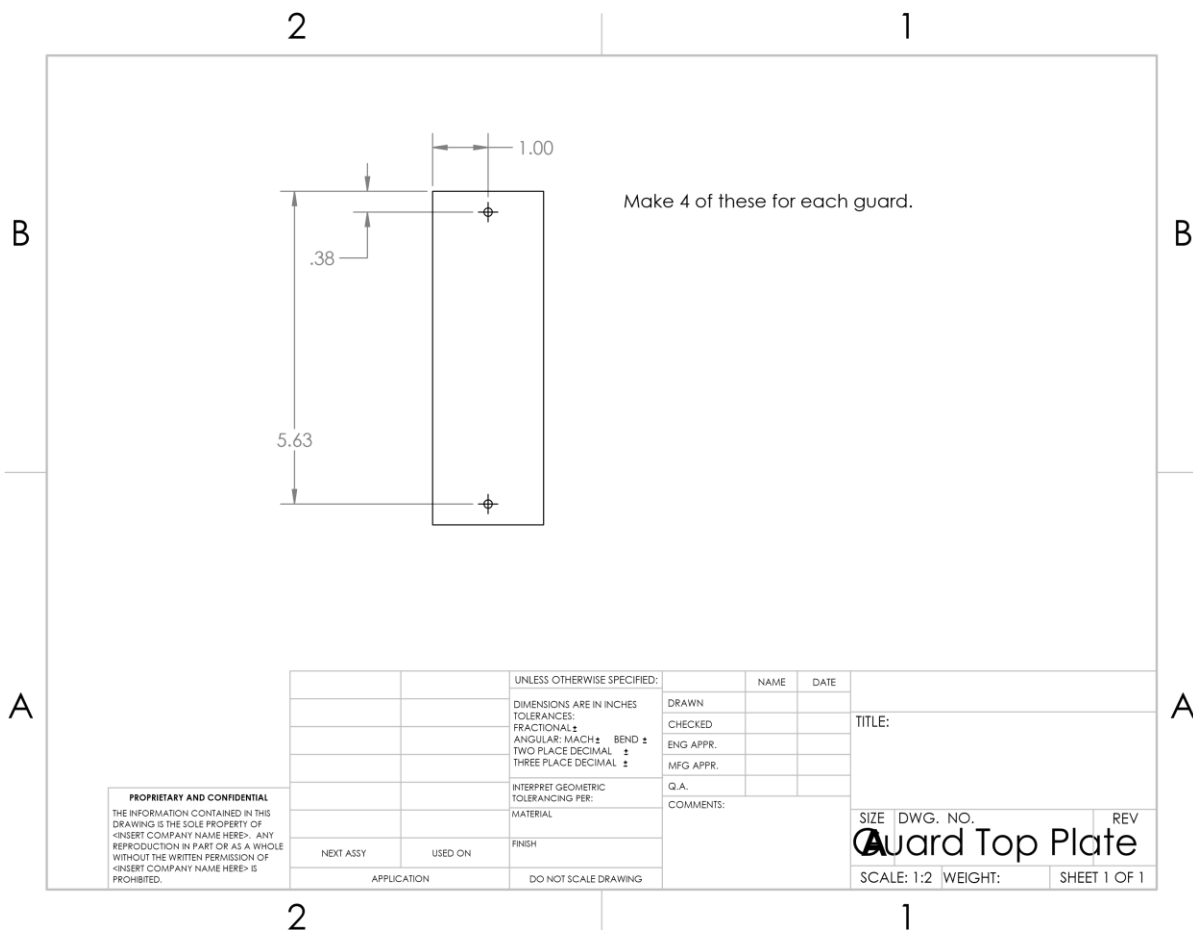


**PROPRIETARY AND CONFIDENTIAL**  
 THE INFORMATION CONTAINED IN THIS DRAWING IS THE SOLE PROPERTY OF <INSERT COMPANY NAME HERE>. ANY REPRODUCTION IN PART OR AS A WHOLE WITHOUT THE WRITTEN PERMISSION OF <INSERT COMPANY NAME HERE> IS PROHIBITED.

		UNLESS OTHERWISE SPECIFIED:	NAME	DATE
		DIMENSIONS ARE IN INCHES	DRAWN	
		TOLERANCES:	CHECKED	
		FRACTIONAL: ±	ENG APPR.	
		ANGULAR: MACH ± BEND ±	MFG APPR.	
		TWO PLACE DECIMAL: ±	Q. A.	
		THREE PLACE DECIMAL: ±	COMMENTS:	
		INTERPRET GEOMETRIC TOLERANCING PER:		
		MATERIAL		
NEXT ASSY	USED ON	FINISH		
APPLICATION		DO NOT SCALE DRAWING		

**Guard Bottom Plate V2-2**

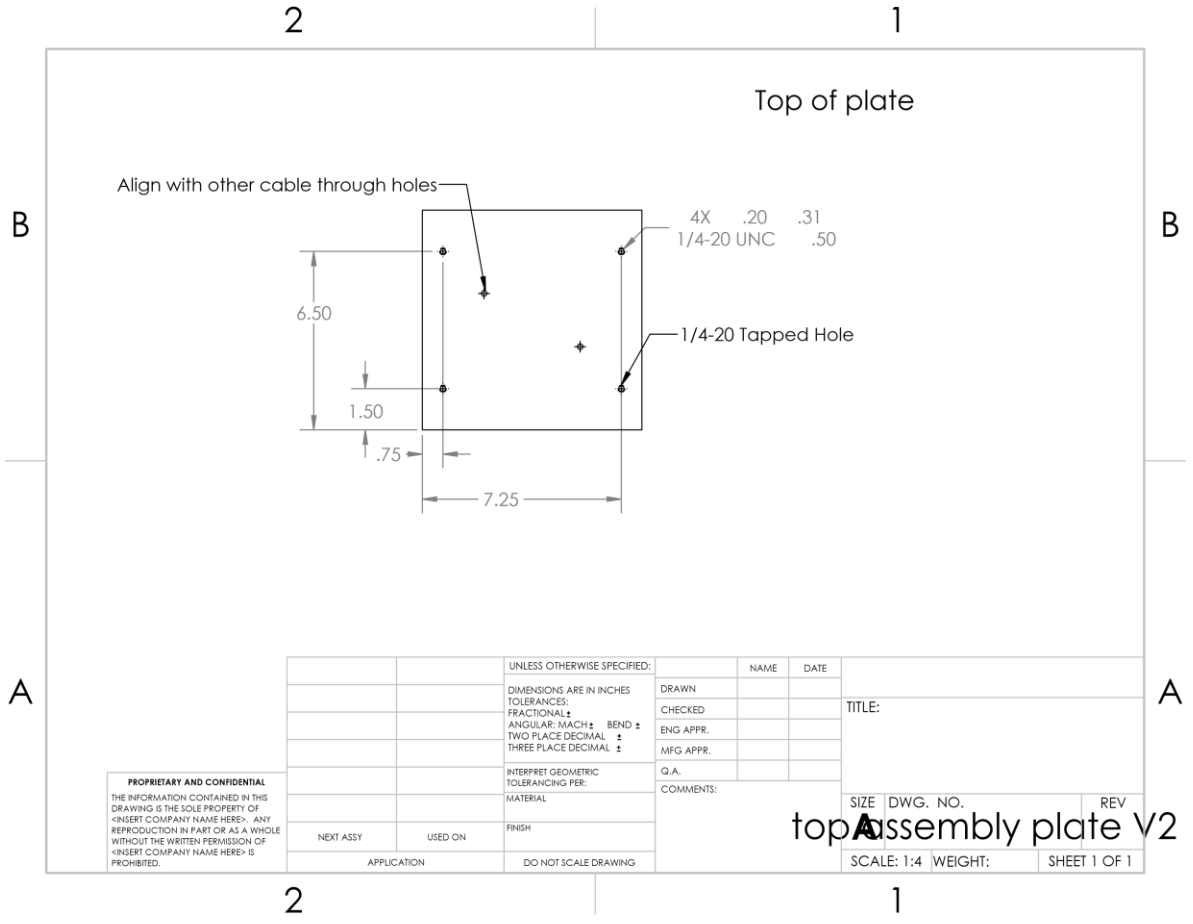
SIZE	DWG. NO.	REV
SCALE: 1:2	WEIGHT:	SHEET 1 OF 1



Make 4 of these for each guard.

**PROPRIETARY AND CONFIDENTIAL**  
 THE INFORMATION CONTAINED IN THIS DRAWING IS THE SOLE PROPERTY OF <INSERT COMPANY NAME HERE>. ANY REPRODUCTION IN PART OR AS A WHOLE WITHOUT THE WRITTEN PERMISSION OF <INSERT COMPANY NAME HERE> IS PROHIBITED.

		UNLESS OTHERWISE SPECIFIED:		NAME	DATE	
		DIMENSIONS ARE IN INCHES	DRAWN			TITLE:
		TOLERANCES:	CHECKED			
		FRACTIONAL ±	ENG APPR.			
		ANGULAR: MACH ± BEND ±	MFG APPR.			
		TWO PLACE DECIMAL ±	Q.A.			SIZE DWG. NO. REV <b>Guard Top Plate</b>
		THREE PLACE DECIMAL ±	COMMENTS:			
		INTERPRET GEOMETRIC TOLERANCING PER:				SCALE: 1:2 WEIGHT: SHEET 1 OF 1
		MATERIAL				
	NEXT ASSY	USED ON	FINISH			
		APPLICATION	DO NOT SCALE DRAWING			

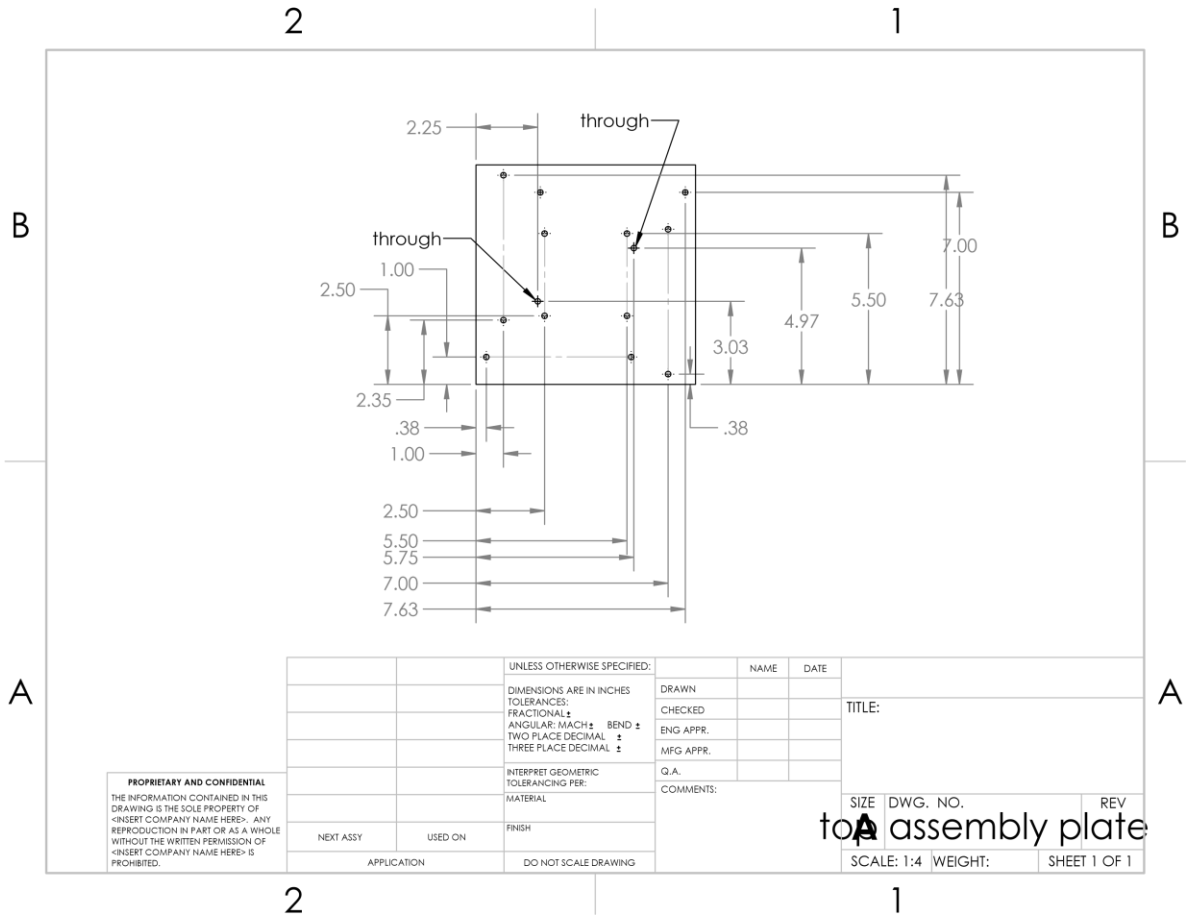


**PROPRIETARY AND CONFIDENTIAL**  
 THE INFORMATION CONTAINED IN THIS DRAWING IS THE SOLE PROPERTY OF [INSERT COMPANY NAME HERE]. ANY REPRODUCTION IN PART OR AS A WHOLE WITHOUT THE WRITTEN PERMISSION OF [INSERT COMPANY NAME HERE] IS PROHIBITED.

		UNLESS OTHERWISE SPECIFIED:		NAME	DATE	
		DIMENSIONS ARE IN INCHES	DRAWN			TITLE:
		TOLERANCES:	CHECKED			
		FRACTIONAL: ±	ENG APPR.			
		ANGULAR: MACH ± BEND ±	MFG APPR.			
		TWO PLACE DECIMAL ±	Q.A.			
		THREE PLACE DECIMAL ±	COMMENTS:			
		INTERPRET GEOMETRIC TOLERANCING PER:				SIZE DWG. NO. REV
		MATERIAL				
		FINISH				
NEXT ASSY	USED ON					
APPLICATION		DO NOT SCALE DRAWING				SCALE: 1:4 WEIGHT: SHEET 1 OF 1

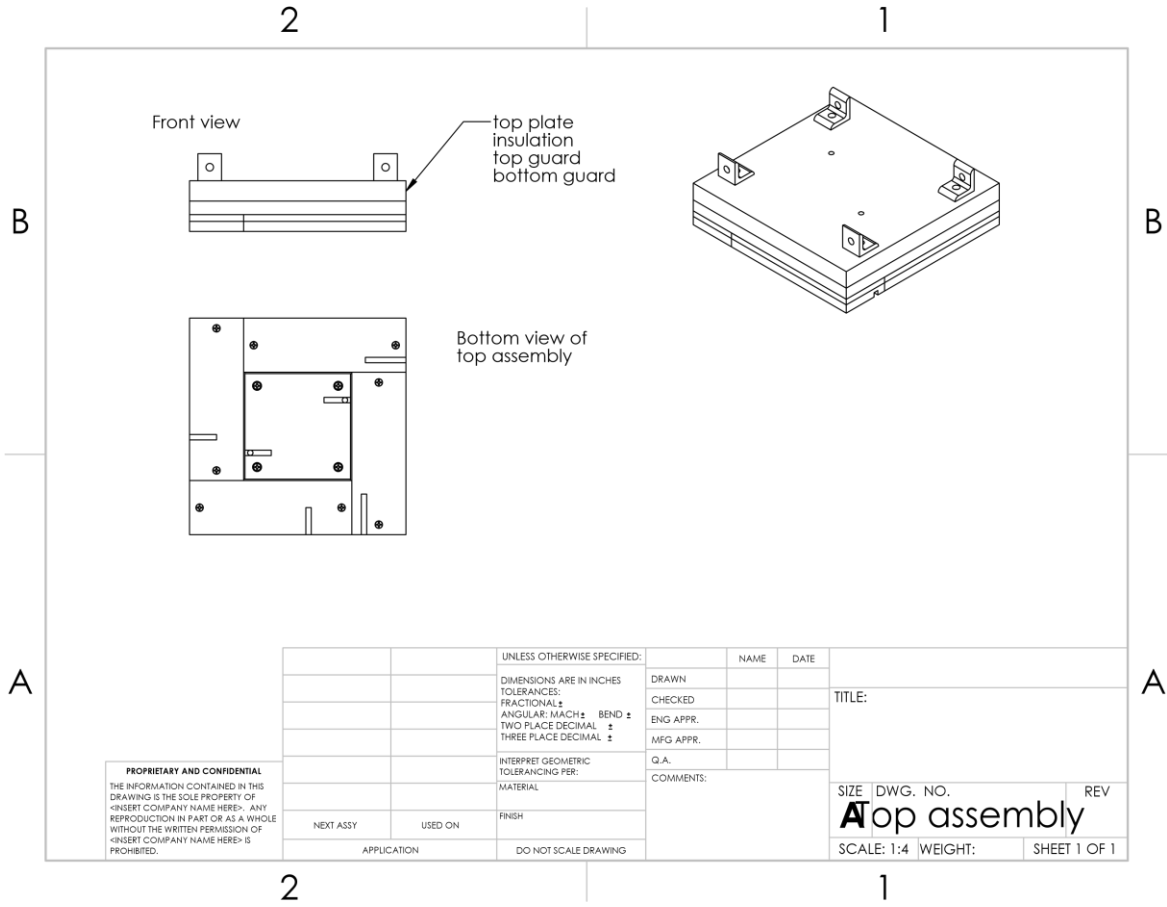
top Assembly plate V2





**PROPRIETARY AND CONFIDENTIAL**  
 THE INFORMATION CONTAINED IN THIS DRAWING IS THE SOLE PROPERTY OF <INSERT COMPANY NAME HERE>. ANY REPRODUCTION IN PART OR AS A WHOLE WITHOUT THE WRITTEN PERMISSION OF <INSERT COMPANY NAME HERE> IS PROHIBITED.

		UNLESS OTHERWISE SPECIFIED:	NAME	DATE	
		DIMENSIONS ARE IN INCHES	DRAWN		
		TOLERANCES:	CHECKED		TITLE:
		FRACTIONAL: ±	ENG APPR.		
		ANGULAR: MACH ± BEND ±	MFG APPR.		
		TWO PLACE DECIMAL ±	Q.A.		
		THREE PLACE DECIMAL ±	COMMENTS:		
		INTERPRET GEOMETRIC TOLERANCING PER:			SIZE DWG. NO. REV
		MATERIAL			to assembly plate
NEXT ASSY	USED ON	FINISH			SCALE: 1:4 WEIGHT: SHEET 1 OF 1
APPLICATION		DO NOT SCALE DRAWING			



## Guarded Hot Plate Coding

## Arduino Code

```

1  #include <Adafruit_INA260.h>
2  #include <OneWire.h>
3  #include <DallasTemperature.h>
4  #include <LiquidCrystal.h>
5
6
7
8  // setup interface with LCD display
9
10 const int RS = 13;
11 const int E = 12;
12 const int DB4 = 8;
13 const int DB5 = 7;
14 const int DB6 = 4;
15 const int DB7 = 2;
16
17 LiquidCrystal LCD(RS, E, DB4, DB5, DB6, DB7);
18
19 // Setup temperatures sensors
20
21 // Data wire is plugged into digital pin 5 on the Arduino
22 #define ONE_WIRE_BUS 5
23
24 // Setup a oneWire instance to communicate with any OneWire device
25 OneWire oneWire(ONE_WIRE_BUS);
26
27 // Pass oneWire reference to DallasTemperature library
28 DallasTemperature sensors(&oneWire);
29
30
31
32 // setup power meter chip and set Digital averaging filter
33
34 Adafruit_INA260 ina260 = Adafruit_INA260();
35
36
37
38
39
40 // Setup variables for temperature reading
41 // addresses on temperature sensors by orientation
42
43 uint8_t sensor1[8] = { 0x28, 0xF4, 0x59, 0x6A, 0x0A, 0x00, 0x00, 0x37 }; //guard 4 right
44 uint8_t sensor2[8] = { 0x28, 0x9C, 0xC0, 0x69, 0x0A, 0x00, 0x00, 0x99 }; //hot Plate 1
45 uint8_t sensor3[8] = { 0x28, 0xC1, 0x36, 0x6A, 0x0A, 0x00, 0x00, 0x4F }; //guard 3 back
46 uint8_t sensor4[8] = { 0x28, 0xB1, 0x54, 0x6A, 0x0A, 0x00, 0x00, 0x45 }; //hot plate 2
47 uint8_t sensor5[8] = { 0x28, 0xD5, 0xD4, 0x69, 0x0A, 0x00, 0x00, 0x19 }; // guard 2 left
48 uint8_t sensor6[8] = { 0x28, 0x1D, 0xC4, 0x69, 0x0A, 0x00, 0x00, 0x5B }; //COLD plate 2
49 uint8_t sensor7[8] = { 0x28, 0x63, 0x79, 0x13, 0x0B, 0x00, 0x00, 0x6B }; //cold plate 1
50 uint8_t sensor8[8] = { 0x28, 0x4F, 0xE8, 0x69, 0x0A, 0x00, 0x00, 0xC2 }; //guard 1 Front
51
52 float T_guard1 = 0;
53 float T_guard2 = 0;
54 float T_guard3 = 0;
55 float T_guard4 = 0;
56 float T_top1 = 0;
57 float T_top2 = 0;
58 float T_bottom1 = 0;
59 float T_bottom2 = 0;
60 float MplateTemp = 0;
61
62
63
64 // store old temperatures values
65
66 float OT_guard1 = 0;
67 float OT_guard2 = 0;
68 float OT_guard3 = 0;
69 float OT_guard4 = 0;

```

```

70 float OT_top1 = 0;
71 float OT_top2 = 0;
72 float OT_bottom1 = 0;
73 float OT_bottom2 = 0;
74 float OMplateTemp = 0;
75
76 //Store Heating outputs
77
78 float H_guard1 = 0;
79 float H_guard2 = 0;
80 float H_guard3 = 0;
81 float H_guard4 = 0;
82 float H_metered = 0;
83
84 //Store Old Heating outputs
85
86 float OH_guard1 = 11;
87 float OH_guard2 = 11;
88 float OH_guard3 = 11;
89 float OH_guard4 = 11;
90 float OH_metered= 11;
91
92 // Store Heating output pins
93 const int guard1Pin = 3;
94 const int guard2Pin = 6;
95 const int guard3Pin = 9;
96 const int guard4Pin = 10;
97 const int meteredPin = 11;
98
99 // setup power storing variable
100 float power = 0;
101
102 // set desired temperature
103
104 float desHPT = 30;
105
106 //setup startup button
107
108 const int resetPin = A2;
109 bool go = false;
110 bool Reset = false;
111
112
113 // define function for codes
114
115 void getTemperatures() {
116
117     sensors.requestTemperatures();
118     delay(250);
119
120
121 float checkTemp1 = 0;
122 float checkTemp2 = 0;
123 float checkTemp3 = 0;
124 float checkTemp4 = 0;
125 float checkTemp5 = 0;
126 float checkTemp6 = 0;
127 float checkTemp7 = 0;
128 float checkTemp8 = 0;
129
130
131 OT_guard1 = T_guard1;
132 OT_guard2 = T_guard2;
133 OT_guard3 = T_guard3;
134 OT_guard4 = T_guard4;
135 OT_top1 = T_top1;
136 OT_top2 = T_top2;
137 OT_bottom1 = T_bottom1;
138 OT_bottom2 = T_bottom2;

```

```

139     OMplateTemp = (OT_top1 + OT_top2) / 2.;
140
141     checkTemp8 = sensors.getTempC(sensor8);
142     if(checkTemp8 > 5) { T_guard1 = checkTemp8;}
143
144
145     checkTemp5 = sensors.getTempC(sensor5);
146     if(checkTemp5 > 5) { T_guard2 = checkTemp5;}
147
148
149     checkTemp3 = sensors.getTempC(sensor3);
150     if(checkTemp3 > 5) { T_guard3 = checkTemp3;}
151
152
153     checkTemp1 = sensors.getTempC(sensor1);
154     if(checkTemp1 > 5) { T_guard4 = checkTemp1;}
155
156     checkTemp2 = sensors.getTempC(sensor2);
157     if( checkTemp2 > 5) {T_top1 = 1.021*checkTemp2-0.5145;}
158
159     checkTemp4 = sensors.getTempC(sensor4);
160     if( checkTemp4 > 5) {T_top2 = 1.011*checkTemp4-0.207;}
161
162     checkTemp7 = sensors.getTempC(sensor7);
163     if( checkTemp7 > 5) {T_bottom1 = 1.009*checkTemp7-0.208;}
164
165     checkTemp6 = sensors.getTempC(sensor6);
166     if( checkTemp6 > 5) {T_bottom2 = 1.002*checkTemp6+.005;}
167
168
169     MplateTemp = (T_top1 + T_top2) / 2.;
170
171     power = ina260.readBusVoltage()/1000. * ina260.readCurrent()/1000.;
172
173 }
174
175
176
177
178 bool changePI = false;
179
180
181 // setup PI control heating Cycle
182
183 void heatingCycle() {
184
185     getTemperatures();
186     delay(275);
187     // PI constants for guard plates
188
189     float H = 0.5;
190     float Kp = 0.5;
191     float Ti = 4;
192
193     if (changePI){
194
195     Kp = 0.5;
196     Ti = 8;
197     }
198
199     else{
200     Kp = 1;
201     Ti = 2;
202     }
203
204
205     float changeguard1;
206     float changeguard2;
207     float changeguard3;

```

```

208     float changeguard4;
209     float changemetered;
210
211
212
213     changeguard1 = Kp*(H/(2*Ti)+1)*(desHPT - T_guard1) + Kp*(H/(2*Ti)-1)*(desHPT -
OT_guard1);
214     changeguard2 = Kp*(H/(2*Ti)+1)*(desHPT - T_guard2) + Kp*(H/(2*Ti)-1)*(desHPT -
OT_guard2);
215     changeguard3 = Kp*(H/(2*Ti)+1)*(desHPT - T_guard3) + Kp*(H/(2*Ti)-1)*(desHPT -
OT_guard3);
216     changeguard4 = Kp*(H/(2*Ti)+1)*(desHPT - T_guard4) + Kp*(H/(2*Ti)-1)*(desHPT -
OT_guard4);
217     changemetered = Kp*(H/(2*Ti)+1)*(desHPT - MplateTemp) + Kp*(H/(2*Ti)-1)*(desHPT -
OMplateTemp);
218
219     H_guard1 = constrain(OH_guard1 + changeguard1,0,255);
220     H_guard2 = constrain(OH_guard2 + changeguard2,0,255);
221     H_guard3 = constrain(OH_guard3 + changeguard3,0,255);
222     H_guard4 = constrain(OH_guard4 + changeguard4,0,255);
223     H_metered =constrain(OH_metered+changemetered,0,255);
224
225     if(desHPT - T_guard1 > -0.2){analogWrite(guard1Pin, H_guard1);}
226     else {analogWrite(guard1Pin, 0);}
227
228     if(desHPT - T_guard2 > -0.2){analogWrite(guard2Pin, H_guard2);}
229     else {analogWrite(guard2Pin, 0);}
230
231     if(desHPT - T_guard3 > -0.2){analogWrite(guard3Pin, H_guard3);}
232     else {analogWrite(guard3Pin, 0);}
233
234     if(desHPT - T_guard4 > -0.2){analogWrite(guard4Pin, H_guard4);}
235     else {analogWrite(guard4Pin, 0);}
236
237     if(desHPT - MplateTemp > -0.2){analogWrite(meteredPin, H_metered);}
238     else {analogWrite(meteredPin, 0);}
239
240
241
242     OH_guard1 = H_guard1;
243     OH_guard2 = H_guard2;
244     OH_guard3 = H_guard3;
245     OH_guard4 = H_guard4;
246     OH_metered =H_metered;
247
248 }
249
250 bool checkStablize() {
251
252     bool yes = true;
253
254     float check = 0;
255     float thresh = 0.2;
256
257     // Check Hot Plate Assembly
258
259     check = abs(desHPT - MplateTemp);
260     if(check > thresh) {yes = false;}
261     check = abs(desHPT - T_guard1);
262     if(check > thresh) {yes = false;}
263     check = abs(desHPT - T_guard2);
264     if(check > thresh) {yes = false;};
265     check = abs(desHPT - T_guard3);
266     if(check > thresh) {yes = false;};
267     check = abs(desHPT - T_guard4);
268     if(check > thresh) {yes = false;};
269
270     //check cold plate assembly
271     /*

```

```

272     check = abs(desHPT - T_bottom1 - 15 );
273     if(check > thresh) {yes = false;};
274     check = abs(desHPT - T_bottom2 - 15);
275     if(check > thresh) {yes = false;};
276 */
277
278     return(yes);
279 }
280
281
282
283
284 void dispStartingMenu() {
285     LCD.clear();
286     LCD.setCursor(0,0);
287     String message = "Push Left:start";
288     LCD.print(message);
289 }
290
291 void dispHeating() {
292
293     LCD.clear();
294     LCD.setCursor(0,0);
295     String message = "Heat Up: " + String(MplateTemp);
296     String m2 = "Push right:stop";
297     LCD.print(message);
298     LCD.setCursor(0,1);
299     LCD.print(m2);
300
301 }
302
303
304
305 void dispstabilizing(int i) {
306
307     LCD.clear();
308     LCD.setCursor(0,0);
309     String message;
310     String m2 = "Push right:stop";
311     if(changePI){message = "hold V: "+String(i/12)+"/150";}
312     else{message = "hold T: "+String(i/12)+"/150";}
313     LCD.print(message);
314     LCD.setCursor(0,1);
315     LCD.print(m2);
316
317 }
318
319 void dispRecord () {
320
321     float sum = 0;
322     LCD.clear();
323     LCD.setCursor(0,0);
324     String message = "recording..";
325     String m2 = "Push right:stop";
326     LCD.print(message);
327     LCD.setCursor(0,1);
328     LCD.print(m2);
329
330 }
331
332 void DispHold(int itt){
333     LCD.clear();
334     LCD.setCursor(0,0);
335     String message = "holding: " + String(itt) + "time";
336     String m2 = "Push right:stop";
337     LCD.print(message);
338     LCD.setCursor(0,1);
339     LCD.print(m2);
340 }

```

```

341
342 // this function sends data to the python script
343
344 void recordData() {
345     float sum = 0;
346
347
348
349
350     Serial.println(power,4);
351     sum = sum + power;
352
353
354
355     // record temperatures
356     Serial.println(T_top1);
357     sum = sum + T_top1;
358     Serial.println(T_top2);
359     sum = sum + T_top2;
360     Serial.println(T_bottom1);
361     sum = sum + T_bottom1;
362     Serial.println(T_bottom2);
363     sum = sum + T_bottom2;
364     Serial.println(T_guard1);
365     sum = sum + T_guard1;
366     Serial.println(T_guard2);
367     sum = sum + T_guard2;
368     Serial.println(T_guard3);
369     sum = sum + T_guard3;
370     Serial.println(T_guard4);
371     sum = sum + T_guard4;
372     Serial.println(H_guard1/255.,3);
373     sum = sum + (H_guard1/255.);
374     Serial.println(H_guard2/255.,3);
375     sum = sum + (H_guard2/255.);
376     Serial.println(H_guard3/255.,3);
377     sum = sum + (H_guard3/255.);
378     Serial.println(H_guard4/255.,3);
379     sum = sum + (H_guard4/255.);
380     Serial.println(sum);
381
382 }
383
384
385
386 void setup() {
387     // put your setup code here, to run once:
388
389     Serial.begin(9600);
390     LCD.begin(20,2);
391     sensors.begin();
392
393     ina260.begin();
394     ina260.setAveragingCount(INA260_COUNT_64);
395     Serial.println(ina260.getAveragingCount());
396
397
398
399     pinMode(resetPin, INPUT);
400     pinMode(guard1Pin, OUTPUT);
401     pinMode(guard2Pin, OUTPUT);
402     pinMode(guard3Pin, OUTPUT);
403     pinMode(guard4Pin, OUTPUT);
404     pinMode(meteredPin, OUTPUT);
405
406
407     analogWrite(meteredPin,0);
408     analogWrite(guard2Pin,0);
409     analogWrite(guard3Pin,0);

```



```

410     analogWrite(guard4Pin,0);
411     analogWrite(guard1Pin,0);
412
413     getTemperatures();
414     delay(250);
415     getTemperatures();
416
417
418
419 }
420
421 void loop() {
422
423
424     // Starting menu Code
425     dispStartingMenu();
426     while(go == false) {
427
428         go = digitalRead(resetPin) == HIGH;
429         dispTemps();
430         getTemperatures();
431         delay(500);
432
433     }
434
435     go = false;
436
437     // Heating up phase of exteriment
438     dispHeating();
439
440     //fastheatup ();
441
442     delay(3000);
443
444
445
446     bool ready2record = false;
447     int i = -1;
448     int ij = 1;
449     int heatsd = 0;
450     int enterHS = 0;
451     bool ready2stablize = false;
452     while(ready2record == false && Reset == false) {
453         heatingCycle();
454         delay(500);
455
456
457         ready2stablize = checkStablize();
458
459         ij++;
460
461         if (ready2stablize) {
462             i++;
463             if(i % 12 ==0) {
464                 if(changePI) {
465                     //Serial.println("stablizing temperature: " + String(i/12) + "/" +
466                                     String(900/12));
467                     dispstablizing(i); //to LCD display
468                 }
469                 else{
470                     //Serial.println("stablizing power: " + String(i/12) + "/" + String(900/12));
471                     dispstablizing(i); //to LCD display
472                 }
473             }
474             if (i > 60) {changePI = true;}
475
476
477

```

```

478
479     if (i > 1800) {
480         //Hold heat stable
481         //     enterHS++;
482         //     DispHold(enterHS);
483         //
484         //     while( heatsd < 20*60 && Reset == false){
485         //
486         //         Reset = digitalRead(resetPin) == HIGH;
487         //         delay(1000);
488         //         heatsd++;
489         //
490         //     }
491         //
492         //     getTemperatures();
493         //     delay(500);
494         //
495         ready2record = checkStablize();
496
497
498     }
499
500 }
501
502 else {
503     i=0;
504     dispHeating();
505
506 }
507 if(ij % 12 == 0){ dispTemps(); ij=1;}
508 Reset = digitalRead(resetPin) == HIGH;
509
510
511 }
512
513
514 int j = 0;
515
516 // Start Collecting Data once SS is reached,
517
518 Serial.println("Ready");
519 dispRecord();
520
521
522 while(Reset == false) {
523
524     // get temperature, control heaters, etc
525     heatingCycle();
526     getTemperatures();
527     delay(1000);
528     showRecord(j/60);
529     //dispTemps();
530
531     Reset = digitalRead(resetPin) == HIGH;
532
533
534     if( j % 60 == 0) {recordData(); }
535
536     if(j > 1800) {Reset = true;}
537
538     j++;
539
540
541 }
542
543 // Done with experiment
544
545
546 Reset = false;

```

```

547 changePI =false;
548 Serial.println("Done");
549
550 analogWrite(meteredPin,0);
551 analogWrite(guard2Pin,0);
552 analogWrite(guard3Pin,0);
553 analogWrite(guard4Pin,0);
554 analogWrite(guard1Pin,0);
555
556 delay(5000);
557
558 }
559
560
561
562 void showRecord (int stepps) {
563
564
565     LCD.clear();
566     LCD.setCursor(0,0);
567     String message = "record: " + String(stepps) + "/30";
568     String m2 = "Push right:stop";
569     LCD.print(message);
570     LCD.setCursor(0,1);
571     LCD.print(m2);
572
573 }
574
575 void fastheatup () {
576
577     int t = 30000;
578
579     analogWrite(meteredPin,255);
580     analogWrite(guard2Pin,255);
581     analogWrite(guard3Pin,255);
582     analogWrite(guard4Pin,255);
583     analogWrite(guard1Pin,255);
584     delay(t);
585     analogWrite(meteredPin,0);
586     analogWrite(guard2Pin,0);
587     analogWrite(guard3Pin,0);
588     analogWrite(guard4Pin,0);
589     analogWrite(guard1Pin,0);
590
591
592
593 }
594
595 void dispTemps () {
596
597     Serial.print(T_guard1); Serial.print("\t");
598     Serial.print(T_guard2); Serial.print("\t");
599     Serial.print(T_guard3); Serial.print("\t");
600     Serial.print(T_guard4); Serial.print("\t");
601     Serial.print(T_top1); Serial.print("\t");
602     Serial.print(T_top2); Serial.print("\t");
603     Serial.print(T_bottom1); Serial.print("\t");
604     Serial.print(T_bottom2); Serial.print("\t");
605
606     //Serial.println("ut");
607
608     Serial.print(H_guard1 / 255.,3); Serial.print("\t");
609     Serial.print(H_guard2 / 255.,3); Serial.print("\t");
610     Serial.print(H_guard3 / 255.,3); Serial.print("\t");
611     Serial.print(H_guard4 / 255.,3); Serial.print("\t");
612     Serial.print(H_metered / 255.,3); Serial.print("\t");
613     Serial.print(ina260.readBusVoltage()/1000.,3); Serial.print("\t");
614     Serial.print(ina260.readCurrent()/1000.,3); Serial.print("\t");
615     Serial.println(ina260.readBusVoltage()/1000. * ina260.readCurrent()/1000.,4);

```

## Python Code

```

1  # -*- coding: utf-8 -*-
2  """
3  Created on Wed Jan 27 12:47:58 2021
4
5  @author: tmtchell
6  """
7
8  # arduino example get data and store in variable
9
10
11
12  # import packages for code
13
14
15
16  import numpy as np;
17  import pandas as pd;
18  import datetime;
19  import serial;
20
21
22
23  # update these items for each test
24
25  filename = "Hemp_r1s1_expl.xlsx"
26
27  thickness = (40.7+42.4+40.1+41.3)/4 # in mm
28
29  filename2 = "warmup_r1s1_expl.xlsx"
30
31
32
33
34  # Connect to arduino
35
36  try:
37      arduino = serial.Serial('COM4',timeout= None,baudrate=9600)
38      print('connected')
39  except:
40      print("ERROR: Please check the port")
41
42
43  area = 0.010066109 # in meters^2
44
45  # Setup Initial Variables
46
47  errmsg = " "
48
49  DataCols = 14
50  e = 1
51  h = 0
52  S = True
53  warmup=True
54  suData = np.zeros((1,DataCols))
55  Sero = np.array([])
56  r_warmup = np.array([])
57
58
59  while warmup:
60
61      serByte = arduino.readline()
62      print(serByte.decode().rstrip())
63      r_warmup= np.append(r_warmup,serByte.decode())
64
65      if serByte.decode().rstrip() == "Ready":
66          warmup=False
67          break

```

```

68
69
70 ss = [" "]
71 pd.DataFrame(r_warmup).to_excel(filename2, header = False, index = False)
72
73 while S:
74     while e <= DataCols:
75         serByte = arduino.readline()
76
77         if serByte.decode().rstrip() == "Done":
78             S=False
79             break
80
81         try:
82             Sero= np.append(Sero,float(serByte.decode()))
83         except:
84             print('not a number')
85
86         e=e+1
87
88     if S:
89         blank = S
90     else:
91         continue;
92
93     ss.append(datetime.datetime.now())
94
95     try:
96         suData= np.append(suData,[Sero], axis = 0)
97     except:
98         print('bad connection')
99
100     e=1;
101     h=h+1;
102     Sero = np.array([])
103
104 # done recording values, organize collected data
105 print("done recording values")
106
107 Data = np.delete(suData,0,0)
108 ss.remove(" ")
109 arduino.close()
110
111 header = ['Sample Name', 'value1', 'value', 'check sum',"errors",]
112
113 # check Data for any errors: Addition Test
114
115 i = 0
116 err = 0
117 adderror=False;
118
119 for rows in Data:
120     check = round(sum(rows)-rows[-1],2)
121     if abs(check - rows[-1]) > 0.08:
122         print(check - rows[-1])
123         err+=1
124         adderror = True;
125
126     i=i+1

```

```

135
136
137 if adderror:
138     err+=1;
139     print("found " + str(err) + " errors in the addition test")
140     errmsg = errmsg + str(err) + "errors in serial input"
141
142 else:
143
144     print("Data Passed addition test")
145
146
147
148 # check Lateral heat distrubution
149
150
151 laterrH = False
152 laterrC = False
153
154 errmsga = " "
155 errmsgb = " "
156
157 hplate =
158     np.array([Data[:,1],Data[:,2],Data[:,5],Data[:,6],Data[:,7],Data[:,8]]).transpose()
159     latfaults =0
160
161
162 for rows in hplate:
163
164     maxtemp = max(rows)
165     mintemp = min(rows)
166
167     if maxtemp-mintemp > 0.2:
168
169         laterrH = True
170         latfaults +=1
171         errmsga = str(latfaults) + " lateral faults detected in hot plate, "
172
173
174
175 Cplate = np.array([Data[:,3],Data[:,4]]).transpose()
176 latfaults =0
177
178
179
180 for rows in Cplate:
181
182     maxtemp = max(rows)
183     mintemp = min(rows)
184     if maxtemp-mintemp > 0.2:
185
186         laterrC = True
187         latfaults +=1
188         errmsgb = str(latfaults) + " lateral faults detected in Cold plate, "
189
190
191
192 if laterrH:
193     errmsg = errmsg + errmsga
194     print(errmsga)
195
196 if laterrC:
197     errmsg = errmsg + errmsgb
198     print(errmsgb)
199
200 if not (laterrH or laterrC):

```

```

201     print("Passed lateral temperature check")
202
203
204 # calculate average thermal conductivity
205
206
207 Power = Data[:,0];
208 i=0
209
210 T_hot = np.zeros(len(Power))
211 T_cold = np.zeros(len(Power))
212 k = np.zeros(len(Power))
213
214 for rows in Data:
215
216     T_hot[i] = (rows[1]+rows[2])/2
217     T_cold[i] = (rows[3]+rows[4])/2
218     i+=1
219
220
221 for idx,x in np.ndenumerate(Power):
222     k[idx] = (thickness/1000)*(Power[idx]) / (area * (T_hot[idx] - T_cold[idx]))
223
224 # Combine all Data into a formatted excel Table
225
226
227 if errmsg == " ":
228
229     errmsg = "no errors ocured"
230     print("No errors found")
231
232
233 summary1 = pd.DataFrame({0:"thickness",1:thickness,2:"K value", 3:k.mean(),4:"error
check",5:errmsg,}, index= [1])
234 addblank= pd.DataFrame({0:" ", 1:" ",2:" ",3:" ",4:" "}, index=[2])
235 Rowlabels = pd.DataFrame({0:"Date", 1:"metered Power",2:"Metered hot plate temp
1",3:"Metered hot plate temp 2",
236                        4:"Cold Plate Temp 1",5:"Cold Plate Temp 2",6:"guard 1
Temp",7:"guard 2 Temp",8:"guard 3 temp",
237                        9:"guard 4 Temp",10:"guard 1 Duty cycle",11:"guard 2 Duty
Cycle",12:"guard 3 duty cycle",13:"guard 4 duty cycle",
238                        14:"SumCheck",15:"k value"}, index = [0])
239
240
241 dfData = pd.DataFrame({
242     0:ss,
243     1:Data[:,0],
244     2:Data[:,1],
245     3:Data[:,2],
246     4:Data[:,3],
247     5:Data[:,4],
248     6:Data[:,5],
249     7:Data[:,6],
250     8:Data[:,7],
251     9:Data[:,8],
252     10:Data[:,9],
253     11:Data[:,10],
254     12:Data[:,11],
255     13:Data[:,12],
256     14:Data[:,13],
257     15:k})
258
259
260 output = pd.concat([Rowlabels,dfData]).reset_index(drop = True)
261 output = pd.concat([addblank,output]).reset_index(drop = True)
262 output = pd.concat([summary1,output]).reset_index(drop = True)
263 output = output.drop(columns=[14])

```

```
264
265
266 output.to_excel(filename, header = False, index = False)
267
268
269
270 print("file successfully saved: experiment is over")
```



## Guarded Hot Plate Bill of Materials

Categories	Item	Description	Supplier	Unit Price	Qty.	Total Cost
Hot Plate Assembly	Aluminum top connector	8x8x0.75 in.	McMaster Carr	\$49.71	1	\$49.71
Hot Plate Assembly	Aluminum bottom guard plates	6x2x0.375 in	McMaster Carr	\$4.62	4	\$18.48
Hot Plate Assembly	Aluminum top guard Plates	6x2x0.25 in	McMaster Carr	\$2.91	4	\$11.64
Hot plate assembly	Aluminum Metered top and Bottom plates	12x4x.375 in	McMaster Carr	\$13.97	1	\$13.97
Cold plate assembly	Aluminum cold plate	8x8x0.375 in.	McMaster Carr	\$26.11	1	\$26.11
Framing	80/20 t-slot framing	10 ft in total	McMaster Carr	\$30.54	1	\$30.54
Framing	Bottom base plate	8x12x1/8	McMaster Carr	\$47.76	1	\$47.76
Framing	Frame dead bolt latches		McMaster Carr	\$20.95	2	\$41.90
Framing	T-slotted brackets		McMaster Carr	\$5.21	14	\$72.94
Framing	T-slotted bracket screws		McMaster Carr	\$1.85	8	\$14.80
Other	6-32 screws		McMaster Carr	\$9.84	1	\$9.84
Framing	T-slotted brackets		McMaster Carr	\$5.21	6	\$31.26
Cold plate Assembly	Water cooled heat sink	6 pass, 3/8 diameter,	Allied Electronics	\$98.37	1	\$98.37
Electronics	MOSFET Transistors		Amazon	\$7.99	1	\$7.99
Electronics	Temperature sensors	DS18B20	Digikey	\$3.92	8	\$31.36
Electronics	Electric heater pad	10x5cm	Adafruit	\$3.95	5	\$19.75
Electronics	12 volt power supply		Amazon	\$15.90	1	\$15.90
Cold plate assembly	Constant temperature water bath		Cole-Palmer	\$2,976.00	1	\$2,976.00
Other	Thermal Compound		Allied Electronics	\$26.44	1	\$26.44
Other	DI water		Grocery store	\$2.5	2	\$5.00
Electronics	RC Resistor		Digikey	\$2.28	1	\$2.28
Other	Cast acrylic Sheet	12x12x1/4	McMaster Carr	\$18.38	1	\$18.38
Electronics	Current / voltage sensor	INA260	Amazon	\$13.74	1	\$13.74
Electronics	Arduino starter kit		Amazon	\$109.9	1	\$109.90
Electronics	Breadboards		Amazon	\$6.99	1	\$6.99
Electronics	DC motor driver	DRV8871	Amazon	\$12.71	1	\$12.71
					Total	\$3,713.76

## Appendix C: Life Cycle Analysis Details

### Section 1. Pre-Manufacturing Embodied Energy Calculation Tables

#### Wood-framed wall details

Name of Material	EE Density from ICE Database (MJ/kg)	Density of Material (kg/m <sup>3</sup> )	Volume of Material (ft <sup>3</sup> )	Total EE (MJ)
Gypsum Board	1.8	800	2.67	108.75
2x6-Wood Stud (16-in OC)	7.4	530	3.67	407.22
Batt Insulation	28	12	25.75	245.02
OSB sheathing	15	700	2.67	792.97
Tyvek Weather Barrier	76.7	970	0.03	73.03
Exterior Cladding	7.4	530	2.67	296.19

#### SIPs wall details

Name of Material	EE Density from ICE Database (MJ/kg)	Density of Material (kg/m <sup>3</sup> )	Volume of Material (ft <sup>3</sup> )	Total EE (MJ)
½-in wood Cladding (Soft Sawn)	7.4	530	2.66	296.1
furring strip(1x2x8)	7.4	530	0.37	41.64
Tyvek weather barrier	76.7	970	0.03	73.03
OSB ½-in	15	700	2.33	693.66
6 in EPS insulation	88.6	23	30	1,731
OSB ½-in	15	700	2.33	693.66
½-in. Gypsum Board	1.8	800	2.67	108.75

## 3D-print wall details

Name of Material	EE Density from ICE Database (MJ/kg)	Density of Material (kg/m <sup>3</sup> )	Volume of Material (ft <sup>3</sup> )	Total EE (MJ)
Gypsum Board	1.8	800	2.667	108.75
3D end Panel (estimated)	6.015	612	2.667	277.99
3D wood structural Matrix (estimated)	6.015	612	3.667	382.20
Cellulose insulation	3.3	43	25.75	103.47
3D end Panel (estimated)	6.015	612	2.667	277.99
Tyvek weather barrier	76.7	970	0.034	73.03
exterior Cladding	7.4	530	2.667	96.19

## CMU wall details

Name of Material	EE Density from ICE Database (MJ/kg)	Density of Material (kg/m <sup>3</sup> )	Volume of Material (ft <sup>3</sup> )	Total EE (MJ)
1 in stucco	5.32	1,860	1.669	467.7
½-in. Gypsum Board	1.8	800	2.667	108.7
CMU block layer - 13MPa	0.71	1,800	13.32	482.0
Mortar (1:1:6) type M	1.18	1,600	1.906	101.9
R-5 rigid insulation (EPS)	88.6	16	13.333	535.2
1/2 in. Gypsum Board	1.8	800	2.667	108.7

## Section 2. Manufacturing Energy Analysis

### Processing the wood flour

Equipment	Machining gross HP	Time for 1 m <sup>3</sup> of throughput	Source
High Powered Grinder	40	1	Vecoplan [48]
Attrition Mill	50	1	Munson Attrition Mills [47]

From the table above, it takes about 90 hp\*hours to make 1 cubic meter of wood flour using the above equipment, if we convert units and multiply by the amount of material needed for the 3D-print panel (0.2548 m<sup>3</sup>), it is estimated that it would take around 61.5 MJ to process the recycled wood.

### 3D-printing process

	Motor Horsepower (HP)	Ideal printing Time (Hours)	Ideal Print Energy Consumption (MJ)	Conservative Print Speed Energy Consumption (MJ)
x-Axis motor	5	18	241.2	482.4
y-Axis motor	5	18	241.2	482.4
Z-Axis motor	5	18	241.2	482.4
Binder spray motor	0.25	18	12.06	24.12
Extruder	5	18	241.2	482.4
mixing chamber	30	3.4	273.36	546.72
		Total Energy estimates (MJ)	1250.22	2500.44

### Section 3. Added Material Properties Input into EnergyPlus Model

#### 3D wall construction properties

Material	Roughness	Conductivity (W/m*k)	Density (kg/m <sup>3</sup> )	Specific Heat (J/kg-K)
Wood Shingle	MediumSmooth	0.11388	426.0908477	1631
3D wood end (estimated)	MediumSmooth	0.104	537.279	1600
3D wood Middle (estimated)	MediumSmooth	0.0413	113.917799	2488
Drywall	MediumSmooth	0.16009	800.922646	1087
OSB	MediumSmooth	0.1163	544.6273993	1213
SIPs insulation	MediumSmooth	0.1428	23	1500

## Section 4. Athena Eco-Indicator Raw Outputs

	Global Warming Potential (kg CO <sub>2</sub> eq)	Acidification (kg SO <sub>2</sub> eq)	Airborne Particles (kg PM <sub>2.5</sub> eq)	Ozone Depletion (kg CFC-11 eq )	Smog Potential (kg O <sub>3</sub> eq)
3D-Print	111	1.2	0.340	2.36E-07	28.6
CMU	568	3.5	0.704	5.87E-06	64.9
SIPs	200	1.77	0.310	1.85E-07	36
Wood-Frame	124	1.24	0.309	3.60E-07	27.5